Automation Of Single-Cell Techniques In Neural Tissue

by

Joseph D. Steinmeyer

B.S. University of Michigan (2008)
S.M Massachusetts Institute of Technology (2010)

Submitted to the Department of Electrical Engineering and Computer Science
in partial fulfillment of the requirements for the degree of

Doctor of Philosophy

at the

MASSACHUSETTS INSTITUTE OF TECHNOLOGY

June 2014

Signature redacted

Author .....
Department of Electrical Engineering and Computer Science
May 12, 2014

Signature redacted

Certified by .....
Mehmet Fatih Yanik
Assistant Professor of Electrical Engineering
Thesis Supervisor

Signature redacted

Accepted by .....
Leslie A. Kolodziejski
Professor of Electrical Engineering
Chair of the Committee on Graduate Studies

Automation Of Single-Cell Techniques In Neural Tissue

by

Joseph D. Steinmeyer

Submitted to the Department of Electrical Engineering and Computer Science
on May 12, 2014, in partial fulfillment of the requirements for the degree of
Doctor of Philosophy

Abstract

The highly heterogeneous nature of cells in the context of native tissue environments necessitates the development of tools and techniques that can manipulate and analyze samples with single-cell resolution. While the past decades have seen significant progress in analyzing individual cells in tissue, both electrically and morphologically, the ability to genetically manipulate and biochemically analyze such cells in a high-throughput manner has seen only limited advances, and therefore a significant technological gap in accessing cells with single-cell specificity in tissue remains. We present a system design and workflow that fills in this gap in technology through the implementation of precision automation and redesign of standard biological techniques, resulting in greatly improved throughput while maintaining single-cell accuracy and precision. This thesis comprises three parts: First we discuss the design and implementation of an expandable computer-controlled automation system enabling the rapid maneuvering and targeting of micropipettes within tissue environments as well as a methodology for cleaning and reuse of these micropipettes to enable significant gains in throughput. Second we apply this automation to transfecting neurons in brain slices with DNA and RNA for subsequent analysis with greater throughput than previous methods. Third, we apply our automation to collecting the contents of single neurons embedded in relevant tissue environments for molecular analysis. The work presented greatly improves the throughput of traditional single-cell methods of transfection and cell-sampling by between one and two orders of magnitude and fills in a gap in the workflow of the rapidly expanding field of single-cell analysis.

Thesis Supervisor: Mehmet Fatih Yanik
Title: Assistant Professor of Electrical Engineering

Acknowledgements

The past years of work would not have been possible without the support of family, friends, and colleagues. I would like to thank my Ph.D. supervisor Dr. Mehmet Fatih Yanik for his support throughout my graduate studies here at MIT. I'm also grateful to Dr. Dennis Freeman and Dr. Jongyoon Han for serving on my thesis committee. My many lab mates have been amazing in helping me learn and carry out research including Matthew Angel, Chris Rohde, Mark Scott, Thomas Dieffenbach, Chrysanthi Samara, Paul Tilberg, Zachary Wissner-Gross, Cody Gilleland, Jaqueline Wolfrum, Steve Sheridan, Yao Zhou, Alexei Finski, Mohammed Azimi, Peter Eimon, and others. Others at MIT who've helped me in countless ways include Professor Joel Voldman, Professor Leslie Kaelbling, Professor Cardinal Warde, Professor Marc Baldo, Adam Hartz, Shawna Young, Julian Greene, and the entire OEOP community, Ron Roscoe, Janice Balzer, Al McGurl, Lourenco Peres, John Sweeney, Cheryl Cheney. Finally for my family, including Libby Steinmeyer and my parents Mark and Mary Ann Steinmeyer, as well as Rachel Greenhaus, Carol Kaye, and the Chesapeake and Ohio Railway who've been the core of my support, I'm very much grateful.

Not that it was beautiful,
but that, in the end, there was
a certain sense of order there;
something worth learning...
-Anne Sexton

Contents

List of Figures

List of Tables

Chapter 1

The Study of Single Cells: Background and Motivation

A significant trend in recent years in the many the sub-fields of the life sciences has been the focus on the biology of individual cells as actually analyzed at the single-cell level[1]. Most of what is considered as "common knowledge" in regards to cell biology today, was not generated by analyzing individual cells directly, but rather by analyzing populations of cells and extrapolating downwards to the single-cell level[1]. This is not to say knowledge gained so far in biology is a waste or without benefit; such a viewpoint couldn't be further from the truth in fact. Throughout the twentieth century, there have been many questions that haven't required the ability to analyze individual cells in order to find answers. However as the life sciences have advanced, new questions have appeared and many of these involve variability at the actual level of single cells. In the case of tumor biology and neuroscience, for example, cell-to-cell variability is at the core of new phenomena just being discovered so it is no longer sufficient to extrapolate information about individual cells from many; direct access to the individual cell is now needed.

This shift in focus has been catalyzed by recent improvements in manipulative and analytic techniques. Historically, the study of cells, regardless of environment or type, has suffered from one major disconnect: the mismatch between the scale of cell parameters, and the scale at which researchers can manipulate and analyze parameters using instruments. This mismatch has at

[1] As opposed to the study of single cells as extrapolated from the study of populations

various points encompassed all physical phenomena, including mechanical, electrical, and chemical, (and continues to do so in subsets of these parameters), and improvements in minimizing or eliminating the difference between what *should* be measured and what *can* be measured has been the core of many, if not all, biotechnological advances. While certain parameters of cells can now readily be manipulated and analyzed at sufficiently low-enough levels, there are still many areas where this measurement/parameter mismatch continues to require researchers to either make assumptions regarding phenomena, or avoid the pursuit of particular lines of inquiry until the mismatch can be overcome.

One of these mismatches recently overcome is single-cell DNA and RNA sequencing [2]. In the past few years, there's been an explosion in the amount of research on sequencing the DNA and RNA transcripts of individual cells. In particular, the ability to analyze copy numbers of low-expression level mRNA species from single cells, something achievable with any regularity and ease only in the past few years, has revealed the potentially questionable nature of previously held assumptions in certain areas of cell biology as well as revealed completely new insights into a far more complex set of heterogeneous cell states than previously thought to exist[3]. The importance importance and promise of these advances are such that the prominent life science journal *Nature* named single-cell sequencing as the "Method of the Year: 2013"[4].

Single-cell transcript analysis needs to be framed in the context of it being as yet one more improvement in a general trend towards complete direct analysis of cells, a gradual trend that has been going on for centuries, and which has advanced rapidly in the last several decades. From a systems engineering perspective, many of the advances in molecular and cellular biology from polymerase chain reaction (PCR), to patch clamping, to microscopy, have been matters of achieving amplification of sufficiently high fidelity to enable manipulation and study of cellular signals. This introduction chapter covers a brief history of single-cell analysis from this engineering perspective, from the earliest work with cells up to the state-of-the-art as of 2014. We then look at a few of the outstanding issues that remain, and show how the bulk of the work in this thesis, specifically the automated platform for single-cell manipulation and analysis that we developed, can be used to fill in some of these technological gaps and enable previously unachievable capabilities in certain analytical dimensions.

1.1 Single Cells in History

For centuries, the study of life was restricted only to what was able to seen, and more generally sensed, by the unaided human. The modern concept of all life being comprised of cells is a relatively recent idea, being traced back to the discovery of cells in the eighteenth century. The first attempts at single-cell analysis coincided directly with the initial observations of cells by Robert Hooke and Antonie van Leeuwehoek using crude microscopes of their own construction[5]. In one letter to Robert Hooke, (who made the first recorded observations of cells in cork and who is widely credited with coining the term "cell") Leeuwenhoek emphasizes the marked difference between different cells and what could be considered among the first single cell analysis[6].

> Examining this water...I found floating therein divers earthy particles, and some green streaks, spirally wound serpent-wise...and I judge that some of these little creatures were above a thousand times smaller than the smallest ones I have ever yet seen, upon the rind of cheese, in wheaten flour, mould, and the like.

What is commonly held to be the birth of cell doctrine in Theodor Schwann's publication of his 1838 work *Microscopic Investigations on the Accordance in the Structure and Growth of Plants and Animals*, stressed both the variability of cell types in organisms and various settings as well as unifying principles that exist across all cell types[7]. Cell-to-cell variability was therefore recognized early on, and as work was carried out in the following centuries on higher-level organisms, more specializations of cell types were found and classified. Researchers discovered that there was no general type of "tree cell", for example, but rather mixes of many different cell types within individual organisms even within specific organs and tissues. The realization of cell heterogeneity was especially important in the development of of modern neuroscience at the end of the nineteenth century where single-cell optical analysis was integral in Ramon Santiago Cajal's development of neural doctrine[8].

1.2 Manipulation and Analysis of Single Cells in Biology

The ability to carry out experimental analysis on single cells requires two major capabilities: the ability to manipulate and the ability to analyze with cellular or

sub-cellular levels of precision and accuracy. The primary difficulty in analyzing the input/output characteristics of a cell is the mismatch of scales between the parameters of a single cell and those capable of being measured and manipulated by researchers. For example:

- A standard mammalian cell has dimensions of maybe 10 μm, far smaller than can be viewed by the naked eye, and therefore a microscope is needed to close the gap.
- The electrical properties of a cell are on the order of millivolts and exist spatially over distances as small as several nanometers[2]. Mechanical devices with fine precision and accuracy as well as high-fidelity electronics are therefore needed to manipulate and analyze these properties.
- The quantity of biomolecules generated by a single cell are far below what can be detected by an unaided human and therefore require amplification techniques. These techniques include enzymatic methods, chain reactions, etc...

This thesis focuses primarily on rapid, targeted single-cell perturbation and analysis of biomolecular parameters (gene expression primarily), and will therefore focus only on that subfield of scaling for single-cell analysis. Optical techniques and electrical techniques as applied to single cells comprise fascinating fields of research in their own right, and for the readers that are interested, there are a number of good reviews on the state of the art can serve as a starting point[9, 10].

1.2.1 Cell Lines as a Means of Biochemical Amplification

The quantity of biological material produced by a single cell is extremely small. For proteins, total amount of material in a cell may be as low or lower than 50 pg, with individual polypeptide species making up tiny fractions of that number [11, 12]. In the case of RNA, total quantity in a mammalian cell is estimated to be approximately 10 pg, of which only several percent is mRNA [13, 14]. In the case of DNA, the total amount of most sequences in a cell will be two. For most of the history of biology, these amounts of starting material were far below what was capable of being analyzed.

[2]the thickness of the cell membrane

The relatively simple solution to this problem was to avoid work on a single instance of a cell and instead the use many identical cells at the same time in order to be able to respond to and produce signals at then obtainable levels of precision and accuracy. This has been the approach for working with most prokaryotic cell types for the last century, where the fundamental unit of analysis in terms of experimental readouts became the clonal population rather than the individual cell. This approach has much justification, since bacteria have amazingly low error rates in replication and transcription, being on the order of ow as 1×10^{-11} errors per base pair copied, and as far as cell types go daughter cells of an E. coli division are about as close to copies as can be achieved[15]. From a systems engineering point of view, the bacteria population themselves act as high-fidelity amplifiers, and utilization of them in such a way proved valuable in early biological work. Consequently, much cell biology, and much of what we know of cells is extrapolated backwards from population-based experiments.

Cell-line amplification has also been applied to higher order cells including many mammalian cell lines. The first expandable human cell line by George Otto Gey in 1951 (the famous HeLa cell) was followed up with numerous other well-established lines, and all together these cell lines have provided what have been viewed as scaled versions of single mammalian cells. By culturing a flask of HeLa Cells, a researcher could obtain μg to mg of molecular species, and the middle decades of the twentieth century saw the development of manipulative and analytical techniques that could work at those levels. Most, if not all modern molecular biology analytical techniques, including Northern, Southern, Western, (and Eastern) blots, Polymerase Chain Reaction (PCR), as well as many "bulk" transfection techniques such as electroporation, lipofection, and viral transfection were all developed in the context of cell line cultures and their associated amounts of material.

(In)Homogenous Cell Populations

In spite of its benefits, there were/are several key limitations to cell line culture. First is that a cell culture is not a collection of *exactly* identical cells. Even in the case of extremely low mutation rates in *E. coli* replication, mutations are inevitable (and in fact necessary for many techniques), so it is impossible to assume that all cells will share identical genomes. Compound this with epigenetic variation heavily present in eukaryotic cells, variations in cell cycle

at any given point in time, as well as the now well-documented stochasticity of mRNA and protein levels in cells, and it becomes nearly impossible to claim that any two cells in a cell line culture are "identical" at any given point in time [16, 17, 18, 19]. Researchers have even come to realize recently that within so-called "homogenous" cell populations, the variability in cell signals and states between two "identical" cells can vary more than that between two averaged populations exposed to different stimuli [20, 21].

Cell cultures and cell lines therefore need to be viewed as biochemical amplifiers with potentially lower fidelity than previously held. This shouldn't suggest that they are useless as a research tool. If the amplitude of the signal being measured exceeds any cell-to-cell variability or "noise" within a cell-culture amplifier, then such a platform is sufficient, but as the amplitude of the signal approaches the cell-to-cell variability for a response, the validity of any readouts generated should be called into question. If a cell culture contains a vast distribution of cell parameters of an unknown nature, in analyzing the population, these trends will be lost. This resulting "averaging effect" can have significant implications, masking trends found both within a population or between populations. Two key issues with the averaging effect are highlighted in Figures 1.1 and 1.2. Many of these issues have in fact been confirmed in cell populations as single-cell analysis techniques have come into popular usage in recent years [20, 21, 4].

(In)Validity of Cell Cultures

Cell culture-based biology and the utilization of cell lines as models has undoubtedly yielded important experimental results for biology and helped to develop knowledge about cellular processes, however in addition to intra-culture variability, there is also a significant concern about the overall validity of cell lines and *in vitro* culture in general as tools for answering biological questions. HeLa Cells are far from a "typical" cell found in the human body [3]. Even the culture of primary cells, cells extracted directly from tissue and then cultured *in vitro*, exhibit vast differences in many parameters. While true for all cell types, this is particularly the case in neurons. A neuron in its native tissue environment in the central or peripheral nervous system will be surrounded by astrocytes and microgila as well as various classes of other neurons and, if in a vertebrate, surrounded by myelinating oligodendrocytes (or Schwann Cells if in the peripheral

[3] cellular immortality and variabile polyploidy being just a few of the issues

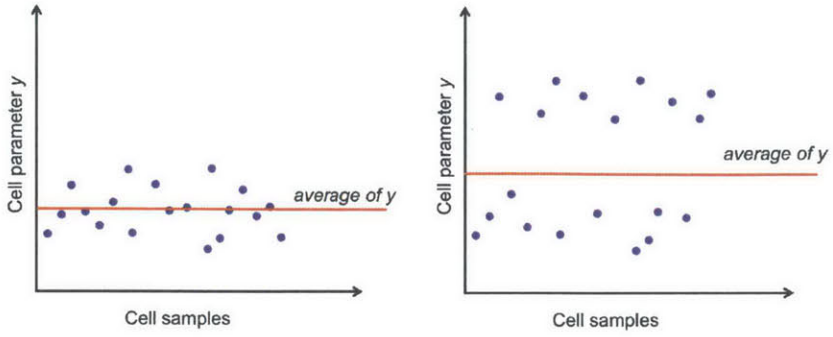

Figure 1.1: Two problems resulting from cell population averaging are demonstrated here. On the left, a collection of cells and their measured value of parameter y are plotted along with their average. At its most basic level, averaging of cells will obscure the distribution. In a situation where the distribution is Gaussian or somethign similar, this won't be a problem necessarily, however it can become a particular issue as shown in the right plot. Here the average obtained from bulk analysis corresponds to a value which no individual cell itself exhbits. This can lead to innacurate assessment of response and analysis.

nervous system)[22, 8]. All of these cells project onto the neuron, maintaining or modulating all aspects of its environment. When removed from this environment, the neuron should be expected to act and respond differently which is problematic in dissecting how native neurons function[23].

1.2.2 Single Cells In Tissue Environments

The goal of biology is the study of life, and therefore the model systems in which work is carried out should be as close as possible to reality while still allowing for the ability to manipulate and analyze the system. Cell culture *in vitro* and established cell lines, obviously make sacrifices in this regard, being significantly deviated from real conditions, but they can still have their use, the validity of which is based upon questions. For example, it is perfectly reasonable to study the question of cellular response to changes in osmolarity in a cell culture platform since one would expect that many general principles will still be present assuming the cells are healthy. It is less relevant to study native neural networks of the brain in dissociated primary neurons; the latter will not model the former very well. In other areas of biology, the behavior of individual tumor cells within a cultured piece of tissue have been found to behave far differently than tumor cells cultured *in vitro*, calling into question of

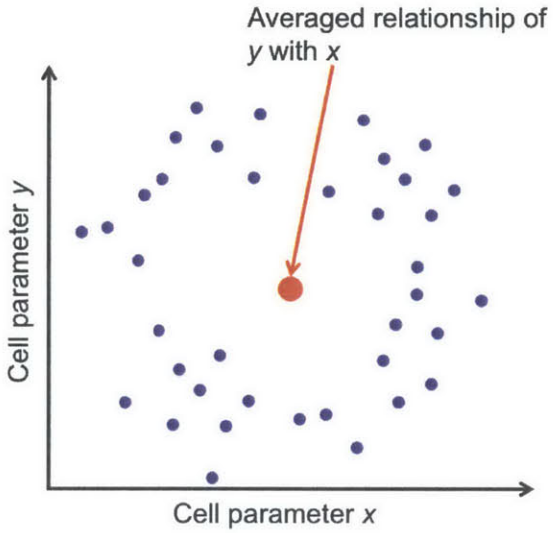

Figure 1.2: In the event of merging a cell population for analysis, the creation of "false states" can occur. Here, the distribution of two cellular parameters (mRNA, protein level expression, etc...) are plotted in a two-dimensional plane. It is obvious to the reader that a circular-distribution exists in the $x - y$ plane, however to a researcher analyzing this collection of cells only at the population level, this pattern will be obscured, resulting not only in a loss of distribution (similar to that shown in the right plot of Figure 1.1), but also in the creation of a non-existent pairing between x and y values.

study and screening of treatments using the latter format[24].

There is consequently a lot of motivation to work with cells when when in their native tissue environments, either *in vivo* or in slice culture format. In working in these environments, however, the researcher can no longer rely upon high (cell-culture amount) levels of starting material for experiments. Instead, due to the heterogeneity of cells in tissue environments, the biochemical manipulation and analysis of cellular state requires direct access to the biochemical state of the individual cells. To varying degrees methods and technologies have been developed in the last two decades towards this end and a brief overview of the benefits and shortcomings of the major groups of single-cell biochemical manipulation and analysis techniques for tissue environments are detailed in the Sections 1.3 and 1.4.

1.3 Single-Cell Manipulation in Tissue Environments

Table 1.1 details available tissue-compatible techniques for obtaining some degree of single-cell biochemical modulation. The limitations are discussed in sections below.

Transgenics

One common means of achieving manipulation with single-cell resolution is through the use of transgenic lines. Many incarnations of this technique have been developed, with the vast majority being primarily in mouse until relatively recently[25]. An extreme implementation of single-cell manipulation in tissue is the so-called "brainbow" series of research carried out by The Carp Lab and associates at Harvard University beginning in 2006, where cells in nervous tissue were combinatorially labeled with a variety of fluorescent species enabling previously unachieved densities of cell imaging and analysis [26, 27]. Transgenic lines can be used to target expression to specific cell types, for example confining the labeling or expression of transcripts to subclasses of cells using cell-type specific promoters. There are several major limitations in transgenic targeting from the point of view of many research studies. First, transgenics are a before-the-fact method, where the targeting is implemented during development and the production and crossing of specific specimen lines. Second, the inherent nature of transgenic technology precludes its use in higher-level tissue work, for

Technique	Single-Cell Precision	Single-Cell Accuracy	Throughput	Wild-Type Tissue
Transgenics	Yes	No	High	No
Viral Transfection	Yes	No	High	Yes
Biolistic Transfection	Yes	No	High	Yes
Bulk Electroporation	Yes	No	High	Yes
Single-Cell Microinjection	Yes	Yes	Low	Yes
Single-Cell Electroporation	Yes	Yes	Low	Yes
Optoporation	No	Yes	Limited	Yes

Table 1.1: Single-cell precision refers the ability to effectively target individual cells when surrounded by many cells, but not the ability to taret a specific cell. Single-cell accuracy refers to the ability to target a specific cell. In general most techniques can be tuned to yield single-cell precision, often times through sparse, stochastic labeling in the case of bulk techniques, however only manual techniques provide full-function single-cell accuracy.

example in human tissue. Researchers have succeeded in culturing post-mortem brain tissue and recent research has found evidence of unique structures or cell subclasses found only in the brains of higher order mammals, including humans [28, 29, 30]. Research published in the last few years on many topics of neural development lend support to several unique features, and if research is to be carried out on single cells in relevant human tissue culture environments, whether post-mortem neural tissue or culture tumor tissue, a technique should need to be able deal with wild-type tissue, ruling out transgenics[31, 32].

Biolistic and other Bulk Transfection Techniques

While transgenics cannot be used to target a given cell in wild-type tissue other techniques can do so[4]. Biolistic transfection is one such method that allows the transfection of individual cells in a tissue environment[33, 34]. In biolistic transfection a device, often termed a "gene gun," fires small gold particles coated with the reagent to be transfected at the tissue sample. Particles and the material they carry then become lodged in the cells and will subsequently be processed or incorporated. Depending on the settings, very sparse to very dense can be achieved. Which cells get transfected is left up to chance however since the gene gun provides only the most basic targeting capabilities, possibly providing slight regional accuracy and precision.

Biolistic transfection can be termed a "bulk" transfection methodology in that it is applied to the greater majority of a given tissue and relies upon parameters and probability to determine how many and which specific cells get transfected. Several other bulk transfection methods exist including bulk tissue electroporation and bulk lipofection[35, 36]. While relying on different physiological properties for operation, both techniques provide means of transfecting pre-defined densities of cells while lacking cell precision and accuracy. Viral Transfection is another possibility for transfecting cells within tissue. In the case of organotypic culture the protocol for transfection is a simple as placing a viral solution above and allowing to diffuse into volume of the tissue. By varying the concentration of virus applied differing densities of transfection can be achieved, however which specific cells get transfected is still largely up to chance. This can be a major limitation in studying a neural circuit for example, where the researcher would want to target a specific neuron that has already

[4]Several of these techniques are actually how you generate transgenic lines in the first place, using bulk electroporation *in utero*

been identified via another method viral for neural tracing [37, 38]. Some degree of cell selection can be implemented with these bulk techniques by using vectors that possess cell-type selective expression controls. These can yield more complex patterns, where expression of a vector is the product of both semi-random transfection (from the bulk method) and cell-type-specific expression (from the vector)[39]. This does not overcome all limitations, however. Labeling cells based off of presumed sub-type categories is inherently limited by knowledge of those subtypes. For years, attempts have been made to subdivide cell types based off of presence/absence of molecular markers, morphological data, electrophysiological responses, and location[40]. Consequently there are experimental situations where the capability to arbitrarily transfect single cells "on the fly" would be desirable.

Single-Cell Microinjection

The techniques described so far can be relatively high-throughput, allowing many cells to be transfected at once, but which exact cells get transfected is still largely up to chance. There also exist a series of techniques that provide single-cell precision and accuracy. Unfortunately these techniques are also often of a much lower throughput than the bulk techniques above. Single-cell microinjection is one such technique where a glass micropipette with tip dimensions usually < 0.1 μm is loaded with a reagent and then used to pierce a cell of interest and introduce the reagent[41, 42, 43]. While this technique is often used in monolayer culture, it does have the drawback of easily getting clogged in tissue environments due to the extracellular matrix and small size of the tip opening. Additionally, the mechanical puncturing of the cell can be violent to the cell resulting in damage or death[41].

Single-Cell Electroporation

Single-Cell Electroporation (SCE) is a variant of standard electroporation where the electroporating field is only applied in the vicinity of single cell [44, 45]. In most modern (last decade) implementations, a micropipette is used as a hybrid electrode and delivery device [46, 47]. Single-cell electroporation (SCE) has emerged as a versatile means for transfecting cells due to its potential for high efficiency[48, 49], its ability to transfect a variety of agents including dyes[50], plasmids[51], and RNAi reagents[52], and its tissue and in vivo compatibility[53, 51, 54]. The fundamental operation of the technique relies

upon loading a micropipette with a transfection reagent, which may contain a mixture of multiple agents such as plasmids, in an ionic solution, and then positioning the tip opening on or near the cell of interest before applying an electrical signal to electroporate the membrane of the targeted cell. The micropipette therefore serves as both a highly-focused electrode and a sample delivery device.

Optoporation/Optical-Mediated Expression

Optoporation is another method that can achieve single-cell specificity in tissue environments approach[55]. Optoporation is similar to single-cell electroporation in many ways relying on targeted environmental change to induce the formation of pores in a cell membrane. Modern optics are more than capable of achieving sub-cellular resolution, and multi-photon systems can provide 3-dimensional accuracy and precision [56]. While SCE utilizes an electrode to deliver its reagents and electric field, optoporation needs only to introduce light to the defined region in order to porate the target cell, minimizing the potential for damage. However, reagents to be transfected still need to be introduced to the region, and in a tissue culture environment, this is very difficult to do without directing deposition using a micropipette. In a cellular monolayer environment, the entire culture solution containing the reagents could be used, using light as the selection mechanism, however this can waste large amounts of expensive reagents and can be difficult to implement in tissue due to limited diffusion of large macromolecules through the intercellular space and because of the rate of degradation, particular of RNA in extracellular solution (See Fig. 4.10)[57]. It use in complex tissue environments is therefore limited when compared to other single cell techniques.

Conclusion of Techniques

It should be apparent that there are two general classes of transfection techniques for cells in tissue environments: So-called "bulk" techniques that are high throughput compatible but lack single-cell accuracy or precision, and a set of techniques that can indeed target single cells with high precision, but do so at a low throughput. Little middle-ground exists.

1.4 Single-Cell Analysis in Tissue Environments

In addition to manipulating single cells in tissue through transfection, there is also a need to biochemically analyze those single cells. Fortunately analytical techniques have been developed with sufficient sensitivity to analyze individual cells for many biochemical parameters including mRNA, DNA, protein, and metabolite content[58]. However, there are still distinct limitations in carrying out these analyses on cells from tissue environments. The current state of the tissue-compatible single-cell sampling methods are shown in Table 1.2. While the following discussion can apply to all single-cell analytics, because of the content of this thesis, we focus primarily on RNA-based analysis.

Dissociation-based Collection of Single Cells

The simplest way in which to achieve single-cell biochemical analysis of cells from tissue is to mechanically or enzymatically dissociate the tissue and sort the cells using either Fluorescence Activated Cell Sorting (FACS) or a similar technology [59, 60, 61]. Such an approach is extremely amenable to high-throughput deployment and has been used in many recent publications in a variety of tissue environments[62, 63]. From an analytical standpoint, however, there are two major issues with this approach. The first is that dissociation of cells takes a long time and is potentially very harsh on the cells. By the time cells are extracted and sorted, they may have started to negatively respond to the dissociation environment/chemicals. Second, when using dissociation and FACS sorting there is no current way to associate morphological information about the cell with its biochemical analysis since the cell identities are mixed and consequently lost during the sorting process. Loss of this information is particularly critical in cases where tissue and cell type heterogeneity is of importance. For example in studying neurons, morphological characteristics, and location, can be as critical in identifying cell subtypes as biochemical markers [40]. Losing one class of data can greatly limit experimental usefulness.

FISH FISSEQ

An alternative to breaking tissue apart and analyzing cells separately is to lock the tissue in place chemically through fixation, and analyze cells using markers and fluorescent labels. This methodology finds its roots in immunohistochem-

Technique	Single-Cell Precision	Single-Cell Accuracy	Context*	Throughput	Live Tissue
Dissociation and FACS Sorting	Yes	No	No	High	Partial(dissociated)
FISH Variants and FISSEQ	Yes	Yes	Yes	High	No
Manual Micropipette Aspiration	Yes	Yes	Yes	Low	Yes
Laser-Capture Micro-dissection	Yes	Yes	Yes	High	No
Optically-Targeted Techniques	Yes	Yes	Yes	Low	Yes

Table 1.2: Single-cell precision refers the ability to effectively sample individual cells when surrounded by many cells, but not the ability to sample a specific cell identified in tissue. Single-cell accuracy refers to the ability to sample a specific cell identified in tissue. In general most techniques can be tuned to yield single-cell precision, but most high-throughput techniques require either fixed tissue, loss of single-cell accuracy or both. Manual Micropipette aspiration can provide both single-cell accuracy and precision in live tissue but suffers from low throughput.
*Context refers to the ability to match morphological information about a particular cell with its biomolecular analysis. Dissociating cells prior to RNA-seq, for example, mixes the cells and therefore lacks this capability.

ical staining and in the case of nucleic acid identification goes back to early fluorescent *in situ* hybridization (FISH) work from the 1980s[64]. More modern implementations have built upon this approach with work in the previous decade developing into single-molecule FISH as well as Fluorescent in Situ Sequencing (FISSEQ) and associated technologies[65, 66, 67, 68]. In this class of approaches, fixed tissue is analyzed for the presence of tags that bind to specific sequences (RNA or DNA), and using fluorescence imaging, allow the detection and even quantification of subspecies at a single-cell level. The obvious benefit of this approach is that it enables analysis while cells are still in the context of their tissue environment, and so is an improvement over dissociation and FACS in that regard. There are limitations in the spatial resolution with current implementations of FISSEQ as well as analytical limitations that are not as good as RNA-seq and similar techniques. Furthermore, this class of techniques does require tissue fixation, which has the limitations discussed in Section 1.4 above[66, 68].

Laser-capture microdissection

Laser Capture Micro-dissection (LCM) is a unique technology that provides a way to extract single cells from tissue environments and then transfer them into high-throughput single-cell analytical devices[69]. At its core LCM relies upon a high-intensity laser to cut out a particular cell from its environment and when coupled with a vibratome and rinsing/deposition tool can provide high-throughput collection of single cell contents coupled to original morphological data taken pre-extraction. LCM, however is generally carried out almost exclusively in pre-fixed tissue [70]. There have been more recent implementations of this technique where live cells can be removed, however to the author's knowledge this was done in cultured cells rather than tissue environments[71, 72]. If LCM can be adapted for use in tissue environments, it will still face the hurdle of content extraction since in live tissue, assuming off-target radiation effects can be minimized, the ability to collect material will still be dependent upon a mechanical means of isolation or which there is no clear solution.

Optical Techniques

The last several years have seen a series of optically-mediated analytical techniques that provide single-cell specificity in live tissue. At the forefront of this is the Transcriptome-*in vivo* Analysis (TIVA) Tag methodology[73]. In this tech-

nique, tissue is globally exposed to specialized RNA tags that are universally taken up by all cells. Upon excitation with light, the tags activate and anneal to all poly-A RNAs in the cell. Targeted illumination of a single cell can therefore tag only that particular cell's poly-A mRNA. Following local tissue extraction, the presence of a biotin label on the tags allows a biotin-strepdavidin pulldown to be carried out, thus collecting the RNA content of the targeted cell. This technique potentially fills several gaps in the field by allowing a means to rapidly target a single-cell for collection using a minimally-evasive method. No fixation is used during the collection process, with only a lysing and disruption step followed by RNA-pulldown. This technique requires regional destruction of the tissue for collection so analyzing adjacent cells is out of the question, however, and it is not readily apparent how such an approach could be varied to allow the handling of multiple samples at once.

Manual Micropipette Aspiration

A simple, yet reliable means of collecting single-cell content from tissue environments is via micropipette aspiration as originally shown in a series of papers in 1992 [74, 75]. In this method, by achieving a low-leakage patch seal on a cell and then applying negative pressure, the content, or at least a portion of it, can be extracted and then deposited for downstream analysis, at which point it can be used to analyze most biomolecules including DNA, RNA, protein, and metabolites [76]. This technique has high spatial accuracy and precision and can also be done on live tissue without the need for fixation. However, this technique is inherently low-throughput. The cytoplasm of a cell is a gelatinous material, not easily aspirated with a micropipette and prone to clogging[77]. When collected into a pipette tip, it is very difficult to free it from the glass. As a result, following aspiration, the tip of the glass micropipette is broken off for collection [78, 79, 80]. Destruction of the tip obviously prohibits reuse of the micropipette for additional samplings, and a one-cell-one-micropipette paradigm is enforced resulting in low throughput, labor-intensive operation.

1.5 Remaining Need and Overview of Work

In surveying the state of the field in the previous two sections and Tables 1.1 and 1.2, it is readily apparent that two general classes of techniques exist for single-cell manipulation and single-cell analysis in tissue environments. On one side,

there are a collection of techniques that are high-throughput compatible, but which lack one or more features such as cellular selectivity or a the inability to work in live tissue. On the other side, there exist single-cell techniques that have sufficient specificity and targeting capabilities, but which are low-throughput and therefore incompatible for high or even medium-throughput use. Very little middle-ground in between these two groups.

1.5.1 Proposed Solution

This thesis introduces several novel techniques and workflows that attempt to fill in the gap between the sets of manipulation and analysis techniques available for the single-cell researcher. By taking the principle operations of a set of traditionally manual, low-throughput single-cell techniques (single-cell electroporation and micropipette-mediated single-cell aspiration), and redesigning to overcome features that make these two useful techniques low-throughput, significant gains in throughput can be achieved while no sacrifice is made in terms of live or wild-type tissue compatibility and single-cell precision and accuracy.

The content of this thesis is as follows:

- **Chapter 2** details the initial and on-going development of a software and hardware package that enables the quick shuttling of a micropipette into and out of a solution bath containing tissue samples as well as a plate assembly for deposition, sampling, cleaning, and rinsing of tips. It will also discuss some the development of a cleaning procedure for micropipettes, however details of its deployment in both a single-cell electroporation setting and a single-cell harvesting setting will be discussed in more detail in Chapters 3 and 4, respectively.

- **Chapter 3** discusses in detail the integration of single-cell electroporation (SCE) into the automated micropipette platform introduced in Chapter 2. High efficiency of SCE as well as its ability to be rapidly switched to transfect different reagents demonstrates an unprecedented flexibility in manipulating individual cells.

- **Chapter 4** details the on-going work to use the system for rapid single-cell sampling (SCS) in tissue environments for downstream analysis using conventional single-cell analytics. While analysis of mRNA transcripts is the major readout analyzed, we also discuss the benefits and possibility of

using the approach demonstrated to analyze proteins and other biological macromolecules.

- **Chapter 5** briefly details on-going work with integrating the platform with electrical recording and SCE and SCS and summarizes the overall contribution of the work to the greater research field.

Chapter 2

Rapid and Scalable Automation for Glass Micropipettes

This chapter covers the development of a novel technique for using conventional pulled glass micropipettes to interface with single-cells in a way that allows reuse and cyclic operation. In addition we discuss the flexible collection of automation hardware and software we developed that greatly increases the throughput of micropipette usage in transfecting and biochemically sampling cells in tissue environment. This increase in speed drastically reduces cost-per-operation in both transfecting cells using single-cell electroporation (SCE) and collecting cellular material using single-cell sampling (SCS), which will be discussed separately in Chapters 3 and 4, respectively. [1]

[1]The system automation and operation workflows developed in this work were carried out over the course of five years in parallel with the single-cell electroporation (SCE) and single-cell sampling (SCS) work discussed in Chapters 3 and 4, respectively. For the sake of ordering in this thesis, automation from all aspects of system development will be covered in this chapter and particular implementations will be covered in later chapters. For an overview and early details from the work on automation, please see the author's Master's thesis[81].

2.1 Glass Micropipettes: Background

Glass micropipettes have been a fundamental tool in interfacing with individual cells for a large portion of the twentieth century[2]. Glass micropipettes are interesting in that they were among the first devices with micron-level features that could be reliably and characteristically manufactured by humans, predating even microelectronic fabrication techniques by several decades. By taking advantage of properties of glass cylinders as they are heated and pulled, macroscopic features (inner-to-outer diameter ratio) can be reliably transformed into microscopic features. Because a glass micropipette is a confining device, isolating its interior environment from the outside electrically, chemically, and too a lesser degree optically and thermally, these scaled physical parameters provide a means of scaling environmental isolation that could otherwise only be implemented macroscopically. For example, placing a metallic electrode into the large end of a micropipette filled with an ionic solution yields an electrode with spatial resolution at or below one micron. Such a tool was fundamental in allowing early electrophysiological recordings of neurons[83]. Further advances in this same technique yielded patch clamping, which allowed interfacing with individual membrane-bound ion channels of cells [84, 85]. Micropipettes also allow a means of obtaining high reagent resolution both for the release or collection of material at the cellular level. For example, researchers can "spritz" chemicals onto specific neural synapses because of the spatial resolution afforded by micropipettes[86]. Merging both of these techniques allows single-cell electroporation (SCE), the transfection of reagents into large cells with minimal off-target transfection. Alternatively, the molecular content from a single cell can be extracted and isolated from cells nearby, and this forms the basis of the work in Chapter 4 of this thesis [74].

In surveying how glass micropipettes are utilized in the biology, it becomes readily apparent that the vast majority of uses are short-term in nature. In almost all cases the lifetime of a micropipette starts when it is pulled, and ends a short time later after it has been used for the delivery of one type or reagent, or the sampling of one specific cell. From an economic and experimental standpoint, this approach makes sense. Micropipettes easily clog and often one "use" is all that can be obtained from them using standard techniques.

[2]A summary of the development and refinement of glass micropipettes can be found first few several chapters of *Advanced Micropipette Techniques for Cell Physiology* by Flaming and Brown[82]

Furthermore, the extremely low cost of glass micropipettes (< 1 USD), leaves little motivation to reuse them if one is not concerned with time.

This disposable usage of micropipettes does have a major disadvantage, however, in that it requires large amounts of time to carry out a series of experiments. Micropipettes are delicate and care must be taken in creating and setting them up for experiments. In addition, variability in protocols for creation of micropipettes often requires multiple attempts, where a researcher will set up the tip, carefully position it, and only then discover that it lacks the correct parameters for use, at which point another micropipette is inserted. This entire process can take tens of minutes, and is labor-intensive. Regardless, the experimental benefit of micropipettes are unmatched, providing a unique means of interfacing with cells both *in vitro* and *in vivo* for the purpose of measuring or manipulating the electrical, chemical, and mechanical state of a cell while minimizing disturbances to the surrounding region. Despite the age of the technology, it is tried and proven and a the devices used to generate micropipettes are standard components of most neuroscience labs.

We initially sought to take the glass micropipette, a device currently limited to a manual, low-throughput deployment, and increase the throughput with which it can be used while maintaining all the benefits of its functionality. The core of this work focuses on three developments:

- **Front-Loading of Reagents** to provide a quick means of loading and releasing arbitrary reagents to cells and small volumes
- **Cleaning and Rinsing of the Micropipette** to overcome the need to dispose between uses
- **Automation** of all non-user-critical steps to improve throughput and minimize support labor for the researcher

2.2 Front-Loading of Reagents

Traditionally micropipettes are "rear-loaded" with the solution or reagent desired by the researcher. This process involves manually filling the micropipette from its non-pulled end and must be done prior to an experiment. While there are times when front-loading is used for injecting materials with limited and/or expensive supply such as proteins, we have not been able to find cases in the

literature where researchers have reused micropipettes between different front-loading cycles[42, 43].

2.2.1 Limited Diffusion of Large Molecules

We began our work by identifying the front-loading of micropipettes as a part of a solution to their manual usage. By loading a micropipette with a generic conducting solution (a basic media which is compatible with all samples), we wanted to see if small volumes could be front-loaded into the tip and then used to carry out tasks such as deposition. In support of this implementation is that in a given micropipette experiment such as single-cell electroporation (see Chapter 3), the vast majority of solution used for loading will not be used. Transfection of a single cell using SCE, for example will require on the order of tens of pL of solution, when the tip will be loaded with on the order of μL of solution, a difference of four or five orders of magnitude. Due to the high hydraulic resistance of the micropipette tip, front-loading of a micropipette was hypothesized to provide a means of volume loading with much finer resolution than possible [3]

Front-loading into a micropipette already loaded with generic solution could raise the question of diffusion or loss of small front-loaded quantities into the greater bulk of the micropipette. As simulations and experiments showed, however, the rate of how fast this happens for relevant biomolecules is slow enough as to allow experiments to be carried out. Figure 2.1 shows that small molecules such as dyes with molecular weights of several hundred Daltons (Da) will relatively quickly diffuse into the greater volume of the micropipette. Larger molecules such as plasmids, with molecular mass on the order of 1 MDa or more remain relatively stationary at the tip of the micropipette, however, providing support for a front-loading prior to usage.

2.2.2 Implications for Use and Reuse

The successful demonstration of front-loading in micropipettes allowed us to then investigate means of reusing micropipettes. Because we could preload a micropipette with a generic solution, and then quickly (10s of seconds) introduce a sufficient quantity of material to the tip to carry out experiments, we then speculated that if we could remove that material with similar speed, multiple

[3]Details of these intial experiments are included in the Author's Master's Thesis and in Section A.2 of this thesis[81].

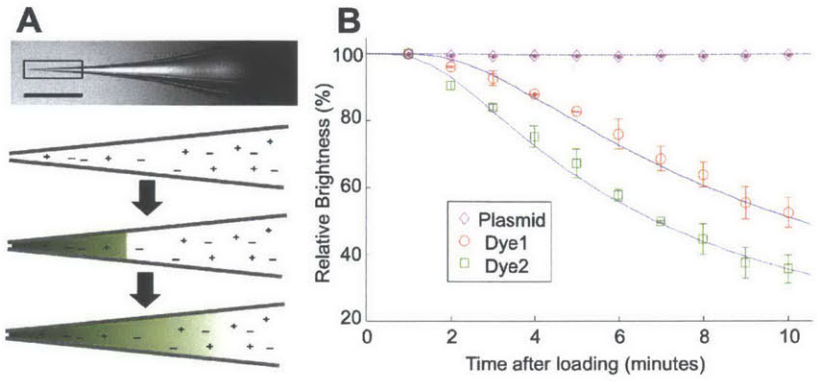

Figure 2.1: A: In a micropipette filled with saline (scale bar 1 mm), a front-loaded reagent diffuses over time, decreasing concentration of the sample at the tip (drawings are not to scale). (b) Approximately 2 nL of three different fluorescent molecules, Alexa Fluor 594 (Dye1) and 488 (Dye2) hydrazide salts and SYBR-Green-labeled pEGFP-N1 (Plasmid), were front-loaded into micropipettes and their fluorescence monitored at 1 minute intervals over ten minutes and compared to simulations (continuous lines). Each data point is the mean ± s.d. of three independent experiments. Concentration was correlated with brightness using standard curves discussed in Figure A.3 and Section A.2

iterations of different materials could be loaded and unloaded into the same micropipette.

2.3 Cleaning and Rinsing of Micropipettes

Optical analysis of loading and reloading cycles with micropipettes using different colored dyes verified that the micropipettes could be reused (data not shown see M.S. thesis), however this did not guarantee that samples were isolated from each other in time. A chemical means of cleaning the micropipette , in conjunction with simple ejection of the previous volume,was then proposed as a way of more effectively isolating separate samples from one another. In addition, because the micropipettes were to be used in a biological tissue environment, early experiments showed that extracellular debris would quickly clog a micropipette tip, preventing the expulsion and reuse of tips.

2.3.1 Sterilization

The need to sterilize a micropipette tip and to clean it of biological detritus in order to reuse it led us to experiment with a vast array of chemicals and methods for cleaning, ranging including an assortment of acids, bases, and detergents. For more on this work please see the author's Master's Thesis[81]. Sodium Hypochlorite exhibited superior cleaning capability on glass micropipettes at varying percentages (from 0.1% to 10%, depending on experiment), and was therefore used for almost all subsequent cleaning work. Sodium Hypochlorite forms hypochlorous acid in an aqueous environment and very aggressively attacks all classes of biological macromolecules [87].

2.3.2 Rinsing MIcropipette Tips

Because sodium hypochlorite destroys most biological materials, its usage in the context of a cyclic micropipette operation needed to be tightly regulated. We developed a series of washing and rinsing steps involving pressure pulses and insertion into water baths in order to eliminate the chance of stray bleach carrying over between samplings in order to destroy sample to be delivered (in the case of SCE) or that had been collected (in the case of SCS). Once effective programs were found, both repeatable cell transfection with different samples (Figure 3.4 and Section 3.2.1) and cell collection (Section 4.6) could take place.

2.4 System Automation

The previous two sections demonstrated a novel means of increasing the throughput of micropipette usage. If still carried out manually by a researcher, however these developments would yield minimal gains in throughput, however. We next set out to design a set of automation software and hardware that could take advantage of our novel micropipette workflow to actually increase the throughput. Drawing inspiration from semiconductor wafer and more recent liquid handling equipment, we developed a simple proof-of-concept system. A basic diagram of the system is shown in Figure 2.2. The system is based heavily off of a standard electrophysiological "rig", including an upright microscope with water-dipping objective, as well as a set of Sutter MP-285 Micromanipulators for control of a micropipette and a stage to hold tissue samples. Critically, however, the system has automated movement paths integrated into it using RoboCylinders

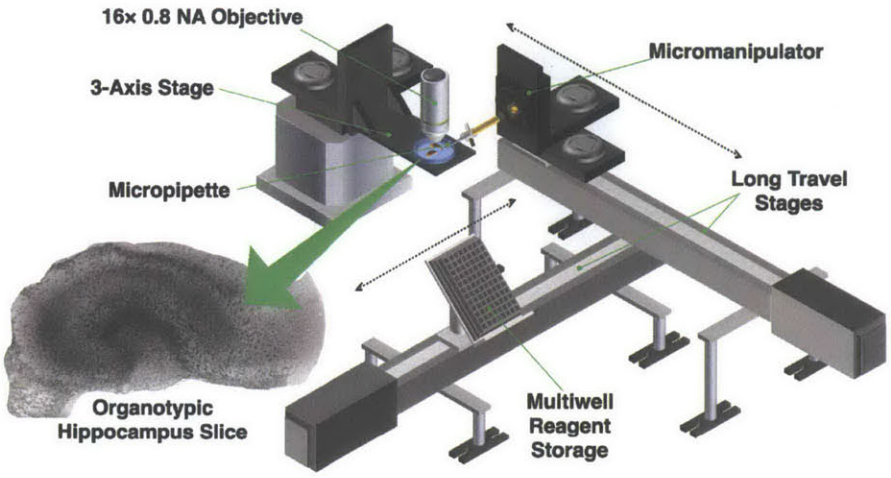

Figure 2.2: All of the automation and experiments detailed in this thesis were built upon the basic layout shown above, first detailed here[81]. A Sutter MP-285 family micrompanipulor is mounted upon a long-travel stage (International Automation Incorporated) with 250 mm travel range. Orthogonal to the micromanipulator axis is a second axis set lower carrying a multiwell reagent plate at an angle matching that of the micropipette to enable direct insertion and withdrawal. Synchronized control of the micromanipulator, the two long-travel stages, as well as the sample stage allowed rapid insertion and removal of delicate glass micropipettes into and near tissue environments.

(International Automation Inc.), which we will term "long-travel stages". Two movement paths were included in the original design: First is a track to move the micromanipulator controlling a micropipette from its operation area at the microscope to a loading position removed from the scope. A second track controls a multi-use well plate holder that contains samples, as well as rinsing and washing equipment. In the original SCE implementation, the plate holder was designed for use with wells at a standard 96-well spacing of 9mm (center-to-center). By integrating computer control of these long-travel stages, with control libraries developed in house to drive the Sutter micromanipulators, as well as a series of valve and pressure controls for controlling inflow and outflow at the micropipette controlled via data acquisition cards (National Instruments) we could implement all portions of the front-loading and reuse techniques developed in Sections 2.2 and 2.3.

2.4.1 System Characterization

Figure 2.3 shows the results of several mechanical tests carried out on the Sutter MP-285 micromanipulator and the long-travel stages, both separately and together. While full-speed (2.9 mm/s) movement repeatability of the Sutter MP-285 micromanipulator is not reported in the product literature, we tested it in-house by putting it through 50-cycle operations and monitoring the displacement of a micropipette tip under a 16× water-immersion microscope objective. Images of micropipette tip position were taken at every cycle step and analyzed. An example data set with just the Sutter micromanipulator is shown in Figure 2.3A. An interesting phenomenon that we observed was that much of the overall drift in position of the micromanipulator takes place very quickly before stabilizing out. This so called "settling-in" process is demonstrated by tracking the average in Fig. 2.3A. Within the first ten cycles, the average magnitude of drift from initial position approach approximately 3 μm however over the next forty cycles, the average drift from the initial position shifts approximately only a further 1μm.

Because the micropipette is free to drift in two dimensions, calculating the magnitude of drift as shown in Figure 2.3 could obscure the variation in moving cycle-to-cycle. To ensure this wasn't being underestimated we calculated the root-mean-square (RMS) drift from cycle to cycle using absolute coordinates of the micropipette in a fixed X-Y coordinate system. For a fixed-in-place Sutter MP-285, we calculated an average RMS drift of 1.96 ± 0.20 μm ($n = 4$), a sufficiently small number for our purposes.

In the system shown in Figure 2.2, the MP285 is mounted on the long-travel stage which then moves between the tissue bath and sample plate. The repeatability and drift of the combination of long-travel stage and MP-285 micromanipulator needed to be analyzed in order to characterize overall system performance. The reported repeatability of an long-travel stage (model RCA2) according to IAI technical specifications is ±0.02 mm or ±20 μm. When running an experiment similar to the case with a fixed MP-285, but now with a movement program each cycle applied to the Long-Travel Stage of:

a) -50 mm at 10 mm/s
b) -25 mm at 50 mm/s
c) +50 mm at 50 mm/s
d) +5 mm at 10 mm/s
e) +20 mm at 25 mm/s

The result of this experiment is shown in Figure 2.3B. Paying attention to the Y-axis on this plot, it is obvious that both the overall drift from start to finish and the RMS drift are larger, with the latter being $11.94 \pm 2.97\mu m$ ($n = 4$). This cycle-to-cycle RMS drift is significantly larger than that when the only the MP-285 is moving (1.96 ± 0.20 μm) ($p \approx 0.007, n = 4$), leading to the conclusion that the majority of the drift is coming from the long-travel stage.

Proper usage of the long-travel stage can abrogate much of this drift arising the manipulator. In particular, maintenance of the long-travel stage at constant speeds, as well as running symmetrical movement patterns with no intermediary stopping points can minimize the overall drift and RMS drift as shown in Figure 2.3C. In this experiment, identical operations were carried out as in the experiment in Figure 2.3B, however the cyclic movement pattern of the long-travel stage was set at:

a) -100 mm at 50 mm/s

b) +100 mm at 50 mm/s

The result of this operation showed a vast improvement. Both the overall drift from the beginning and the RMS drift became much lower than with the more arbitrary long-travel stage operation program. The average RMS drift with the symmetrical movement pattern was 1.80 ± 0.39 μm ($n = 4$ experiments). This measurement was significantly different from the arbitrary pattern ($p \approx 0.005, n = 4$). In fact, much to our surprise, there was no significant difference in RMS drift between combined movements of both micromanipulator and long travel stage together and just micromanipulator.

2.4.2 Human-Control and Software

The automation above could effectively carry out all the steps required to load, unload, clean, rinse, and position a micropipette with sufficient precision and accuracy. While we initially carried out experiments with automating the actual targeting of single cells for electroporation the efficiencies achieved were too low and we instead chose to focus on only on the automation aspects discussed above[81]. While future work on this project may lead to additional levels of computer control, including fine-targeting of cells based off of optical or electrical measurements and utilize recent developments in auto-targeting and computer vision for identifying cells, current state of the automation is focused on elimination all steps that can be automated with high efficacy, and releasing to human control for the actual targeting of cells [88]. Gains in timing

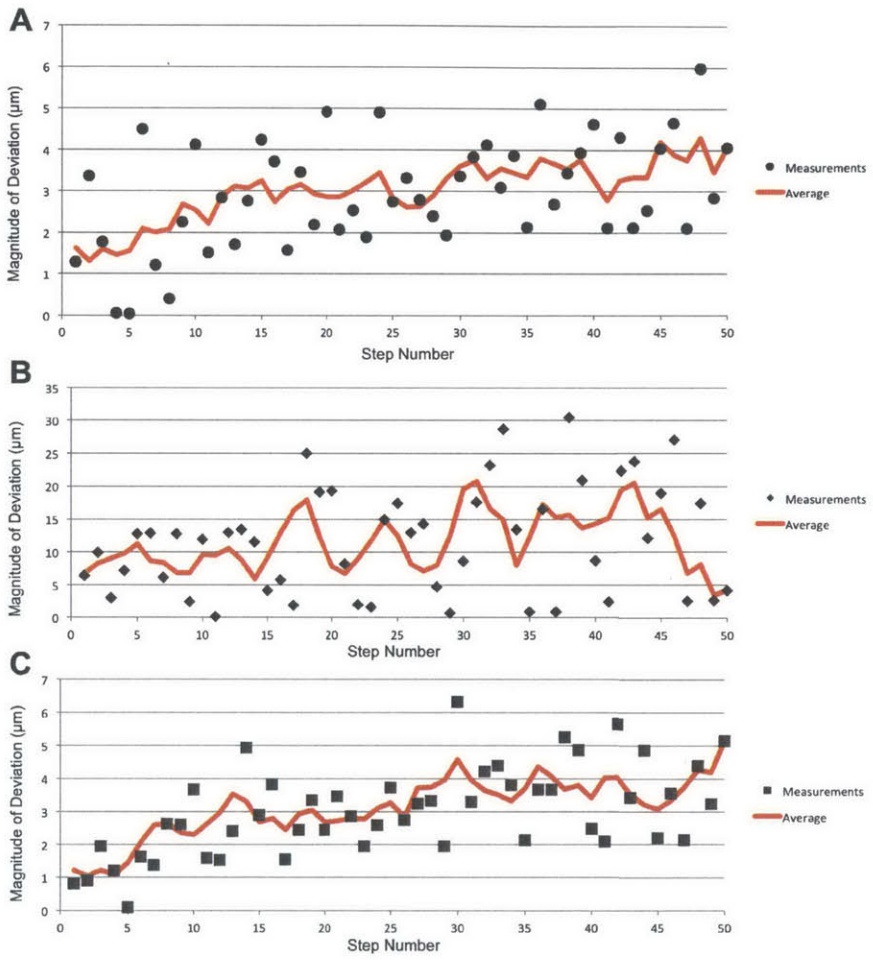

Figure 2.3: Examples of Micropipette Drift over 50 cycles for A: a fixed MP-285, B: an MP-285 mounted on a RCA2 RoboCylinder (long-tavel stage) with poorly-planned movement pattern, C: an MP-285 mounted on an long-travel stage with well-planned movement pattern. A: A standard insert-remove movement pattern for fixed MP-285 micromanipulator demonstrated an RMS drift of 1.96 ± 0.20 µm. B: Adding to this movement by the MP-285, a poorly-executed movement pattern by the RoboCylinder that exacerbated back-lash in the gearing increased the RMS drift to 11.94 ± 2.97µm. This cycle-to-cycle RMS drift was significantly larger than that when the only the MP-285 was moving (1.96 ± 0.20 µm) ($p \approx 0.007, n = 4$). C: With a well-planned movement pattern for the Robocylinder, minimizing the effect of back-lash, the RMS drift was 1.80 ± 0.39 µm, which showed no statistical difference from a stationary MP285. In all cases, 50-cycle experiments were run four times ($n = 4$).

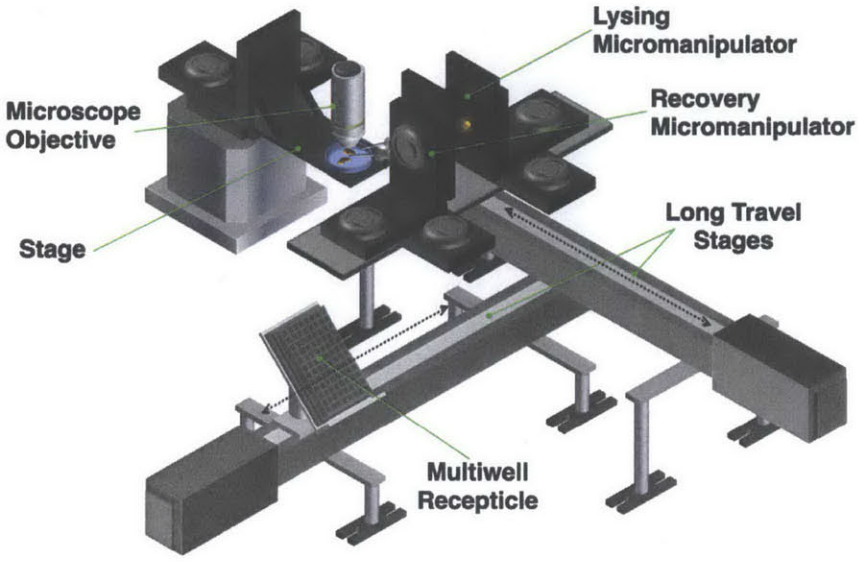

Figure 2.4: Version 1 of the dual-micropipette system: Initial efforts at using two separate micropipettes involved mounting a second independent micromanipulator onto the same long-travel stage that was already present in the original system.

are still significant, however, as shown and discussed in Chapters 3 (Figure 3.5 and 4, because the vast majority of time spent in deploying manual micropipette techniques is focussed on tasks that are now automated in this new system.

Control software was developed in MATLAB due to its wide utilization and familiarity in the academic, engineering, and scientific communities[4]. Screenshots of the software from the SCE and the SCS implementations are included in Figures 3.6 and 4.6, respectively. Further discussion of software is included in Section A.1.

2.5 Expanding Automation for Single-Cell Sampling

As discussed in Chapter 4 of this thesis, collecting the cytosolic content of single cells (single-cell sampling (SCS)) in tissue was found to require two microma-

[4]Software for interfacing with Sutter equipment is now available on the Sutter website. We have maintained and updated the original MATLAB-based control library developed in 2010, and it is still freely available to researchers upon request. Contact the author for the latest version

nipulators, each controlling a separate micropipette[5]. In order to minimize modification to the original, system, to accommodate two micropipettes we initially developed a modified micromanipulator mount for one of the long travel stages that could hold both manipulators, as shown in Figure 2.4. This approach had the advantage of needing only minor changes to the original system (Figure 2.2), however placing both micropipettes on the same side of the field of view greatly limited the flexibility when varying SCS parameters (see Chapter 4). In addition, penetration of the field of view and tissue from the same angle ultimately proved to be a hindrance to effective cell content collection. As a result, this design was abandoned and instead replaced with a second version shown in Figure 2.5

Version 2 of the dual-micropipette automation greatly improved functionality. Because each micromanipulator/micropipette pair was independent in this setting, the design offered greater flexibility in all steps of system operation. As is discussed in Section 4.4, this flexibility permitted a more efficient workflow and improved the full-cycle speed when compared Version 1[6]. Version 2 of the dual micropipette configuration was characterized as we did previously, we ran a series of analyses as shown in Figure 2.6.

2.5.1 Well Format Modifications

Because of dilution restrictions on collected cellular material (see Section 4.1), version 2 of the dual-micropipette system had a plate handler with 384 well format. With well-to-well spacing of 4.5 mm, and area and depths approximately 80% less those found in the comparable 96 well format, a revised alignment procedure was developed[7]

2.6 Discussion

The developments outlined in this chapter on workflow and automation provide the basis for the work carried out in the subsequent two chapters. By develop-

[5]The system as a whole became comprised of three micromanipulators: One for each micropipette and one to control the tissue stage.

[6]Due to limitations in Sutter software control with MP285 and MPC2000 systems, each micromanipulator needed a separate ROE-2000 and control box in order to permit simultaneous movement of the two micromanipulators

[7]With 96-well format, spacing tolerances were low enough so as to minimize the need for recalibration of alignment. With 384 well format, while the automation was sufficient to handle the finer tolerances, alignment required longer to carry out, and disturbance of the components warranted realligning more often.

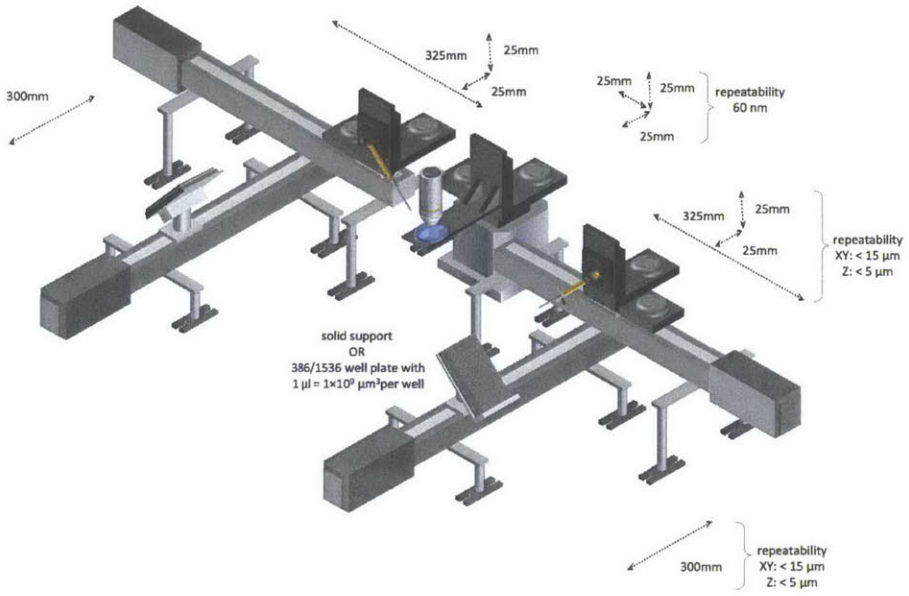

Figure 2.5: Version 2 of the dual-micropipette system: Two mirror-image systems, each controlling a separate micropipette and its supporting cleaning/rinsing/deposition wells were constructed. This setup allowed maximum flexibility in developing SCS. An enlarged version of this diagram is shown in Figure A.7. Photographs of the actual system can be seen in Figures A.4 and A.5.

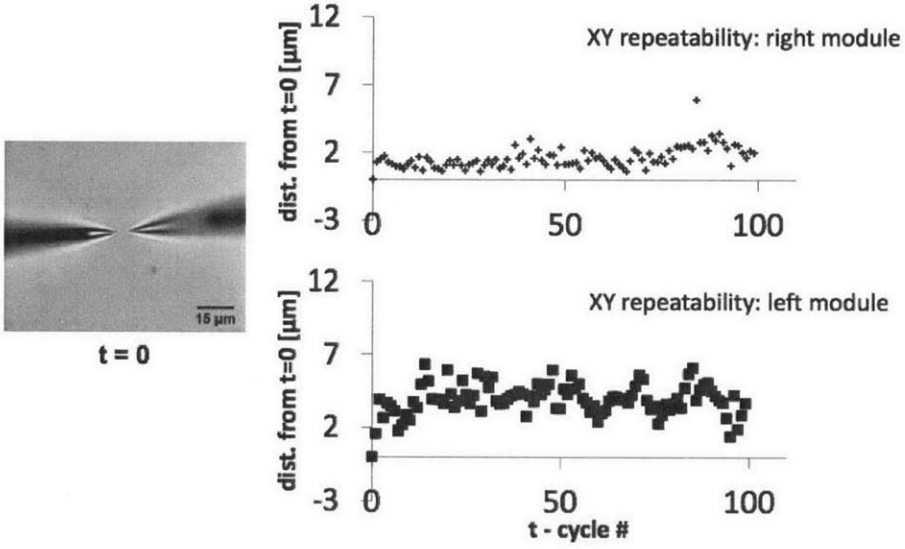

Figure 2.6: Point-to-point reproducibility in movement was found to be similar to what was observed with only one micromanipulator. Carrying out well-behaved movement plans as was originally used for studying single micromanipulator system operation in Figure 2.3, the RMS drift of the left micropipette was 0.92 ± 0.30 µm while the RMS drift fo the right micropipette was somewhat larger at 2.58 ± 0.44 µm ($n = 4$ subdivided samplings). These two values were found to be significantly different ($p < 0.05$), however because the scale of the difference was so small, it could be readily accounted for in regular system operation.

ing a novel micropipette technique that allows reuse with cells and biological samples, and by removing manual procedures, the automation and workflow allows the ability to carry out most varieties of traditional micropipette work with greatly increased throughput and decreased labor on the part of the user. To our knowledge, the automation and workflow we developed is the first to demonstrate the reuse of a glass micropipette for repeated use. In the next two chapters, the automation and workflow are applied first to rapid single-cell transfection (Chapter 3) then second to rapid single-cell content sampling (Chapter 4), with both carried out exclusively in tissue environments.

Chapter 3

Automating Single-Cell Transfection in Tissue Environments

3.1 Single-Cell Electroporation: Background

Electroporation has been used for decades to transfect cell types ranging from bacteria to stem cells[1]. As shown in Figure 3.1, electroporation is based off of raising the magnitude of the cell's transmembrane potential V_m to a level above a certain threshold at which point pores form in the membrane. The value of this threshold varies widely according to many parameters and reports, however it is generally agreed upon being in the range of several hundred millivolts to over 1 Volt [90, 91]. There are limitations in the electric field applied, however with too large being applied for too long irreversibly damaging the cell and leading to its death. All electroporation relies upon the generation of holes in a cell's membrane to facilitate passage of material from inside the cell to outside the cell, however a number of additional phenomena play a significant role in how effectively this actually happens. Smaller molecules, such as dyes, small proteins, or possibly even short nucleic acid oligos can most likely passively transfer in the cell's internal volume via diffusion and possibly electrophoretic and/or electroosmotic flow, while larger molecules such as plasmids, RNA, or

[1] Work in this chapter was originally published in PLoS One by author in 2012[89]

larger proteins have been shown to take many minutes to several hours to be transferred into the cell, which suggests an active process such as endocytosis is taking place (See Figure 3.1.)

Early electroporation relied upon placing cells in an ionic media suspension containing the reagents to be transfected between two electrodes and applying the electric field (Figure 3.2A). This style of electroporation can be classified as "bulk transfection." In tissue environments, bulk electroporation can also be applied by placing a tissue slice between two electrodes. This method is coarse in spatial resolution, with only the minimal form of regional specificity being achievable. Cell type selection does not occur at the transfection step in this case, but cell-specificity can be achieved by relying upon functionality of the vectors being introduced, however this offers little to no benefit over other bulk techniques[2].

An alternative to bulk electroporation is single-cell electroporation (SCE) (Figure 3.2B) where the electroporating field is spatially confined to the region of a single cell. This technique was first accomplished by using carbon microelectrodes in 1999 [44, 45] on single cells in suspension. In subsequent papers, this methodology was modified to allow for sample delivery and electric field delivery from the same implement (glass micropipette) [46, 47]. Further work saw the technique successfully implemented in tissue environments [53, 92, 54, 51].

Single-cell electroporation (SCE) has emerged as a versatile means for transfecting cells due to its potential for high efficiency[48, 49], its ability to transfect a variety of agents including dyes[50], plasmids[51], and RNAi reagents[52], and its tissue and in vivo compatibility[53, 51, 54]. The fundamental operation of the technique relies upon loading a micropipette with a transfection reagent, which may contain a mixture of multiple agents such as plasmids, in an ionic solution, and then positioning the tip opening on or near the cell of interest before applying an electrical signal to electroporate the membrane of the targeted cell. The micropipette therefore serves as both a highly-focused electrode and a sample delivery device. The efficiency of the technique can vary widely depending on cell type and vector delivered.

[2]The specificity is obtained through selectivity in expression of the vector. For example a plasmid expressing a gene of interest under a promoter highly upregulated into astrocytes could provide a degree of astrocyte specificity in expression even though the transfection efficiency had little selectivity

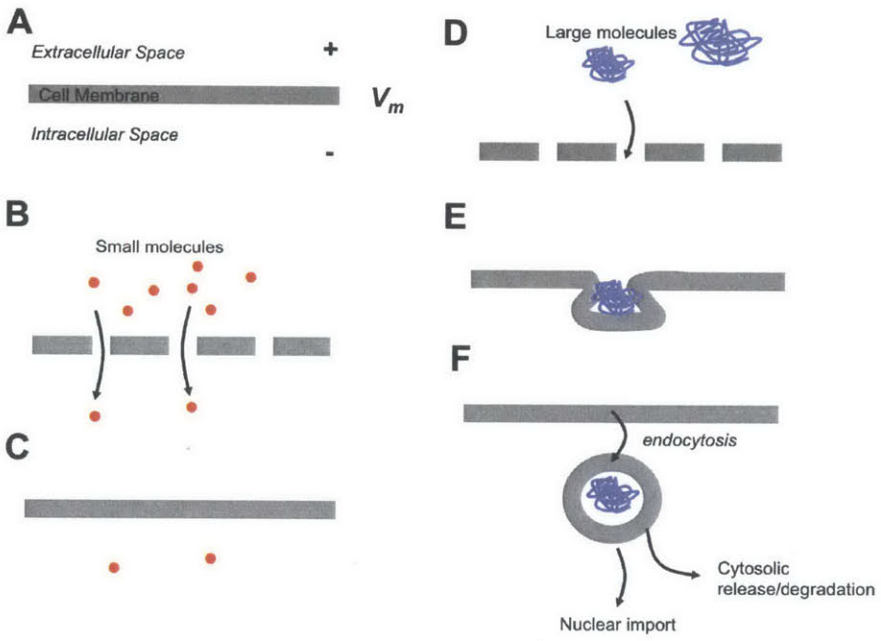

Figure 3.1: Electroporation results from modifying the transmembrane potential V_m (A) to a value greater than a set threshold, thus inducing the formation of pores in the phospholipid bilayer of the cell. The pore size is a function of the nature of the electric field (amplitude, frequence, polarity, etc...), however for cell survival, pore size is small enough to allow small molecules including dyes and smaller proteins to pass into the cell via diffusion, electrophoretic, and electroosmotic flow (B). After a certain period of time, the cell membrane will reseal, leaving the material that moved into the cell, remaining in the cell (C). In the case of larger molecules, such as plasmids, synthetic RNA, or proteins, the pore size is most likely too small to permit diffusion through or very far into the cell (D). Evidence suggests that an active process follows up electroporation (E) with the transfected molecules being imported to the cell via endocytosis, and subsequently either released into the cytoplasm, transported to the nucleus, or degraded by the cell (F).

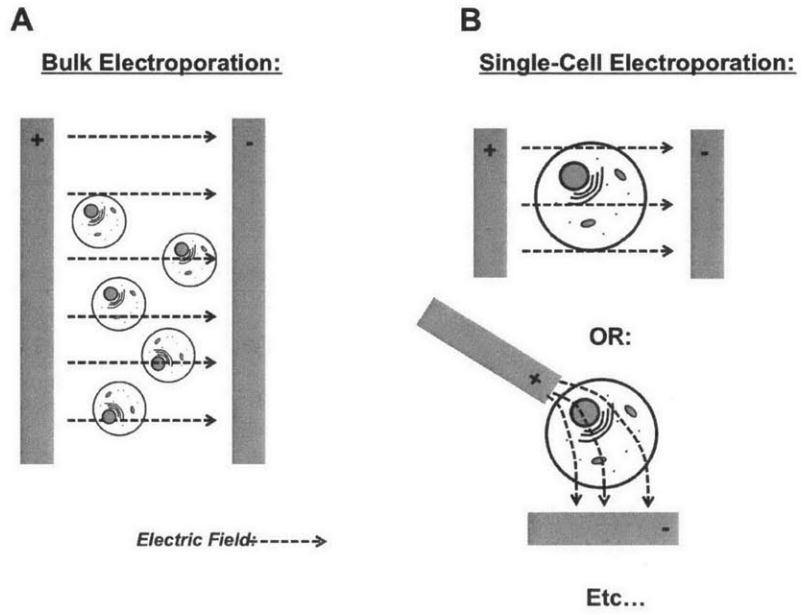

Figure 3.2: In bulk electroporation (A), a large quantity of cells are suspended in a ionic solution containing the reagent to be transfected (plasmid, dye, etc...) between two electrodes. A voltage is applied across the solution, often on the order of 100V. The voltage applied can be DC, sinusoidal, or some other waveform (of varying frequencies), with much research claiming improved yields for certain cell types with certain conditions. Following electroporation cells are replated and allowed to develop. In single-cell electroporation (B) sufficiently high electric field for poration is confined to the region of one cell. Many manifestations in design and approach have been used, including microfluidic chips as well utilization of a micropipette as a focussed electrode, which is the technique used in this thesis.

3.1.1 Limitations with Single-Cell

Being a technique that relies upon micropipettes, SCE falls prey to the general limitations with all micropipette-mediated methodologies as discussed in Chapters 1 and 2 of this thesis. While the spatial selectivity of SCE is superior in its ability to target arbitrary cells in a tissue environment, including wild-type tissue, its low-throughput limits its applicability in screening, circuit tracing, and other medium to higher-throughput applications. Using the platform and workflow developed in Chapter 2, we were able to overcome these limitations while maintaining the benefits of SCE in neural tissue [37].

3.2 Single-Cell Electroporation using Front-Loaded Micropipettes

Starting with the system described in Section 2.4 and Figure 2.2, and adding an electrical interface (See Section A.1) to the micropipette we front-loaded a plasmid encoding a fluorescent protein under a high-expression viral promoter (pEGFP-N1) and proceeded to electroporate individual neurons in in organotypic tissue. At 24 hours following electroporation (Fig. 3.3), the transformation efficiency as determined by EGFP expression was 79.1±8.7% with very high repeatability ($n = 72$ cells from six independent experiments), comparable to the best efficiencies reported in conventional SCE methods[54, 49]. It should be noted that in these experiments, no expression of fluorescent protein was observed in any of the cells that were not targeted for electroporation, including adjacent cells. Additionally, expression of plasmids in cells was consistently long-term, with sufficient expression in cells at 7 days post-transfection for both dendritic spine counting as well as neurite morphology analysis (Fig. B.3).

3.2.1 Repeated SCE of Multiple Vectors

We next investigated if micropipettes can be completely cleaned of reagents, and subsequently reloaded without any cross-contamination, therefore allowing the transfection of multiple reagents. As mentioned in Chapter 2, during standard use, micropipettes frequently clog with debris, an issue which can be monitored by visual analysis of dye outflow at the tip and by measurement of the electrical conductivity of the tip. The major contributing factors to clogging are debris arising from the cell-to-micropipette contact and the precipitation of

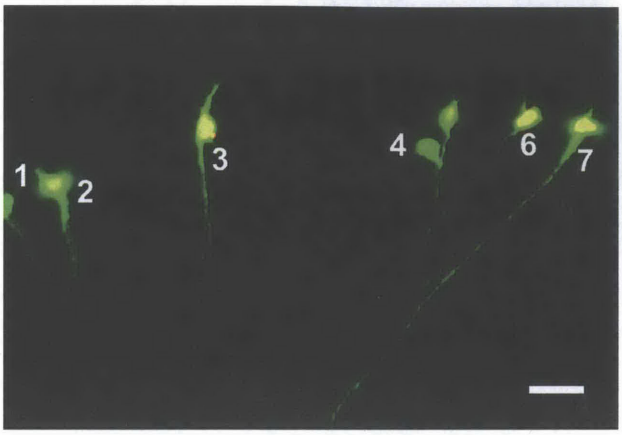

Figure 3.3: A micropipette was front-loaded with pEGFP-N1 by applying a negative pressure to for 20 seconds. The concentration of plasmid in the tip of the micropipette remained stable enough to reliably transfect multiple cells with pEGFP-N1. 79.1±8.7% of the transfected cells expressed EGFP 24 hours following transfection (n = 72 from six independent experiments, where 12 cells were transfected within 2 minutes in each experiment). Scale bar 50 μm.

plasmids at the tip, both of which greatly inhibit the ability of a micropipette to be flushed beyond several sample-rinse cycles. In the case of plasmid transfection, we utilized the sodium hypochlorite-based cleaning a robust method for cleaning the tip by immersing the tip of the micropipette into a well containing a continually-perfused (1.5 mL·min-1) solution of 0.25% sodium hypochlorite solution and by applying 20 seconds of alternating +30 psi and -30 psi gauge pressure pulses with a 2:1 positive/negative duration ratio. The resulting net positive flow out of the tip ensured that sodium hypochlorite was not left in the conductive saline bridge of the micropipette. Immediately following the cleaning step, the micropipette was withdrawn and the tip inserted into a well containing a continuous perfusion of deionized water (1.5 mL·min^{-1}). +30 psi was then applied to the micropipette for five seconds to further ensure remaining sodium hypochlorite was removed. Using this technique, the micropipette could be successfully cleaned and reloaded 92 ± 3.2% of the time ($n = 100$, based on 25 sequential load-clean-rinse cycles from four independent experiments).

To characterize how capable our cleaning methodology was at minimizing cross-sampling (from residues of previous loadings), we next performed a sequential four-part transfection experiment on cells of the CA3 pyramidal cell layer (PCL) which consisted of pCAG-EGFP, then vehicle, then pCAG-dsRed,

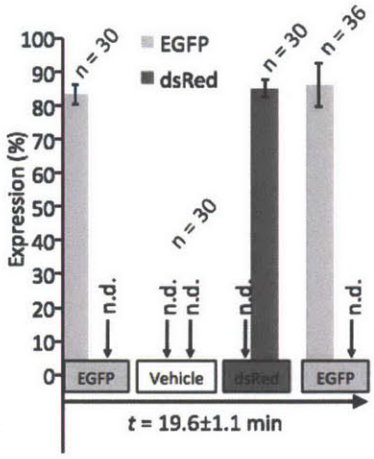

Figure 3.4: Sequential transfections were carried out on groups of single cells using the same micropipette, in which pCAG-EGFP was transfected first (efficiency: 83.3±2.9%*), followed by a reagent containing only the fluorescent vehicle solution (plasmid contamination: 0%), then pCAG-dsRed (efficiency: 85±2.9%) plasmid cross-contamination: 0%), and finally pCAG-EGFP again (efficiency: 86.1±6.4%, plasmid cross-contamination: 0%). The entire sequence took 19.6±1.1 minutes.
(n.d. = not detected) Results are mean ± s.d. of three independent experiments in which 129 total cells were transfected. *Efficiency assayed as EGFP expression at 24 hours post transfection.

and then pCAG-EGFP (Figure 3.4). At 36 hours post-transfection, cells were analyzed for fluorescent expression. We observed 86.1±6.4% overall efficiency (n = 99 cells) with 100% sample specificity (0% cross contamination). Even when all system operations (including loading, targeting, electroporating, washing) are taken into account, it takes only 27.3±1.5 seconds per cell (n=129 cells) (Fig. 3a).

3.2.2 System Throughput

While the user selects the cells to be targeted and transfect, a single high-level control allows triggering of the system to withdraw, clean, rinse, reload, and finally reposition the micropipette. Long-travel servos move the entire micromanipulator at 100 mm/s between the slice bath and the tip cleaning/reagents, which minimize chances for clogging due to exposure to air. A computer-controlled bank of valves as well as pressure and vacuum regulators then precisely rinse, clean, and load the micropipette. Each full transfection cycle (including cleaning and loading) takes only 88.9 ± 8.6 seconds (Fig. 3.5), ($n = 100$

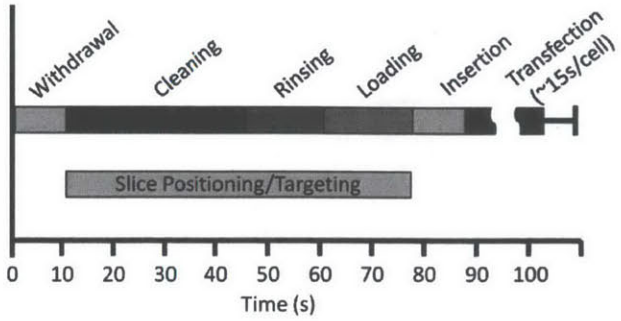

Figure 3.5: Shown is the average time of different steps in a full transfection cycle. Withdrawal, cleaning, rinsing, loading, and insertion to slice bath of the micropipette take 88.9±8.6 seconds (from four independent experiments, n = 25 per experiment). Transfection/dye uptake of single cells takes on average 14.8±6.2 seconds per cell (n = 56 from five separate experiments).

from four independent experiments of 25 transfection cycles each). The targeting and transfecting of individual CA1 and CA3 pyramidal cells generally requires on average 14.8±6.2 seconds per cell ($n = 56$).

3.2.3 Software

Software for implementing SCE using the automation system was contained within a large GUI shown in Figure 3.6 with a detailed version in Figure A.1. A dual-monitor setup allowed simultaneous viewing of the microscope view using the attached video camera. In addition to the core system operations including, long-travel stage, micromanipulator, vale, and pressure regulator controls, the system also allowed variable inputs for SCE parameters (discussed in detail in Section B.6) as well as real-time electrical measurements which could be used for tip clogging and other variables.

3.2.4 Long-Term Operation

We found that commonly used Ag/AgCl wire electrodes are not compatible for long durations of operation because the repeated hyperpolarizing pulses eventually release Ag+ ions into solution even after the wire had been properly chloridized, resulting in variation in electrical conductivity. The presence of Ag+ ions in solution is also potentially toxic to cells. Critically, the Ag+ ions in solution also react with sodium hypochlorite during the washing step to form AgCl in the proximity of the micropipette tip, which precipitates leading to the

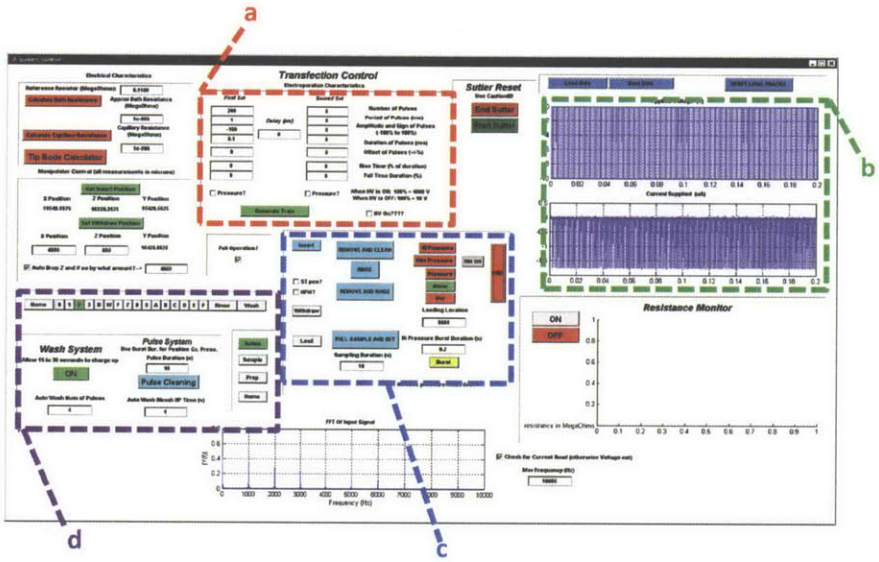

Figure 3.6: All major controls are contained within a single window. (a) Single-cell electroporation parameters, (b) Applied SCE voltage signal (top) and measured SCE current (bottom). (c) Micropipette pressure controls, high-level controls for automated system operation, and micropipette manipulator controls. (d) Micropipette position control, micropipette clean/wash parameters, and multiwell and washing equipment position controls. A detailed view of several panels is provided in Figure A.1

clogging of the tip. To avoid these shortcomings, we used an electrode holder containing a 30 American Wire Gauge (AWG) platinum wire that does not degrade. We found that electrical resistance (measured with a hyperpolarizing 5V DC voltage) to vary by only about 3% per hour of usage (n = 10 micropipettes from 10 independent experiments).

With all of these developments, we were able to continuously recycle and use a single micropipette for over six hours. Only the amount of solution initially backfilled into the micropipette limited this operation duration because each transfection cycle results in a net loss of saline in the micropipette. A micropipette loaded with 6μL of solution was capable of providing three hours or more of operation, and when initially filled with 12 μL, six hours of continuous usage was possible.

3.3 Multicolor Combinatorial Labeling of Single Cells

SCE of plasmids was capable of generating very high expression of fluorescent proteins in target cells. The ability to uniquely label individual cells permits tracking and analysis of multiple cells within complex brain tissues. The "brainbow" technique[26] is a pioneering method to achieve multicolor single-cell labeling, however the need to engineer transgenic animals, and the density and the stochasticity of labeling limits its wide-range use. The capability to rapidly and deterministically label single cells with multiple combinations of colors and without using transgenic animals provides significant flexibility. Using our system, we were able to transfect multiple adjacent pyramidal neurons within minutes of one another (Fig 3.7a) with different fluorescent reporter plasmids (Section B.3). We were also able to easily differentiate the dendritic processes of multiple neurons (Fig 3.7b) as well as dendrites and axons (Fig 3.8).

Testing effects of multiple genetic perturbations in tissues while simultaneously labeling cells with fluorescent reporters for tracking, traditionally requires the development and use of specialized vectors expressing multiple proteins. However, because SCE can transfect mixtures of multiple plasmids, we proposed that mixing plasmids encoding genes of interest along with known fluorophore-encoding plasmids would allow for a means of rapidly analyzing effects of these genes. In addition, this same methodology could allow co-transfection with multiple fluorescent reporters enabling the labeling and differentiation of greater

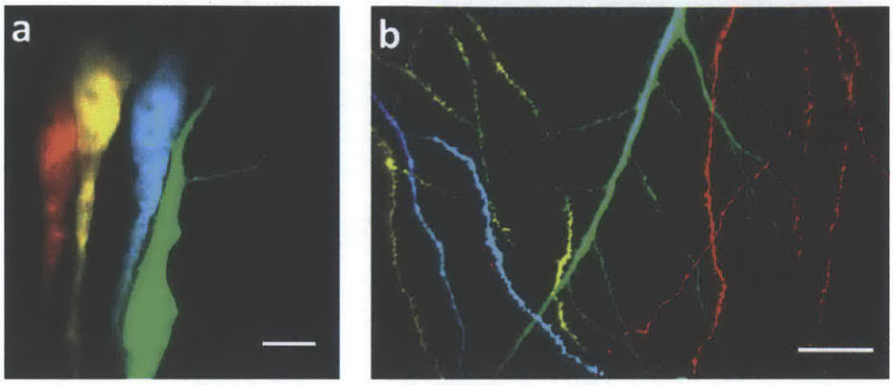

Figure 3.7: Multiple fluorophore-encoding plasmids (pCI-tdTomato, pCAG-YFP, pCAG-Cerulean, and pCAG-EGFP) are transfected into neighboring cells in the same slice. (b) Overlapping processes can be easily distinguished.

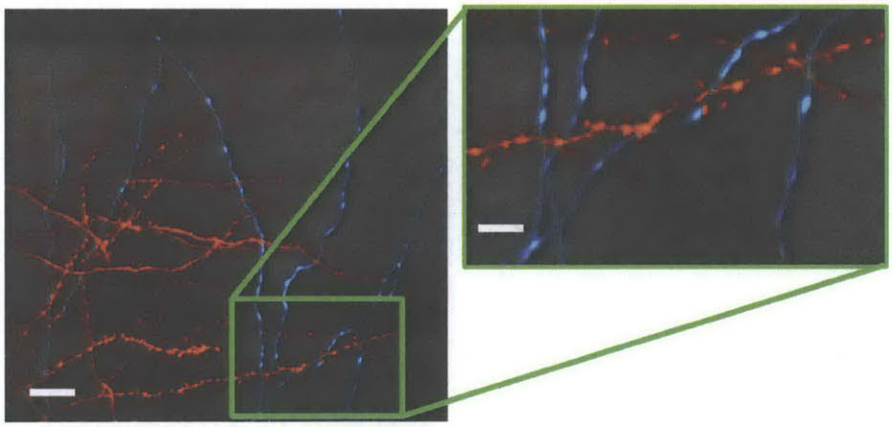

Figure 3.8: Neurons expressing different fluorphores can be readily discerned form one another using confocal microscopy. Here an axon from a nearby cell transfected with pCAG-Cerulean (cyan) innervates with the dendrites of a cell transfected with pCI-tdTomato (orange). Note the axonal boutons and dendritic spines are clearly visible in the inset. Scale bar 20 μm in main figure, 5 μm in inset.

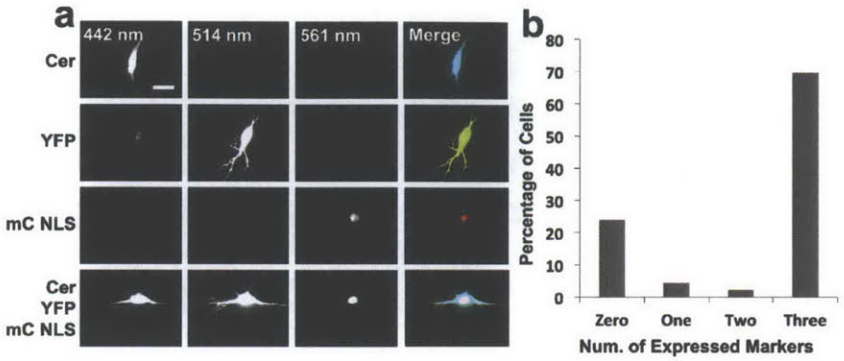

Figure 3.9: (a) pCAG-Cerulean, pCAG-YFP, and mCherry-Lac-Rep express three spectrally distinguishable fluorescent markers: cytosolic 442/470 nm (ex/em), cytosolic 514/530 nm (ex/em), and nuclearly-localized 561/610 (ex/em), respectively, as shown in the top three rows. They were used to determine co-transfection efficiencies of multiple plasmids, as shown in the bottom row. (b) A mixture containing 300 ng·μL^{-1} of both pCAG plasmids and 347 ng·μL^{-1} of mCherry-Lac-Rep was transfected using our front-loaded SCE methodology into CA1 and CA3 pyramidal cells in organotypic hippocampal slices and imaged 24 hours later for expression patterns. 92 cells total were transfected, with 23.9% expressing no visible fluorescence signal, 4.3% expressing only one type of fluorescent protein, 2.2% expressing only two types of fluorescent proteins, and 69.5% expressing all three types of fluorescent proteins. Scale bar in panel a is 10 μm, and in b and c is 20 μm.

numbers of densely packed cells in a given brain slice. To ensure co-transfection could reliably be performed using our modified SCE techniques, we transfected cells with a sample comprised of 1:1:1 molar ratios of three plasmids: pCAG-Cerulean, pCAG-EYFP, and mCherry-Lac-Rep (nuclearly-localized mCherry), at concentrations of 300 ng·μL^{-1}, ng·μL^{-1}, and 347 ng·μL^{-1}, respectively, as well as 50 μM Alexa Fluor 594 in Ringers solution (Fig. 3.9a). 92 CA3 pyramidal cells were electroporated in eight different organotypic slices with this three-plasmid mixture. 24 hours following transfections, fluorescence was observed in 70 of the electroporated cells. Of these 70 cells, 64 (91%) expressed all three fluorescent signals, while 2 cells (2.8%) expressed only two at significant levels, and 4 cells (5.6%) expressed only one fluorescent maker, indicating a very high triple-transfection rate for multiple plasmids (Fig. 3.9b).

3.3.1 Combinatorial Genetic Modification of Single Cells within Brain Slices

The ability to rapidly genetically modify single cells can allow parallel analysis of many genetic modifications in a single brain slice. The protein Kalirin is a Rho guanine nucleotide exchange factor (RhoGEF) which exists as a number of alternatively spliced isoforms in the mammalian brain[93], and its functions have been investigated in a series of elegant papers[94, 95, 96, 97, 98, 99, 100, 101]. The exogenous expression of several Kalirin variants, notably Kalirin-7, has been shown to significantly modify dendritic spine morphology in cultured cortical neurons[102] as well as hippocampal interneurons[95]. We selected three plasmids encoding Kalirin-5, Kalirin-7, and Kalirin-9 with a myc-tag (see Methods) for use in a combinatorial fluorophore plasmid test on linear dendritic spine density in cells of the CA3 PCL.

To check whether the labeling with different fluorophores introduce bias in the observed linear spine density, we transfected a total of 120 cells in the CA1 and CA3 PCLs with the four different fluorophore-encoding plasmids to be used. Linear spine densities of the basal dendritic arbors of the cells were counted for each population of cells at 24 hours post-transfection (n = 120 cells total) (Fig. B.4). No statistical difference in spine density among the populations of cells transfected with the fluorophores Cerulean, EGFP, YFP, and tdTomato was observed. (Fcrit = 2.63, F = 0.29 and 0.62 for CA1 and CA3, respectively).

To verify successful expression of the Kalirin isoforms, each plasmid was co-transfected along with pCAG-Cerulean into CA3 pyramidal cells in organotypic slices. 24 hours following transfections, slices were fixed, stained, and imaged for myc-tag and Cerulean expression (Fig. 3.10a). Differences in cell staining patterns were readily apparent, with the cells transfected with Kalirin-5 and Kalirin-9 exhibiting myc staining in the cytosol, while cells transfected with Kalirin-7 exhibiting localized myc-labeling in the dendrites (Fig. 3.10b), in agreement with the evidence for Kalirin-7 localization to the post-synaptic densities due to its Sec14p/spectrin-like repeat region unique amongst the Kalirin isoforms[99]. Co-transfection rates, determined by co-localized Cerulean fluorescence and anti-myc staining, were 88.2±2.2% (n = 24), 77.1±11.1% (n = 21), and 71.9±5.5% (n = 20) for Kalirin-5, Kalirin-7, and Kalirin-9, respectively. (Fig. 3.10c).

We next transfected individual cells in the CA3 PCL with one of four different plasmid mixtures: tdTomato (control), Cerulean/Kalirin-5, EGFP/Kalirin-

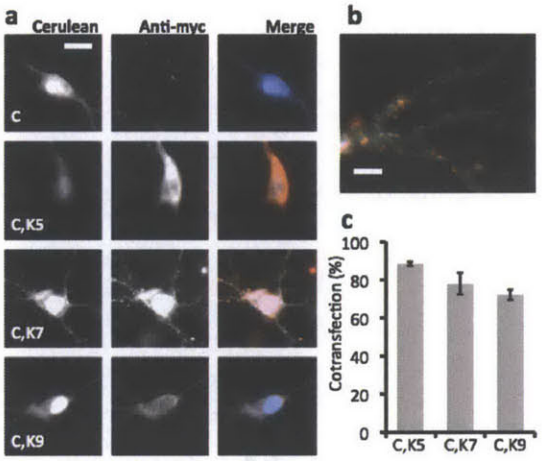

Figure 3.10: (a) Plasmids encoding the three isoforms of Kalirin (Kalirin-5, Kalirin-7, and Kalirin-9) were each co-transfected with pCAG-Cerulean by our system into CA3 pyramidal cells in hippocampal slices. 24 hours following transfection, slices were fixed and stained for the myc tag from the Kalirin isoforms before imaging for Cerulean (cyan) and myc (orange). Scale bar 15μm. (b)Anti-myc staining in Kalirin-7-transfected cells shows localization into fine points on the dendrites. Scale bar 5μm. (c) Co-transformation efficiencies determined by co-staining for pCAG-Cerulean and the three pEAK-His-Myc-Kalirin vectors, were 88.2±2.2% (n = 24), 77.1±11.1% (n = 21), and 71.9±5.5% (n = 20) for Kalirin-5, Kalirin-7, and Kalirin-9, respectively.

7, and YFP/Kalirin-9. Linear spine densities of the basal dendrites were analyzed 24 hours post transfection (Fig. a). Because each isoform was co-transfected with a known and unique fluorophore, we could readily distinguish and analyze cells that had been transfected with different Kalirin-isoform-encoding plasmids in the same tissue slice even for neighboring cells with significantly overlapping processes. When compared to the control cells with an average of 6.7±1.0 spines/10μm ($n = 95$ segments from 19 cells), no statistical difference in linear spine density was observed in Kalirin-5-transfected cells (6.65±2.0 spines/10μm, $n = 60$ segments from 12 cells, $p = 0.74$), as well as Kalirin-9-transfected cells (7.6±0.6 spines/10μm $n = 55$ segments from 11 cells, $p = 0.08$). However, a statistically significant difference in linear spine density was measured in Kalirin-7-transfected cells (8.6±0.9 spines/10μm, $n = 70$ segments from 15 cells, $p < 10^{-4}$) (Fig. b). Our results are in agreement with the previous studies on the effects of Kalirin isoforms[94, 95, 102, 97, 96, 98, 99, 100, 101], which suggest that our methodology based on co-transfection of multiple plasmids provide statistically significant results in a high-throughput, single-cell manner.

Acute hippocampal slices were also tested, in order to assess the systems operational characteristics in a tissue environment more closely resembling in vivo conditions (Figure B.5). Because plasmid expression in acute slices cannot be compared directly to expression in organotypic slices due to the limited lifetime of acute slices (several hours), we compared the cell targeting and electroporation efficiency of our system between acute and organotypic slice cultures, which we define as the percentage of cells intentionally and successfully electroporated and filled with fluorescent dyes (determined visually by dye uptake). No significant difference was found between the two tissue cultures: In acute slices, the targeting efficiency was 95.3±4.2% ($n = 62$ in five separate experiments) while in organotypic slices it was 96.0±5.4% ($n = 56$ in five separate experiments). No off-target electroporation, which we define as the electroporation of unintended adjacent cells, was observed in either case. The higher density of cells in acute slices made the average cell-targeting time longer however: In acute slices, it took 26.5±8.9 seconds per cell, ($n = 62$ cells in five separate experiments) while it took 14.8±6.2 seconds per cell in organotypic slices ($n = 56$ cells from five separate experiments) to achieve the level of electroporation efficiency reported above. This significant difference in timing ($p < 10^{-5}$) was primarily due to the extra time needed in targeting cells with less-clearly defined somatic boundaries in acute slices, as well as the slower movement of the micropipette in acute

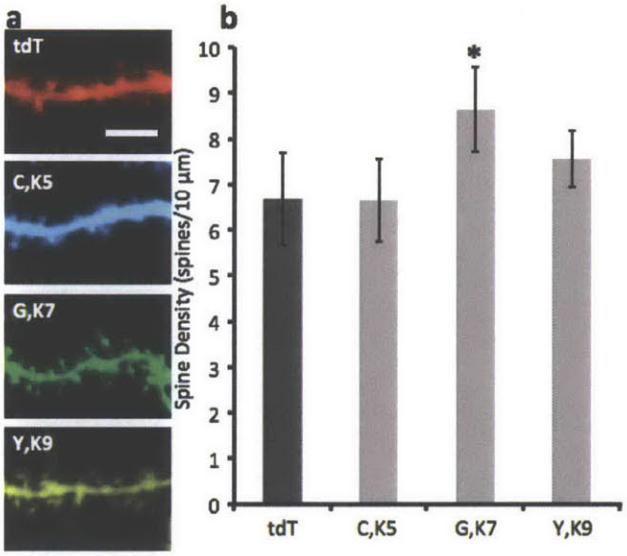

Figure 3.11: (a) A series of transfection cycles were carried out on CA3 pyramidal cells in the same slice (8 total slices) to analyze the effects of exogenous expression of the three Kalirin isoforms on linear dendritic spine density of basal dendrites. Cells were transfected with either tdTomato (tdT) as a control, Cerulean and Kalirin-5 (C,K5), EGFP and Kalirin-7 (G, K7), or YFP and Kalirin-9 (Y, K9). Spines were imaged 24 hours post-transfection. Scale bar is 10µm. (b) Linear spine densities for four groups: tdT cells had an average of 6.7±1.0 spines/10µm (n = 95 segments from 19 cells). C,K5 exhibited no statistically higher spine density (6.65±2.0 spines/10µm, n = 60 segments from 11 cells, $p = 0.74$) and so Y,K9 (7.6±0.6 spines/10µm n = 55 segments from 9 cells, p = 0.08). G,K7, however, did show a statistically higher linear spine density (*) compared to tdT (8.6±0.9 spines/10µfm, n = 75 segments from 15 cells, $p < 10^4$).

slices. These results were expected, based on the often-observed flattening and thinning of organotypic slices when compared to acute slice environments[103].

3.4 Discussion

We demonstrated a novel automated system that greatly improves the throughput of single-cell transfection in tissue environments. Our system can be readily applied to both organotypic and acute slice formats (Fig. B.5), the two primary tissue culture methodologies. A wealth of research exists in using brain slice platforms, and particularly organotypic cultures, in modeling many human diseases including Alzheimer's, Parkinson's, and epilepsy, all of which could benefit from the increased throughput in single-cell manipulation and analysis[104, 105]. In addition to plasmids encoding cDNA, shRNA-encoding plasmids can also be transfected as well as both long coding RNA and siRNA using SCE [52, 106]. Optogenetic proteins could also be transfected with single-cell resolution [107, 108]. The throughput of our technology also makes possible the use of brain slices in high-content, single-cell resolution screens. For instance, large libraries of cDNA or RNAi encoding vectors could be rapidly tested for their effects on neurite and synaptic morphogenesis in brain tissue. Fast-acting reagents such as multiplexed fluorophores, calcium-sensing, and voltage-sensing dyes can also easily be transfected via SCE into both acute and organotypic slices using our system providing a means of real time connectivity and circuit analysis at cellular resolution[109]. Additionally, we can also sequentially transfect reagents into the same cells, enabling pre-and-post transfection analysis[110] (Fig. B.6). Furthermore, it is also feasible that our system can be used in conjunction with single-cell electrophysiology techniques using conventional micropipettes and labeling as shown by Rancz et al. or with novel nanoprobe electrical recording techniques demonstrated by Qing et al. [111, 112]. It is not beyond possibility that the micropipettes in this demonstration could also be replaced with microfluidic chips designed for electroporation, which could potentially provide more flexibility and an avenue through which to integrate additional features [113].

Cell-type-specific transfections could be carried out by using either (a) tissues from transgenic animals that express fluorescent reporters driven by cell-specific promoters, or (b) wild-type tissues labeled with fluorescent reporters (driven by cell-specific promoters) delivered using bulk transfection through viral or biolis-

tic techniques. Once the subpopulations of cells are labeled with fluorescent reporters, their identification, targeting, and transfection with reagents is readily possible with our platform. Additionally, since larger plasmids (up to 13 kbp were transfected in this paper) can be introduced using SCE, cell-type specific promoters can be incorporated into transfected vectors in order to add a further level of specificity to our system.

Chapter 4

Automation of Single-Cell Sampling

After having developed a means of transfecting single-cells in tissue with medium- to high-throughputs, we asked if we could extend the system functionality to collecting the contents of single cells with high spatial and temporal resolution[1]. At its most basic level, the idea for the second portion of this project was to reverse the workflow of transfection from Chapter 3, where instead of going: microplate → cell → clean → repeat, we would operate as: cell → microplate → clean → repeat. as shown in Figure 4.1.

Researchers previously demonstrated the successful collection of cellular contents for downstream molecular analysis using micropipettes as far back as 1992[74, 75]. Subsequent years have allowed a firm foundation for the technique to be established[79, 114, 115, 116]. As was the case when initially adapting single-cell electroporation in Chapter 3, however, we discovered that all previous published uses of micropipettes collecting single-cell contents were "single-use" meaning one micropipette corresponded to one micropipette. In fact, in almost all protocols we surveyed in the literature that used micropipettes for single-cell harvesting, the micropipette was actually broken off in the final receptacle in order to ensure successful release of harvested material [79, 114, 115, 117]. Such an approach obviously precludes reuse, and so our initial work focussed on investigating if a micropipette could collect material from a cell and subsequently

[1]Work in this chapter carried out in collaboration with Dr. Alexei Finski. The initial development of the single-cell lysing technique was carried out by Dr. Finski during his doctoral research at Harvard Medical School.

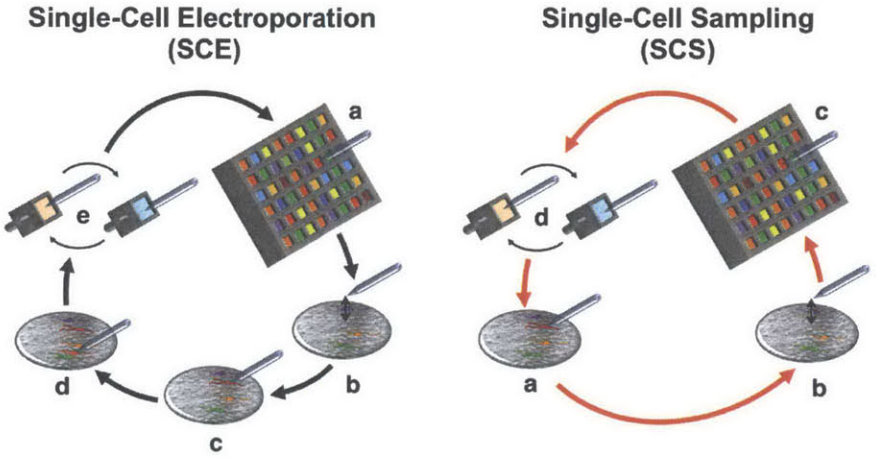

Figure 4.1: In Single-Cell Electroporation (SCE) Mode a micropipette collects a small volume of the vector to be transfected (a), and rapidly electroporates it into targeted cells in tissue environments (b through d), before being cleaned and rinsed and made ready for reuse (e). In Single-Cell Sampling (SCS) Mode a micropipette collects the molecular content from a targeted cell (a, b) before rapidly depositing it into a well for later analysis (c), and finally being cleaned and rinsed for reuse(d). While modifications and additions were needed, this approach ultimately proved successful and will be the basis of the current chapter

deposit it in such a way so as to enable its reuse and for the accurate analysis of deposited material [118, 119].

We had already discovered that glass micropipettes can be cyclically exposed to tissue, cleaning, and rigorous washing environments for hours and many cycles with little to no damage to the tip (analyzed both using optical analysis of mechanical parameters and electrical parameters including resistance and time constant). From prior SCE work (Chapter 3), it was well known that exposure of the tip to a bleaching solution followed by a rigorous rinsing procedure permitted low carry-over/cross-contamination between different pools of nucleic acid for transfection as well. It was therefore hypothesized that similar procedures could be used to ensure separation of biomolecular signals collected from multiple cells harvested with the same micropipette. From an automation and control standpoint and based on our previous work with repeatable SCE, no major issues prevented the reuse of a micropipette for single-cell sampling if two conditions could be met:

- The material collected from a single cell in a micropipette could be reliably deposited into a sufficiently small volume to permit proper analysis. The smallest volume wells we reliably sampled from in the case of automated SCE were 0.2 mL PCR-stripe style microtubes filled with approximately 50 to 100 µL of sample, a volume far too large for reliable measurements of low-copy number RNA transcripts. As a result, a means of depositing into smaller volumes without damaging the micropipette tip needed to be developed.

- The micropipette could could collect cell contents in such a way that did not inhibit further usage. In particular, it needed to be determined if the collection of biomaterials from single cells into the tight confines of a glass micropipette was predisposed to clogging the micropipette to such an extent as to prevent release from a micropipette, or if the same or a derivative cleaning procedure developed for SCE could be deployed to enable reuse.

The investigation of both of these questions is detailed in the sections below.

4.1 Sample Deposition

When handling single-cell level quantities of material for analysis, dilution must be kept to a minimum to avoid signal loss[120]. A sphere-shaped cell with radius 5 μm, will have a total volume of less than 1 pL. For the work in this thesis, we chose to focus on mRNA transcript analysis, and in most procedures analyzing single cell transcripts, the total diluted volume of a single cell's contents is kept at or below about 5 μL in order to ensure successful readout of most transcripts. As a result, deposition into larger 200 μL "PCR" style tubes of the type used for sampling dyes, RNA, and DNA in the SCE work of the prior chapter was therefore not an option.

Two solutions were proposed and investigated to overcome this issue. The first relied upon deposition of the cellular sample into large volume of low-viscosity silicone oil. Initial experiments showed that the sampled cellular volume, being aqueous in nature, would remain together when deposited into an oil environment. Following deposition, a combination of spinning down and harvesting with larger aqueous droplets then allowed the sample to be collected with little dilution. A major benefit, and the original motivation for using oil was that it required no improvement in the alignment and calibration procedure as developed for SCE (Section 2.5.1). In addition, the volume of deposited samples could be maintained at levels on the order of one nanoliter, providing a pathway for possible microfluidic integration. We encountered significant compatibility issues with the lysis buffer reagents (see Section 4.2) and the oil, however, which resulted in unpredictable depositions from the tip. In addition because of the general novelty of the technique, significant chemical verifications would be needed in order to verify its acceptability for downstream analysis, and while still a valid long-term solution for low-dilution collection, we chose to instead shift to a second deposition workflow that differed less than current standard methods in the field.

While the benefits of oil deposition were obvious, we instead decided to focus on an alternative solution to deposition by redesigning the automation control and calibration procedures to enable the targeting of individual wells of a 384 well plate containing approximately 5 μL of aqueous recovery solution. To verify the ability to deposit nucleic acids, a glass micropipette with dimension similar to one used for SCE was loaded with PBS containing YFP-encoding mRNA at a concentration of 2 ng/μL. The micropipette was then moved between wells of a 384 well plate and deposited varying amounts of its contents

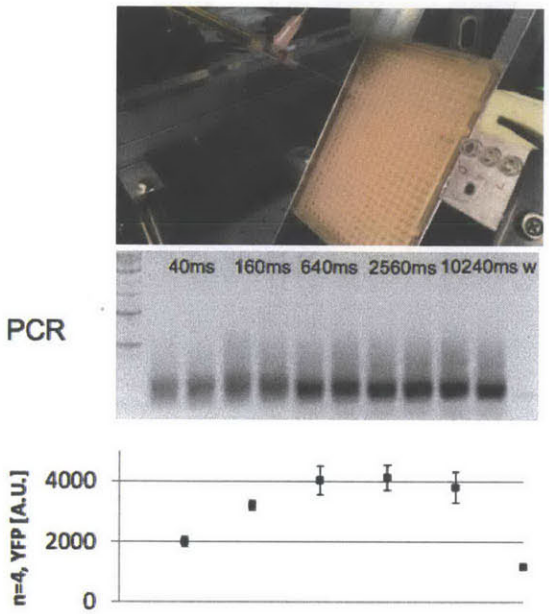

Figure 4.2: An angled standard 384 well plate containing approximatley 5 μL of water with RNAse inhibitors was used for targeted deposition by a glass micropipette loaded with PBS and 2 ng/μL of YFP RNA. Varying deposition periods were applied across multiple wells and the readout was analyzed using standard RT-PCR reactions described in the Appendix.

into the wells. The material in each well was analyzed via standard RT-PCR reactions(SectionB.8.2) as shown in Figure 4.2. A clear correlation between deposition duration and the quantity measured is apparent.

4.2 Sample Collection from Single Cells

The collection of cellular material from individual neurons was originally shown in a series of papers in 1992 [74, 75]. This initial work relied upon achieving the low-leakage conductance seal required for effective patch clamp. The cytoplasm of a cell is a gelatinous material, that is not easily aspirated with a micropipette [80]. When collected into a pipette tip, it is very difficult to free it from the glass. This is, at least in part, one of the reasons why when carrying out a patch-clamp style harvest of cell material, the tip is broken off in the final receptacle [78, 79, 80]. Destruction of the tip obviously prohibits reuse

of the micropipette for additional samplings, and therefore this cell harvesting approach was incompatible with the goals of our research. Early attempts on our part to collect cellular material using direct aspiration into micropipettes followed by deposition into low volume wells were largely unsuccessful, in large part because the sampled material became lodged in the micropipette tip.

Much of the gelatinous nature of the cytoplasm, and its propensity for clogging micropipettes, arises from the cytoskeleton, a complex network of structural proteins that can be subdivided into three main groups: microfilaments, intermediate filaments, and microtubules[121]. All of these classes of cytoskeletal elements are comprised of protein subunits. In the case of microfilaments, the subunits are actin, a 42 kDa protein. In the case of intermediate filaments, the subunits are a large class of proteins featuring a central alpha-helical rod domain, and include subtypes such as keratin and laminin [122]. In the case of microtubules, the subunits are the alpha and beta-tubulin protein subtypes[121]. In all cases, the mechanical structure of the cytoskeletal material can be compromised when exposed to denaturing agents such as anionic detergents. Based off of previously described work, we investigated whether the introduction of a protein-denaturing detergent could be introduced into the interior of a cell in order to neutralize the internal structures that were inhibiting successful uptake and then deposition into the micropipette[123].

4.2.1 SDS Injection

Injection of high concentrations of anionic detergents into cells in the context of tissue environments was recently conceived and developed several years ago at Harvard Medical School[123][2] In their original work, a micropipette filled with a high concentration of lysis buffer, generally a high percentage of anionic detergent sodium dodecyl sulfate (SDS), is directed towards a single cell in a tissue environment. Lysis buffer is subsequently applied to the cell from the micropipette. The stream of high concentration SDS released from the micropipette is of sufficient strength to disrupt the phospholipid membrane of the cell enabling more of the stream to enter the cell. The high concentration of SDS buffer rapidly denatures proteins inside of the cell. The lysed material

[2]for details concerning the original development of this SDS-injection approach please see Alexei Finski's doctoral thesis[123]. This initial work is also contained with several pending patents for Dr. Finski et al. Its adaptation to an automated system, enabling cyclic reuse of single capillaries to enable rapid single-cell selectivity of multiple cells, and its development for use in deeper tissue environments as well as associated analytic techniques for nucleic acid analysis is the topic of this thesis chapter.

is then able to be collected and analyzed. In the original work, protein content was analyzed, but for our work we wanted to utilize it for RNA collection and downstream analysis. The unique ability of this previously established single-cell lysis technique to collect cell material made it ideal for integration into a cyclic system for single-cell collection, and a collaboration between the two research teams was established.

4.3 Micropipette Tip Geometry Considerations

The geometries of micropipettes including tip opening and taper were swept in order to find ideal parameter sets for both the role of lysing and collection/uptake of cellular material. In the case of targeted lysing, too large of an opening resulted in off-target introduction of SDS to other cells both adjacent to the target cell as well as while the tip moved through the tissue. Too small of a tip opening in the lysing micropipette resulted in persistent clogging of the micropipette tip. An ideal value of several 100 nm tip diameter was optimum (approximately 0.25 μm). For the role of the uptake of cellular content both too large and too small of a micropipette tip resulted in persistent clogging before, during, and after content collection[3]. A tip opening diameter close to 2 μm was found to be optimal for collection in tissue environments[4]. A conclusion of this trend is shown in Figure 4.3. Little to no overlap in the functional geometries for both roles could be found. While we had originally desired to conduct both lysing and collection using a single micropipette, due to the large difference in optimum parameters we decided to utilize separate two micropipettes at their individual optimal dimensions as shown in Figures 4.3 and 4.4.

4.4 Cell Sampling

Having settled upon using a a pair of micropipettes for the system, we developed the workflow shown in Figure 4.4. Essentially an expanded derivative workflow of what was used for SCE, the workflow required the separate, simultaneous control of the two micropipettes to improve throughput, allowing them to carry out separate tasks simultaneously, all under computer control. A streamlined

[3]Larger capillaries on the order of 5μm are also very difficult to reliably obtain using a filament micropipette puller such as a Sutter P-97 or P-1000

[4]It should be noted that this parameter is very similar to that found in many patch micropipettes as well as the value we used in the SCE work of Chapter 3.

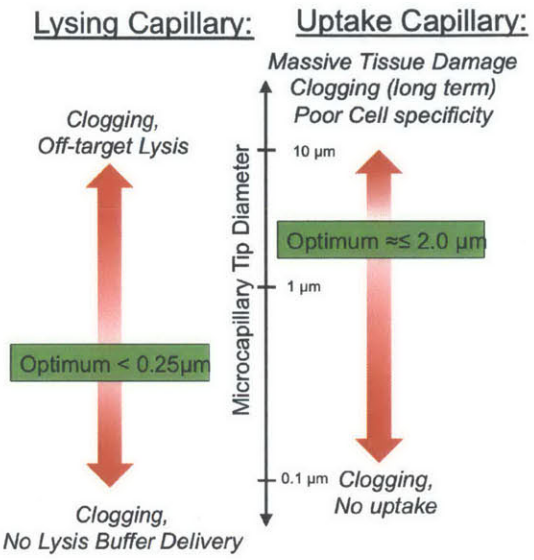

Figure 4.3: Inside of a tissue environment, the optimal geometric paratmeters for micropipettes performing lysing and collection of cellular content were found to differ significantly from what had been found previously[123]. In addition little overlap existed between the optimal parameters for each role necessitating the utilization of two micropipettes.

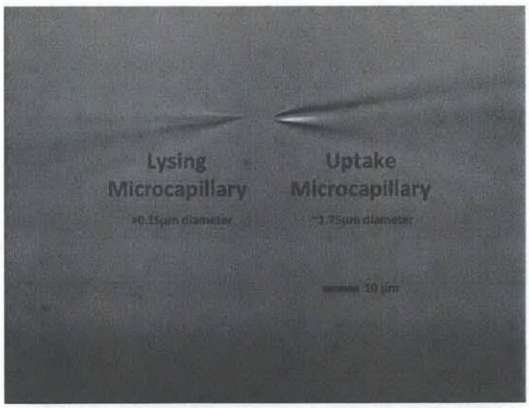

Figure 4.4: The dual micropipette setup was settled on, with two distinctively different micropipette geometries since it provided the fewest compromises in terms of system operation, however it did require a more complicated automation system (see Figures 4.5 and A.7.

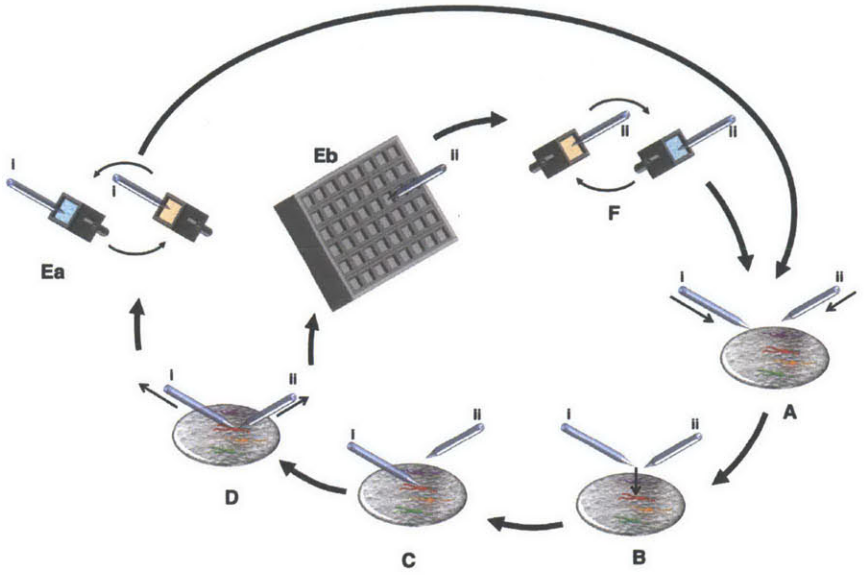

Figure 4.5: Two micropipettes, one a lysing micropipette (i) and one a collection micropipette (ii) approach the target cell in the tissue environment (A,B,C). With both micropipettes in place, lysing buffer is applied to the cell while negative pressue is applied to the collection micropipette. Once collection is complete (<30 seconds), the lysing micropipette is immediatley cleaned and rinsed (Ea), while the collection micropipette is rapidly moved to deposit its sample into a small aqueous volume in a 384 well plate (Eb). Following depostion, the collection micropipette is itself cleaned and rinsed before being ready along with the lysing micropipette for another sampling cycle.

software control was developed based off of the original underlying SCE automation control package, however because fewer parameters needed to be optimized, the control panels could be greatly simplified (Figure 4.6).

Actual sampling and recovery of the cellular material was handled in real time by the researcher in a similar manner to the semi-automated SCE of Chapter 3. A standard operation cycling involved targeting a cell, introducing lysis reagent, monitoring the uptake into the collection micropipette via fluorescence of a dye (included in the lysis buffer to aid in visualization), and releasing the micropipettes to computer control for deposition, cleaning, rinsing, and repositioning. Details are shown in Figure 4.7.

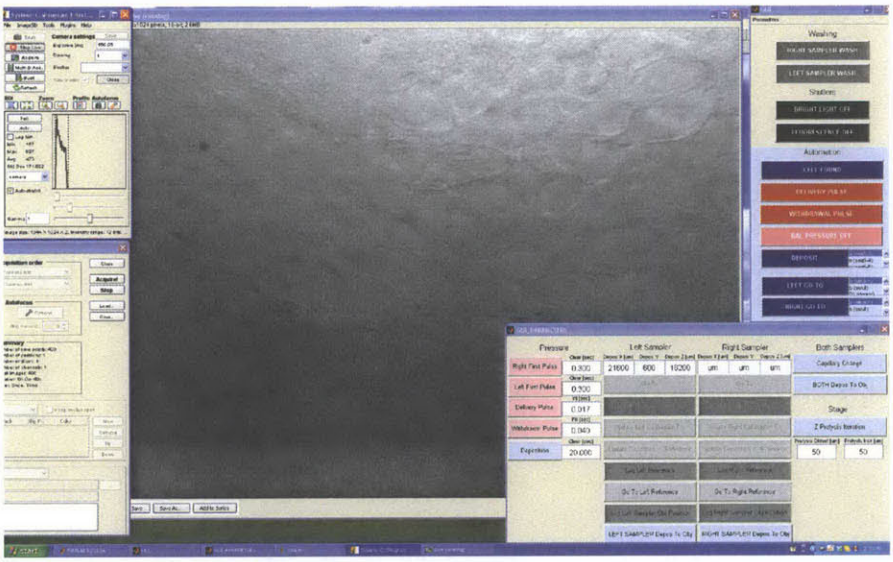

Figure 4.6: SCS control software differed significantly from the versions used for SCE (Chapter 3, Figure 3.6), partially because fewer parameters needed to be varied and partially because of different hardware (new camera). By this point in the automation development, less flexibility was needed to experiment with manual positioning of long-travel stages so options for these were removed as well.

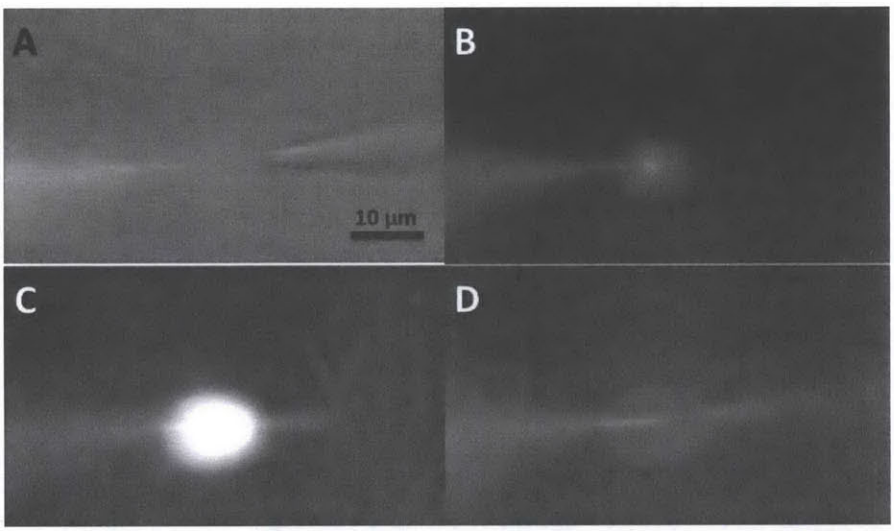

Figure 4.7: A: The two micropipettes are brought into the user's field of view with the lysing micropipette on the left and the collection/uptake micropipettemicropipette on the right. Using brightfield phase contrast imaging, the user brings both micropipettes into contact with the target cell. B: Initial bursts of lysing solution (containing SDS and an indicator dye Alexa Fluor 555 conjugated to 10kDa dextran) are applied to the cell and its soma quickly fills. C: After a period of time the collection micropipette begins to take up dye and cellular content through the application of negative pressure and gradual decomposition of cellular membrane. D: Application of lysis buffer is stopped to prevent bursting of the cell while collection continues until fluorescence is sufficiently low in the cell volume. Following this the micropipettes are automatically extracted and transferred for sample deposition and recycling for the next cell sampling.

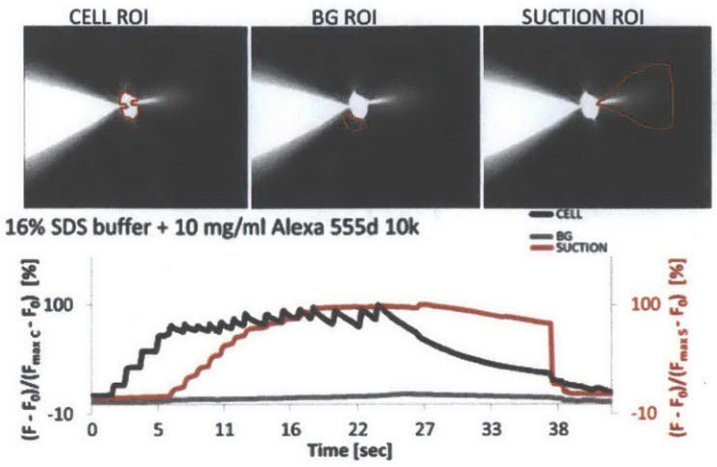

Figure 4.8: Fluorescent measurments of the cell and collection micropipette during a sampling cycle. Plotted are the fluorescent intensities normalized to both background fluorescence and peak value of the specific region of interest plotted. Cell fluorescence is in black and the uptake/collection micropipette is in red. Spikes in the cell are the result of lysis buffer bursts applied by the researcher.

4.4.1 Sampling Timing

In order to better quantify the single-cell sampling behavior the fluorescent intensity of Alexa Fluor dye in the lysis buffer was quantified as it spread first to the cell and later to the uptake micropipette. As can be seen in Figure 4.8 and more generally in Figure 4.9, the entire sampling procedure takes less than 40 seconds for most cells, and this can most likely be shortened in the future. In comparing to other single-cell harvesting techniques in tissue environments, particularly patch clamp aspiration, this value is at or below the timing it takes per cell using those methods, not counting preparatory work. In fact in several papers on patch aspiration procedures, the authors note that negative pressure should be applied for up to 20 minutes to ensure proper collection without inhibitory clogging [124]. Deposition, Rinsing and other steps in the cycle take approximately 90 seconds as of the writing of this thesis, however we expect to get these down to a shorter period as we optimize deposition and cleaning procedures. Overall, however, at a conservative estimate of 2 minutes per cell, the automation and workflow we provide here provides at least an order of magnitude improvement in throughput over other micropipette-mediated collection techniques without sacrificing any of their benefits.

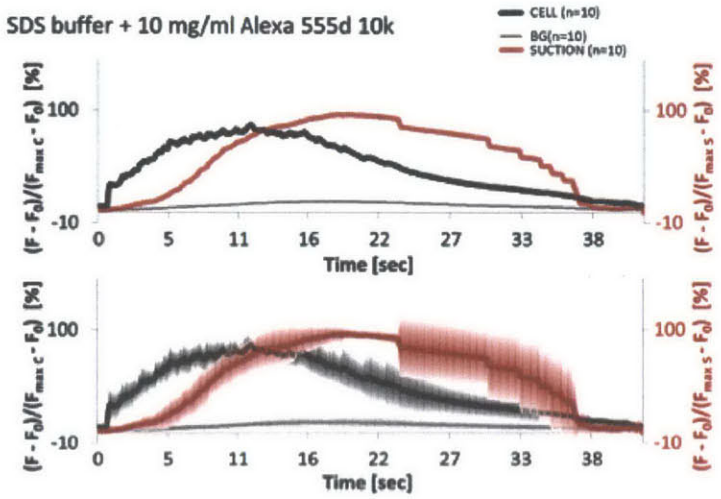

Figure 4.9: The average of ten measured single-cell samplings plotted without (top) and with (bottom) ±s.d. In general the same trend is observed in all cells. Individual traces used to generate this figure can be found in Fig. B.10.

4.5 Benefits and Concerns with High Concentration SDS

While high concentration of SDS facilitated efficient collection of cellular material while avoiding clogging of the micropipette tip, its presence in our workflow needed to be analyzed more fully to ensure no complications on system operation. In particular, the high sensitivity of downstream procedures such as reverse transcription to SDS is well known and we needed to verify it would not be a problem. During this exploration several benefits for SDS were also uncovered.

Rapid Fixation of Target Cell

As shown in the original work, the introduction of lysis buffer to the cell rapidly denatures its protein population. Because the enzymatic capacity of the various components of intracellular environment is rapidly shut down, this methodology effectively chemically freezes the cell close to the moment of collection. The timescale from initial approach to fixation is on the order of seconds, and therefore drastically cuts down on the time available for the cell to respond to disturbance induced by the collection, or for post-collection molecular degrada-

tion to take place.

Flexibility in Analytics

While the main focus in developing this platform is to achieve RNA transcript analysis, single-cell lysis and extraction also enables protein analysis as well as metabolomics.

Ribonuclease Inhibition

Ribonucleases (RNAses) are a superfamily of enzymes found in all cells that are used in the regulation and recycling of RNA in cells [125]. In the cell environment they are tightly controlled, however some cell types secrete various RNAses into the extracellular environment, and upon disruption or death of a cell, many of the biochemical methods that keep the RNAses in check can be compromised. Consequently, degradation of mRNA transcripts from RNAse can have a huge effect on the signal generated from cell content harvesting. A common solution used by researchers is the addition of various natural or recombinant RNAse inhibitors. While these are used at all possible steps, during the actual harvesting of the cell content, it could be difficult to ensure survival of mRNA. Interestingly, an unforeseen benefit of lysing cells with the high SDS concentrations used in this method, RNAse activity is significantly inhibited as evidenced in the experiment detailed in Figure 4.10.

SDS Dilution from Sample

It is well known that the reagents used in both reverse-transcription and PCR are sensitive to even low concentrations of SDS[126]. To confirm that SDS deposited along with cell samples does not inhibit downstream analysis using enzymes (particularly reverse transcriptase), the efficiency of standard RT-PCR reaction sets were analyzed at varying concentrations of SDS as shown in Figure 4.11. As reported in literature, even seemingly low concentrations of SDS in an RT reaction can completely eliminate product generation. We observed improving gains in RT-PCR efficiency down until SDS dilutions of approximately 0.003% before efficiency surprisingly decreased somewhat to results achieved with no SDS present. This trend was found to be repeatable and robust across multiple transcripts. In the case of β-Actin mRNA amplified from serial dilutions of murine whole brain lysate, the signal generated from 10 pg of starting material was found to be 54.3± 8.2% greater than without SDS ($n = 3$), for

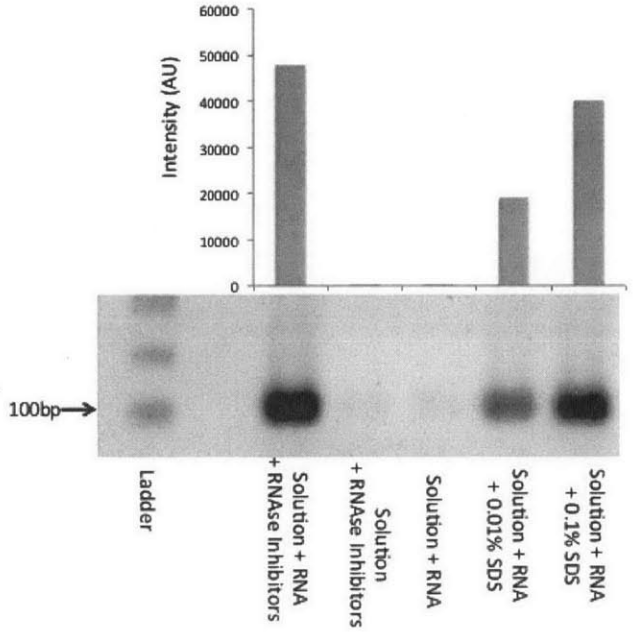

Figure 4.10: mRNA will readily degrade due to Ribnuclease (RNAse) activity from extracellular solution. When murine RNA is added to the extracted extracellular solution of an organotypic murine brain culture in the presence of RNAse-Inhibitors, a strong signal is generated from RT and PCR reactions (left most lane). The extracellular solution on its own exhibits little viable mRNA on its own due to the rapid degradation of transcripts in solution (second lane from left). Even when murine RNA is added to the solution, incubated for thirty minutes and then analyzed little signal appears, (third lane from left) further suggesting the the presence of RNAse activity. Interestingly when low concentrations of SDS are added to the media, the integrity of mRNA added to the mix is maintained (fourth and fifth lanes from left), suggesting SDS, because of its denaturing of proteins, prevents RNAse activity. All experiments involved incubation at room temperature for 30 minutes followed by reverse transcription and PCR analysis for β-Actin signal

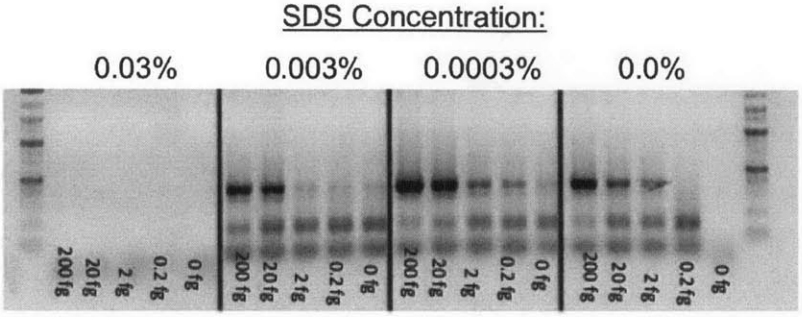

Figure 4.11: The effect of SDS on RT-PCR at various concentrations of synthetic mRNA enconding YFP was assayed. SDS can completely inhibit RT-PCR reactions even at concentrations of 0.03%. At a concentration 0.003% amplification of low starting material is still inhibited when compared to control (right side 0.0%. Interestingly, the efficiency of the RT-PCR reaction improves at low dilutions (0.003%) above what is observed with no SDS at all. Because the dilution of SDS in the tip of the deposition micropipette is on the order of RT was carried out as described in Appendix and PCR was carried out using YFP primer set-1 from Table B.3 at 32 cycles.

example. The rationale for this slight improvement in reaction efficiency within a certain window of SDS concentration is not known, but may be rooted RNAse activity inhibition, the denaturation of proteins and structures inhibiting efficient reverse transcription, or the inhibition of adsorption onto the walls of the reaction vessels.

Doing rough "back of the envelope" calculations we can determine that the final concentration of SDS in a deposited sample will be at or below 0.0005% [5] Initial cell samples in fact were found to benefit from the addition of 0.0003% SDS to their RT-PCR reactions, suggesting that actual final concentration from SDS from deposition is at least an order of magnitude less than that estimate.

These experiments provide significant evidence that deposition of samples collected using targeted lysation using high concentrations of SDS should be compatible with down-stream enzymatic analysis.

[5] Assuming a worst case concentration of 20%SDS in the recovery micropipette tip and a deposition volume of a 100 pL into a volume of 3 to 5 μL, the concentration of SDS in the sample will be at most $20\% \times \frac{100 \times 10^{-12} L}{3 \times 10^{-6} L} \approx 0.00033\%$.

Temperature Requirements

The high concentration of SDS in the lysing micropipette (4% to 16% depending on experiment) required that the micropipette contents be kept at or above 25°C in order to keep the SDS in solution, otherwise the formation of SDS crystals would clog the system operation [127]. When in the tissue culture bath, the entire environment is kept warmed to 37°C anyways for the sake of the tissue viability, however a separate heating element (See Fig. A.6) had to be constructed during cleaning and rinsing steps.

4.6 Recovery Rate Analysis

In conjunction with developing the sampling technique we used RT-PCR analysis of samples to acquire estimates of cellular material recovered. Details of these analyses are included in Section B.8.2 and associated supporting material. In particular we analyzed the presence of several "housekeeping genes" and using serial dilutions of murine brain tissue to generate a standard curve, estimated the quantity of total cell RNA collected from a cell. Significant cell-to-cell variability in house-keeping gene expression is expected to exist even within subclasses of cells, and so while these numbers were used to provide an estimate of RNA content collected, they are by no means a definitive measurement[65].

In order to measure the amount of cellular RNA collected using the procedure we developed, the following experiments were carried out: Cortical neurons were targeted for collection in the cerebral cortex of murine organotypic brain slices. Following collection of cell material, the collection micropipette would immediately deposit its sample into 3 subsequent wells. Multiple wells were used in order to determine if all material was deposited upon first deposition or if multiple depositions were required. A graphical explanation of this experiment is shown in Figure B.8. An initial experiment in which we analyzed the readout from six cell sampling cycles on four cells a piece is shown in Figure 4.12. As can be seen in this plot, signal is heavily biased towards initial wells in each experiment cycle, with very low readouts in most cells sampled after the initial. Because there was a high correlation with successful cell signal and fresh, non-recycled micropipette tips, we reasoned that insufficient washing of leftover sodium hypochlorite from the cleaning step may be destroying cell signal. To check for this we increased the washing steps by 5 times in duration and increased the bias for outward pressure in the micropipette tip when

cleaning in sodium hypochlorite solution in order to minimize the amount of the chemical that moves into the greater micropipette volume. The result of these improvements are displayed in Figure 4.13 and showed a large improvement in cell collection efficiency (82.14% (23 out of 28 cells) as opposed to 37.5% (9 out of 24) prior to more thorough rinsing. Importantly, the results in Figure 4.13 do not exhibit any bias towards earlier sampling as was the case in Figure 4.12, and therefore demonstrate the feasibility for sampling multiple cells in a sequence using the same micropipette, a capability not shown before in the literature.

The quantity of material collected in both samplings was not statistically different, in part because of the rather large variations between samplings. In the data set from Figure 4.12 the average yield of successfully collected cells was 13.21 ± 9.79 pg (s.d), while in the data from the experiment set in Figure 4.13, the average yield of successfully collected cells was measured at 10.15 ± 5.82 pg. (s.d). Ranges of measured total RNA varied widely from several pg up to over 30 pg. These numbers are within the range of estimates reported in the literature[128]. Caution must be exercised in using these readouts however since there is little data in the literature reporting how much (in terms of number of copies) we should expect from neurons. In conjunction with this is that we don't know the cell-to-cell variability to expect for genes such as β-Actin or GAPDH, other than that they are most likely present in at least some level. β-Actin in particular has been shown to vary in neurons depending on state [65]. Most information based on cell-level estimates are derived for non-neural cells, so in taking a conservative approach to these readouts we can claim that we show reliable collection of relevant cellular material, but will stop short of claiming specific numbers. Using the results from RNA-sequencing will provide us with a more standard metric (number of unique reads) that we can use to estimate and compare the amount of RNA collected. This work will be carried out in the near future.

4.6.1 Quantitative Analysis

4.7 Cross-Contamination Analysis

In collecting the contents of cells from tissue environments significant attention should be paid to contamination, and off-target material must be characterized in order to verify the selectivity of a sampling method. There are well-known markers that can be used to define cell subtypes that have little to no observed

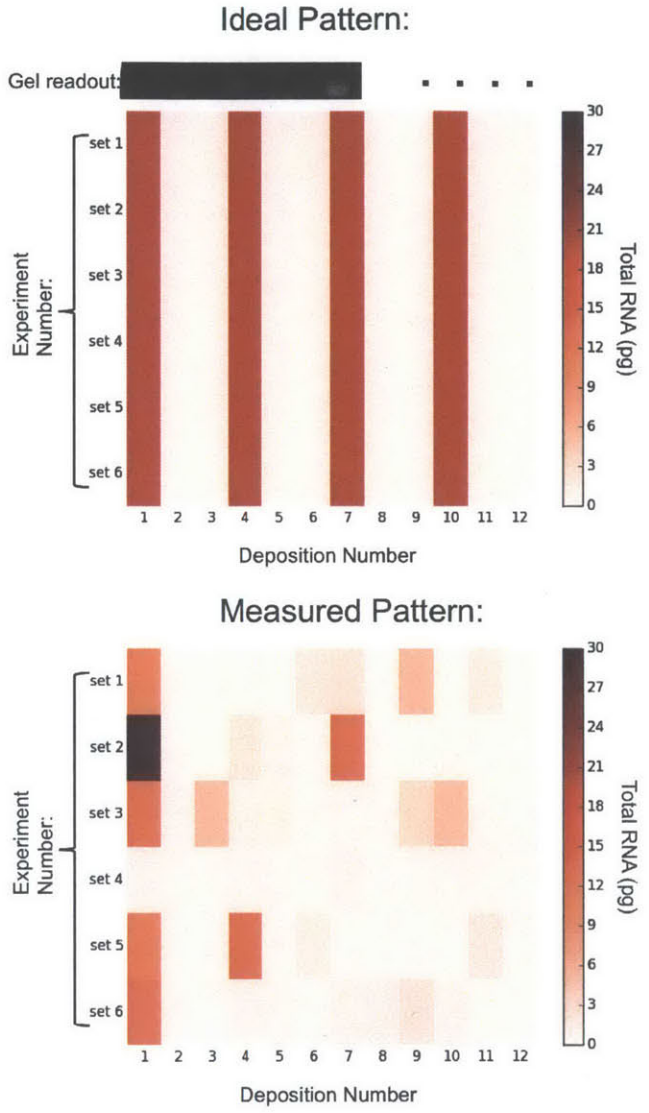

Figure 4.12: The top chart indicates the expected readout for six consecutive sampling experiments (24 total cells), with 4 depositions for each cell. An estimate of 20 pg was used as an expected value, however this is expected to vary widely based off of literature so should only be used as a rough benchmark. The bottom chart indicates the actual readout from six sample sets. This initial sampling revealed a significant bias towards early samples. In the six experiments depicted here, colleciton efficiency*in the first cell sampled (prior to bleach-based cleaning) was 83.33% (5 out of 6), however following the first sampling overall collection efficiency dropped to 22.2% (4 out of 18). The average yield of successfully collected cells was 13.21 ± 9.79 pg (s.d).
*Collection efficiency is defined as a measured signal greater than 2 pg.

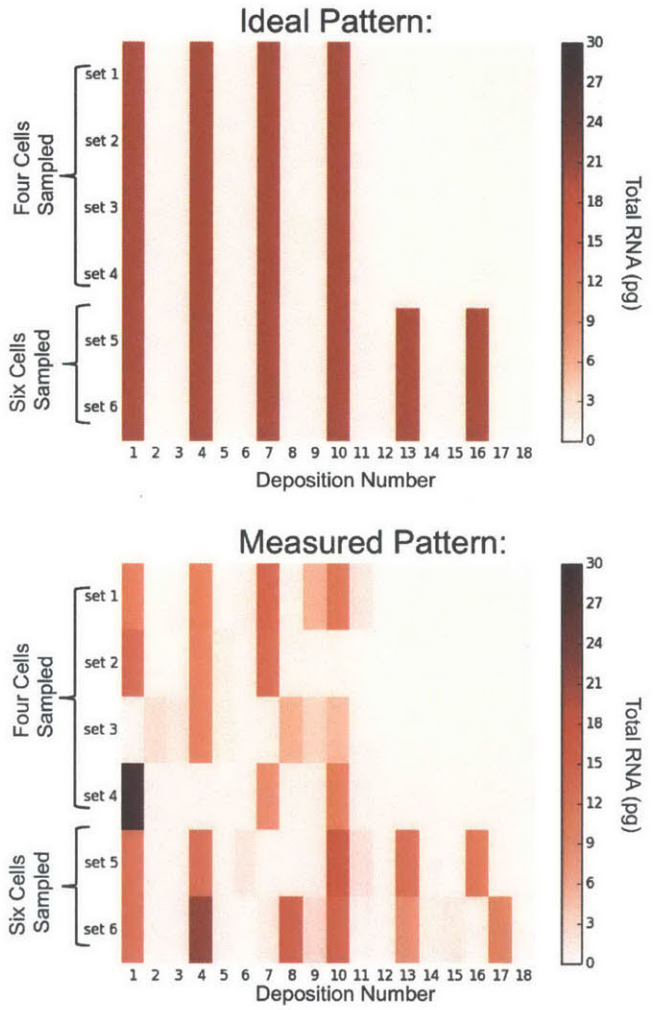

Figure 4.13: Following a more thorough rinsing of the lysing micropipette as well as collection micropipettes to ensure sufficient removal of bleach the overall yield of cell collection was vastly improved. The top depicts the expected experimental readout (note two experiments involved sampling of six sequential cells rather than four), while the bottom depicts the measured readout. In the six experimental runs depicted here, collection efficiency* was 82.14% (23 out of 28 cells sampled). The average yield of successfully collected cells was measured at 10.15 ± 5.82 pg. (s.d)
*Collection efficiency is defined as a measured signal greater than 2 pg.

co-expression in naturally occurring cells[58]. For example, Glial fibrillary acidic protein (GFAP) is often used as a marker of astrocytes in the mammalian brain, and will not be expressed in neurons, while Class III β-Tubulin will be found exclusively in neurons. Similarly within subtypes of cells, certain markers are rarely co-expressed. Cortical inhibitory genes such as *Gad1*, *Gad2*, and *Slc32a1* are rarely found in neurons expressing excitatory markers such as vesicular Glutamate Transporter 1 (vGlut1) and others[129].

In order to begin to characterize the cross-contamination present in this sampling method, a selection of cell markers were assayed using Nested PCR (see Section B.8.2) for β-Actin, GAPDH, GFAP, β-III tubulin, GAD1, vGlut1, and TH (Tyrosine Hydoxlyase a marker of dopaminergic neurons). Four single-cell analytical readouts are shown in Figure 4.14 below, with cell A being identified as a GABAergic neuron, cell B an unknown cell type, cell C an astrocyte, and cell D a glutamatergic neuron. Tabulating these readouts along with others yields Table 4.1. As can be seen, out of the 13 cells we analyzed, all tested positive for housekeeping genes β-Actin and GAPDH. 7/13 tested positive as neurons, 3 tested positive as astrocytes, with no overlap between the two populations. Within the neuron pool, 3 neurons tested positive for inhibitory marker GAD1, 1 neuron tested positive for Glutamatergic marker vGlut1, 3 for no specific subtype, and 0 for dopaminergic marker TH. This preliminary result suggests little to no contamination from non-targeted cells. Of particular note, the lack of GFAP signal in harvested neurons is promising since astrocyte contamination has proven high in other neural collection techniques previously[58].

4.8 Discussion

This chapter covered the development of a system and workflow that enables the rapid sampling of cytoplasmic content of single cells in a way that is compatible with live tissue environments and which generates minimal peripheral damage to cells. This technique does not require whole-tissue fixation, disaggregation, or other global treatments that may affect readouts. While there are a number of techniques available for extracting the cytoplasmic material from single cells, true single-cell collection techniques are historically low throughput and error-prone in implementation. Our system provides true single-cell sampling capabilities on time scales that are over an order of magnitude faster than traditional manual methods (2 minutes per cell in current form), with high

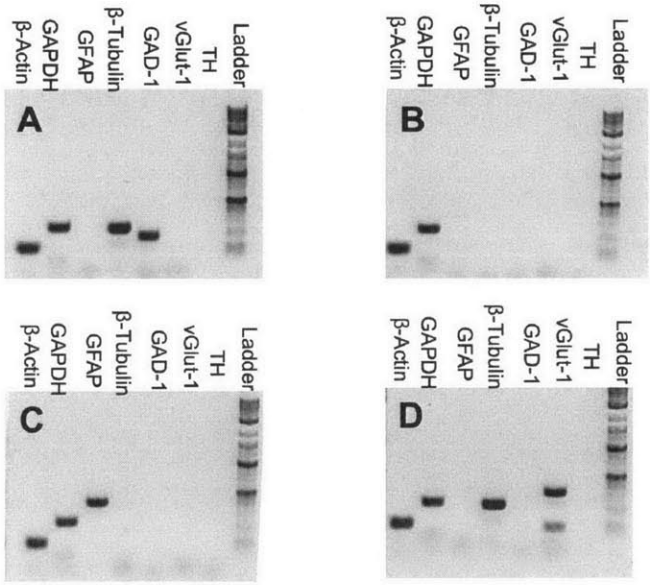

Figure 4.14: Nested PCR analysis was carried out on single cell samplings taken from neural tissue and tested for housekeeping gens β-Actin and GAPDH, astrocyte marker GFAP, neural marker β-III tubulin, and neural subtype markers GAD1, vGlut1, and TH. For examples are shown A identified as an inhibitory neuron, B identified as an unknown cell type, C identified as an astrocyte, and D identified as glutamatergic neuron. These four cells correspond to cells 1, 2, 3, and 4 in Table 4.1. Expected product lengths were β-Actin: 106bp, GAPDH: 252bp, GFAP: 455bp, β-III tubulin: 274bp, GAD1: 198bp, vGlut1: 410 bp , and TH: 311bp.

Cell	Est. Quantity (pg)	β-Actin	GAPDH	GFAP	βIII-tubulin	GAD1	vGlut1	TH	Cell Type
1	8.9	Y	Y	N	Y	Y	N	N	Neuron Inhibitory
2	12.5	Y	Y	N	N	N	N	N	Unknown
3	4.1	Y	Y	Y	N	N	N	N	Astrocyte
4	10.2	Y	Y	N	Y	N	Y	N	Neuron, Glutamatergic
5	13.5	Y	Y	N	Y	N	N	N	Neuron, undefined
6	5.2	Y	Y	N	Y	Y	N	N	Neuron, Inhibitory
7	13.1	Y	Y	N	Y	N	N	N	Neuron, undefined
8	7.4	Y	Y	N	Y	Y	N	N	Neuron Inhibitory
9	12.0	Y	Y	N	N	N	N	N	Unknown
10	6.4	Y	Y	Y	N	Y	N	N	Astrocyte
11	12.2	Y	Y	N	N	Y	N	N	Unknown
12	15.6	Y	Y	N	Y	N	N	N	Neuron, undefined
13	9.0	Y	Y	Y	N	N	N	N	Astrocyte

Table 4.1: Tabulated Nested PCR analysis of single cell samplings taken from neural tissue and tested for housekeeping gens β-Actin and GAPDH, astrocyte marker GFAP, neural marker β-III tubulin, and neural subtype markers GAD1, vGlut1, and TH . All cells tested positive for both housekeeping genes. 7/13 tested positive as neurons, 3 tested positive as astrocytes, with no overlap between the two populations. Within the neuron pool, 3 neurons tested positive for inhibitory marker GAD1, 1 neuron tested positive for Glutamatergic marker vGlut1, 3 for no specific subtype, and 0 for dopaminergic marker TH. A positive signal was defined as anything above the noise level for a specific gene primer set. A negative signal was defined as indistinguishable from the noise level. PCRs were run in duplicate for each cell for verification. No mismatches between duplicates were observed.

collection efficiency and deposition into a standard analytical format. There is a real gap in the technology field that our system addresses, allowing for the first time possibility the sampling of dozens to hundreds of cells from a tissue region in a period of hours, all while collecting morphological information about those cells. These numbers and data sets that cannot be acquired using current technologies, and we therefore believe that the principles of our system will readily find use in the life sciences.

Chapter 5

Continuing Development

The previous chapters demonstrate a novel system and workflow that greatly increases the throughput of single-cell transfection and sampling by redesigning previously established techniques (Single-Cell Electroporation and Single-Cell Aspiration) and combining them with automation to replace the majority of manual steps. This chapter briefly details several future directions we intend to investigate, and we conclude with a brief discussion on the overall impact of the work.

5.1 Further RNA Sampling Analysis

Having shown that the automated single-cell sampling platform can reliably and repeatably collect the contents of cells from tissue environments and deposit them into 384 well plates for downstream processing, we next intend to further quantify total cell content yields when compared to other single-cell techniques as well as further quantify the degree of contamination exhibited[58]. The 5 µL of solution we deposit into is compatible with most RNA-sequencing formats, allowing us to carry out first strand (and second strand if desired) cDNA production, as well as antisense RNA (aRNA)[130, 80]. We will also carry out analysis on pre-labeled cells using primer sets detailed in Figure B.9. Because single-cell RNA-seq results in large numbers of sequence reads, the diversity of which are used to estimate overall quantity of material collected, we will be able to use results from such analyses to directly compare our technique to other developing technologies [73].

5.2 Expandability and Merging Other Techniques

In Chapter 3, the micropipette used for SCE had an approximate tip opening of 2 to 3 μm, which is also in the acceptable size range for the collection/uptake micropipette used in SCS in Chapter 4. An obvious and readily implemented extension of the current work will be to merge both SCE and SCS functionalities into the system at one time. A standard lysis micropipette used in conjunction with a dual-use transfection or sampling micropipette could be readily created since their are no incompatibilities with the two techniques. While the current electrical interface is capable of stimulation for only SCE, it could easily be modified to handle both its SCE operation and an electrophysiological unit for stimulation and recording, since patch-clamp micropipettes are often made up of very similarly-shaped micropipettes. This would continue the trend started in other research of trying to extract multiple classes of cellular parameters from patch clamping neurons[131, 132, 133, 114, 78, 134, 115, 124]. Furthermore, merging recently published patch-clamp automation with the automation and workflow we developed here, could result in even greater throughput gains [88]. In bringing all of these techniques together into the automated system presented in this thesis, and coupling it with an optical system of sufficient resolution, we could generate a means of easily and arbitrarily manipulating and analyzing all relevant cellular parameters in individual tissue-bound cells, with particular benefits for neural circuit analysis. These studies could be carried out in real-time, in the moment, rather than requiring pre-planned transgenic tissue generation or slower manual methods, and could therefore become a form of "cellular multimeter", allowing the flexible and on-the-spot analysis of parameters of neural circuits or cell-to-cell variability in tumor environments.

5.2.1 Protein Analysis at the Single Cell Level

While we focused the work in this thesis on manipulation and analysis of nucleic acid content, there is also the potential to investigate protein content [123]. Low-level protein analysis is different from its upstream nucleic acid cousins because there lacks a readily available means of amplifying the initial starting material. While DNA and or RNA can be amplified exponentially with very high fidelity, protein analysis lacks such capability and analyses must therefore be carried out in very small volumes (on the order of nL) in order to ensure efficient analysis In order to successfully merge our system with modern protein

analytical techniques, biomolecular preconcentrators could provide one method for capturing the cellular content from μL-level volumes as currently generated in our work and forcing them down into the nL scale in which many protein or metabolite assays are effective [135, 136]. Our research into oil deposition (discussed briefly in Section B.9) is another potential means of minimizing dilutions and could provide a means of interfacing with microfluidic analytical chips. Microfluidics fit this niche very well, allowing reactions to take place at the sub-nanoliter level which is sufficient for analysis, and the readout can then be readily amplified (optically or chemically).

5.2.2 Microfluidic Adaptation

Our system currently relies upon pulled glass micropipettes. This was largely due to the flexibility and ease in their manufacture, their ability to readily penetrate tissue environments, and the precedent for their use in the neuroscience community. Replacing these micropipettes with specially designed microfluidic probes for contacting single cells could provide numerous benefits, including the creation of far more complex probes[137]. Microfluidic probe/chip combinations have already been derived for several means of manipulation and analysis of single cells including electroporation and protein analysis, with significant benefits in the latter case due to a minimization of sample dilution[113, 138]. Long-term development of specialized microfluidic probes that are compatible with tissue environments, when used in conjunction with the washing, rinsing, sampling, and deposition techniques we developed in this work, could result in even greater improvements in system throughput and versatility.

5.3 Summary of Work

The future of cellular analysis lies in the study of cells in their natural environment, and less so in artificial cell culture environments, since the former is much closer to the reality of a cell's existence than the latter. Key to achieving this goal are the development of technologies that allow the sampling and manipulation of cells in tissue environments. In the case of both single-cell manipulation and single-cell analysis, available technologies are either high-throughput but insufficiently specific, or have single-cell specificity but are low throughput, with little middle-ground. In tissues such as the brain where even the simplest circuits are comprised of dozens of cells, proper studies need to be able to feed

inputs and measure outputs from the cells in the system in arbitrary patterns that neither class of manipulation/sampling technologies allows. What we have set out to do in the work shown in this thesis is to bridge the gap between the two classes of technologies and find a middle-ground with clear application in tissue studies. By taking techniques that are normally implemented in low-throughput manual ways and increasing their throughput dramatically via redesign and automation we have generated a set of technologies with all of the benefits of the low-throughput manual methods, but with drastically decreased limitations. The technology comfortably sits in the medium-throughput field and will hopefully contribute to the development of a future wave of biological techniques as the life sciences field shifts its focus more and more to single cells. The analysis of single-cells in a tissue environment is very similar to the problem faced by an Electrical Engineer debugging an unknown circuit PCB complete with components. The spatial context of the components must be maintained in order for it to make any sense, and what we have proposed here are a set of technologies that bring us closer to analyzing the cell in its native environment as one would study an unknown circuit component in its native environment.

Our system could in principle be adapted for deeper tissue and even in vivo single-cell manipulations using cranially accessible preparations and multi-photon microscopy [139, 38, 51, 54]. When working at greater depths in vivo, the speed of the system would need to be decreased in order to avoid damage to both tissue and micropipette as we did for acute slices above. However, because in vivo preparations can be operated on over longer time periods than acute brain slices, it should still be feasible to perform large-scale in vivo single-cell manipulations through cranial window preparations. By enabling more variables to be tested within the same tissue and on specific anatomical regions, the effect of variability between multiple tissue preparations and between animals can be avoided. More efficient utilization of tissues could also enable larger scale studies.

Appendices

Appendix A

System Hardware and Automation Methods

A.1 Automating Interfacing with Micropipettes

The electronic setup used for SCE in this thesis is similar in manipulating equipment to most previous SCE implementations, however it departs from convention by relying solely upon a data acquisition card (specifically National Instruments Data Acquisition Card (NIDAQ) card) for both stimulation voltage trains and recording of stimulation current, an approach previously demonstrated in only one publication[92]. Even at the low-end of the cost and feature spectrum, NIDAQ cards offer multiple channels of analog and digital I/O with voltages output and input ranges up to ± 30 V, depending on make and model, which are sufficient in magnitude to electroporate even large plasmids from our experience. An analog output (AO) channel drives the stimulating electrode with the user-specified pulse train. An in-series resistor (R1) of 100 kΩ(metal-film, 0.01% tolerance) is used to form a simple current sampler by having the voltage developed across it fed into an analog input (AI) channel during application of stimulation train[1] . We have found that no amplification is needed between the resistor and NIDAQ card, provided that proper shielding of the cable is in

[1]Because the 100 k$\Omega$is in series with the entire circuit including the entire micropipette with resistance on the order of 10 MΩ, its resistance is negligible and can therefore be used to relatively accurately assess the current in real time

place, with average noise recorded at the input of the NIDAQ card from the resistor found to be $V_{RMS} = 4.4\ mV_{RMS}$ equating to approximately 40 nA of current-read noise, a value sufficiently low for analyzing the μA-level current produced in most SCE trains.

Detailed views of the SCE control software can be seen in Figure A.1. The stimulation parameters are built around the pulse as a unit, with the user specifying the number of pulses, as well as the period, duration, amplitude of each pulse. An offset voltage can also be entered to cancel any DC noise in the recording. A flow diagram of the software is shown in Figure A.2. Upon pressing the Fire button, the function establishes connection to the NIDAQ card, preps the analog input and output channels, loads the stimulation train into the NIDAQ output buffer, triggers the card, and then following the delivery of the stimulation train, reads out the AI signal before immediately severing communication with the NIDAQ card and plotting the complete, scaled voltage and the current trains in synchronized plots to allow easy analysis of the transfection by the user. While introducing no noticeable lag into system operation, this "grab-and-release" treatment towards the NIDAQ card minimizes the amount of time it spends occupied with SCE delivery, and therefore maximizes the amount of time it can be used for other functions. This characteristic is key to the software's flexibility and compatibility with more complex control systems.

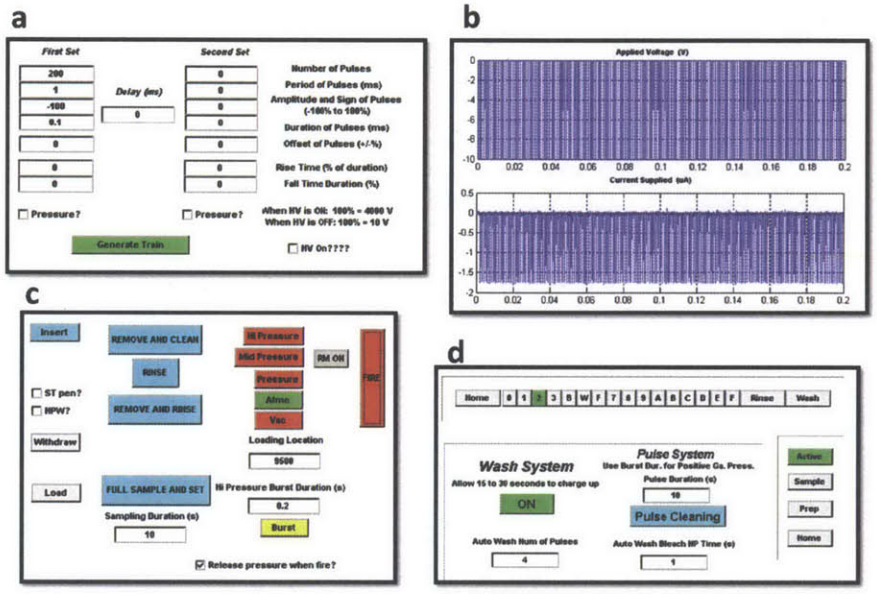

Figure A.1: Detailed images of the portions of the control window, including (a) Single-cell electroporation parameters, (b) Applied SCE voltage signal (top) and measured SCE current (bottom). (c) Micropipette pressure controls, high-level controls for automated system operation, and manipulator controls. (d) Micropipette position control, clean/wash system parameters, and multiwell/washing equipment position control.

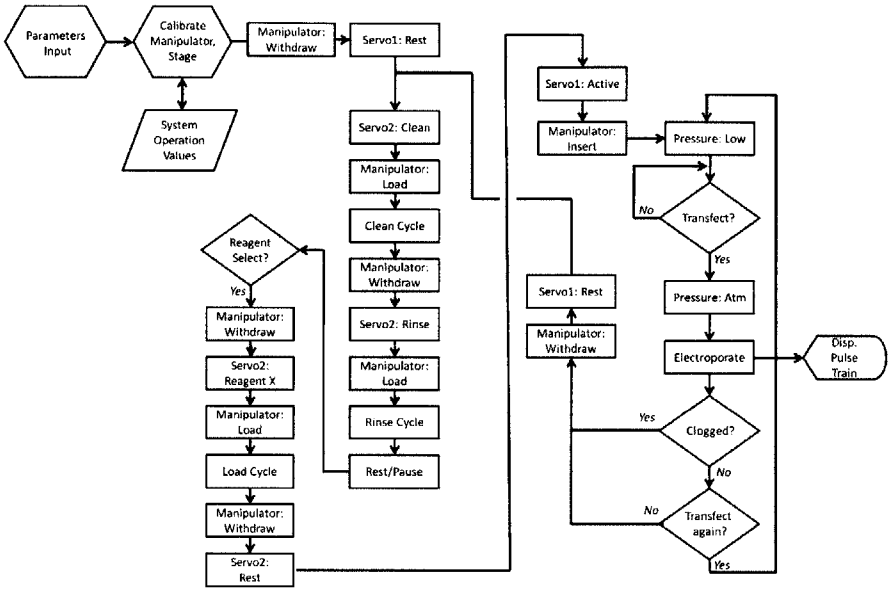

Figure A.2: Boxes are actions and processes, hexagons are preparation steps, diamonds are decision/pause points, parallelograms are data storage. Servo1 refers to the micropipette/manipulator positioner, and Servo2 refers to the multiwell and washing equipment positioner.

A.2 Diffusion Measurements and Simulations

Diffusion measurements were carried out by front-loading micropipettes with samples of known concentration. Brightness was correlated to concentration using calibration curves derived from large volume (several μL) samples rear-loaded into similar micropipettes and then imaged (Fig. A.3). Images were captured every minute, with fluorescence exposure occurring only during image acquisition to avoid bleaching of dyes. A tip-diffusion model was developed in MATLAB to study the recorded measurements. To generate a structural model, micropipettes were imaged under low magnification (Figure 2a) and we traced the outside of the glass to get total micropipette cross-section, which assuming longitudinal symmetry could be used to calculate total volume of the tip. Next, using the assumption of a constant ratio of outer to inner diameter of the micropipette glass we calculated the internal volume profile[140]. This internal calculated volume of the micropipette was then binned into 1 μm^3

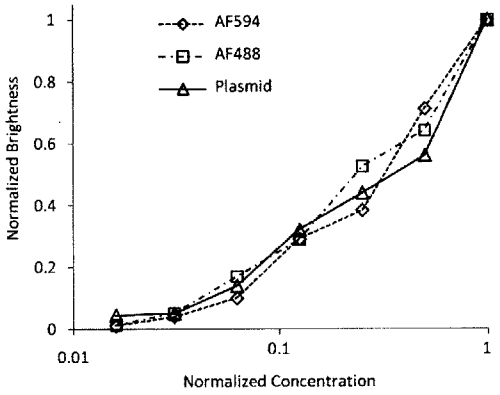

Figure A.3: Micropipettes were rear-loaded with approximately 4 μL fluorophores at varying concentrations to generate a calibration curve for measured fluorescent intensity versus concentration. Samples were measured from a concentration of 500 μM (for the Alexa Fluors) and 500 ng·μL^{-1} (for the plasmid/SYBR Green mixture) and stepped by dilutions of two to approximately 8 μM (for the Alexa Fluor species) and 8 ng·μL ^{1} (for the plasmid/SYBR Green mixture).

cubes for the purposes of simulation. To begin simulation, a sufficient number of volume bins (starting from the tip) were filled with the start concentration in order to generate a longitudinal concentration profile as shown in the middle drawing of Figure 2.1. No diffusion was assumed to take place through the glass, and diffusion out of the micropipette tip was assumed to be negligible. Fick's Law was used to model diffusion:

$$J = -D\nabla c \tag{A.1}$$

where J is diffusive flux, D is the diffusion coefficient, and ∇c is the spatial concentration gradient of the molecular species in question. The simulation took advantage of the longitudinal axial symmetry of the micropipettes to break down simulation into two phases for each time step. First longitudinal diffusion (down the length of the micropipette) was simulated in two dimensions. Second, cross-sectional diffusion of each plane of the micropipette was carried out in two dimensions. Diffusion was calculated between each block and all adjacent blocks. Empirically determined diffusion coefficients taken from the literature were 430 μm^2·s^{-1}, 370 μm^2·s^{-1}, and 3.5 μm^2·s^{-1}, for Alexa Fluor 488 hydrazide, Alexa Fluor 594 hydrazide, and pEGFP-N1, respectively[141, 142].

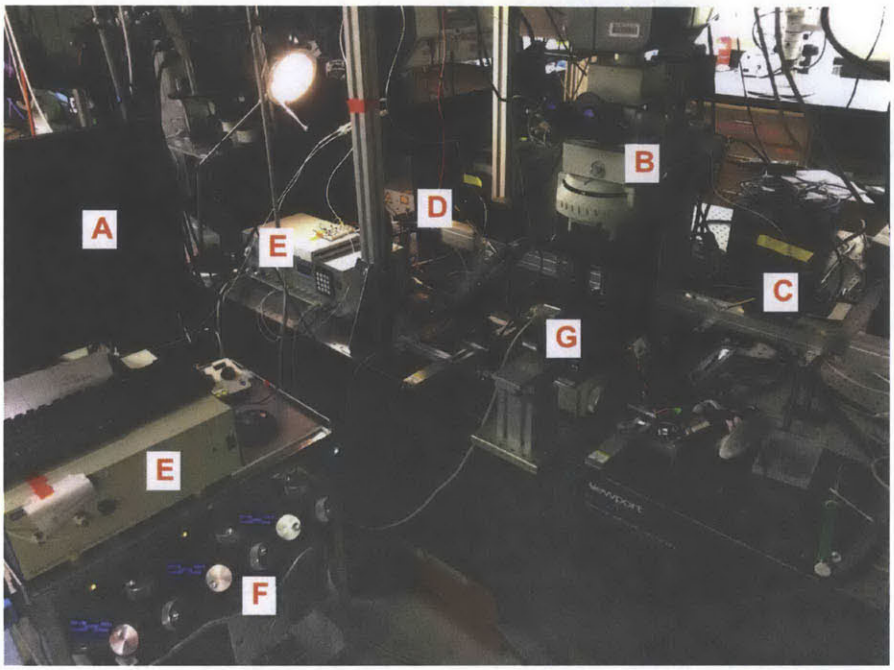

Figure A.4: Overall image of Single-Cell Sampling System. A: Computer for control. B: Microscope. C: Micromanipulator controlling Lysing Micropipette. D: Micromanipulator controlling Collection Micropipette. E: Pressure Controllers. F: Controllers for Micromanipulators. G: Micromanipulator for tissue handling.

A.3 System Images

The following images detail the system at the time of its dual-micropipette implementation used for single-cell sampling. Images of the original SCE system (one micromanipulator) can be found here[81].

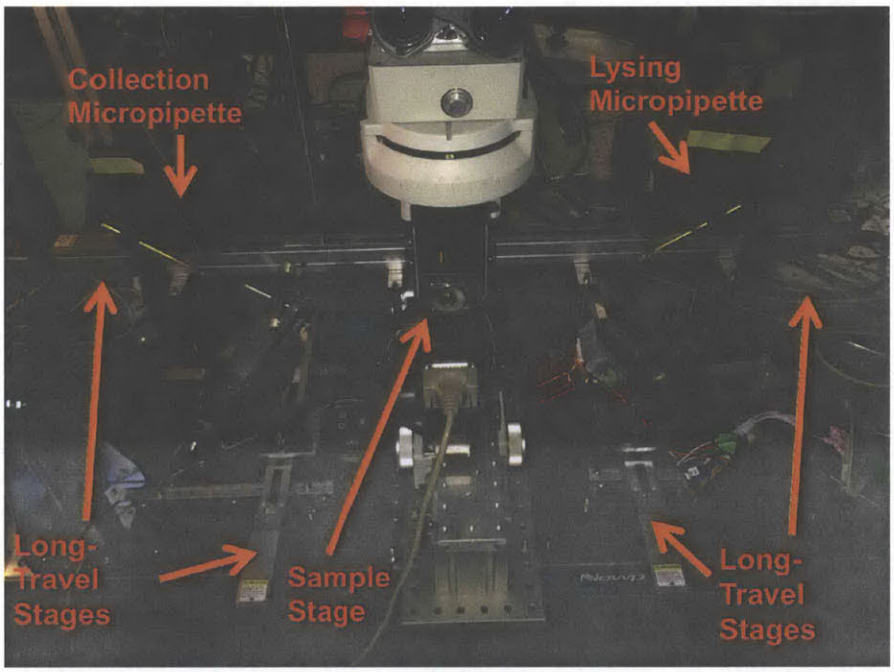

Figure A.5: Detailed view of Single-Cell Sampling System

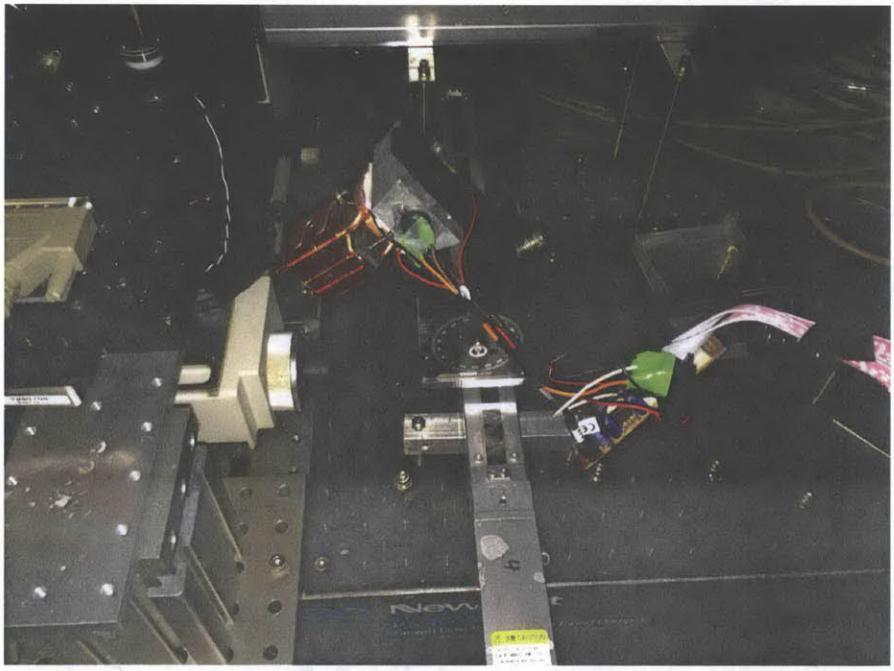

Figure A.6: The high concentration of SDS in the lysis micropipette necessitated its maintenance at temperatures in excess of of 25°C. A peltier heater was constructed and fashioned for tip temperature maintenance when outside of the tissue culture bath.

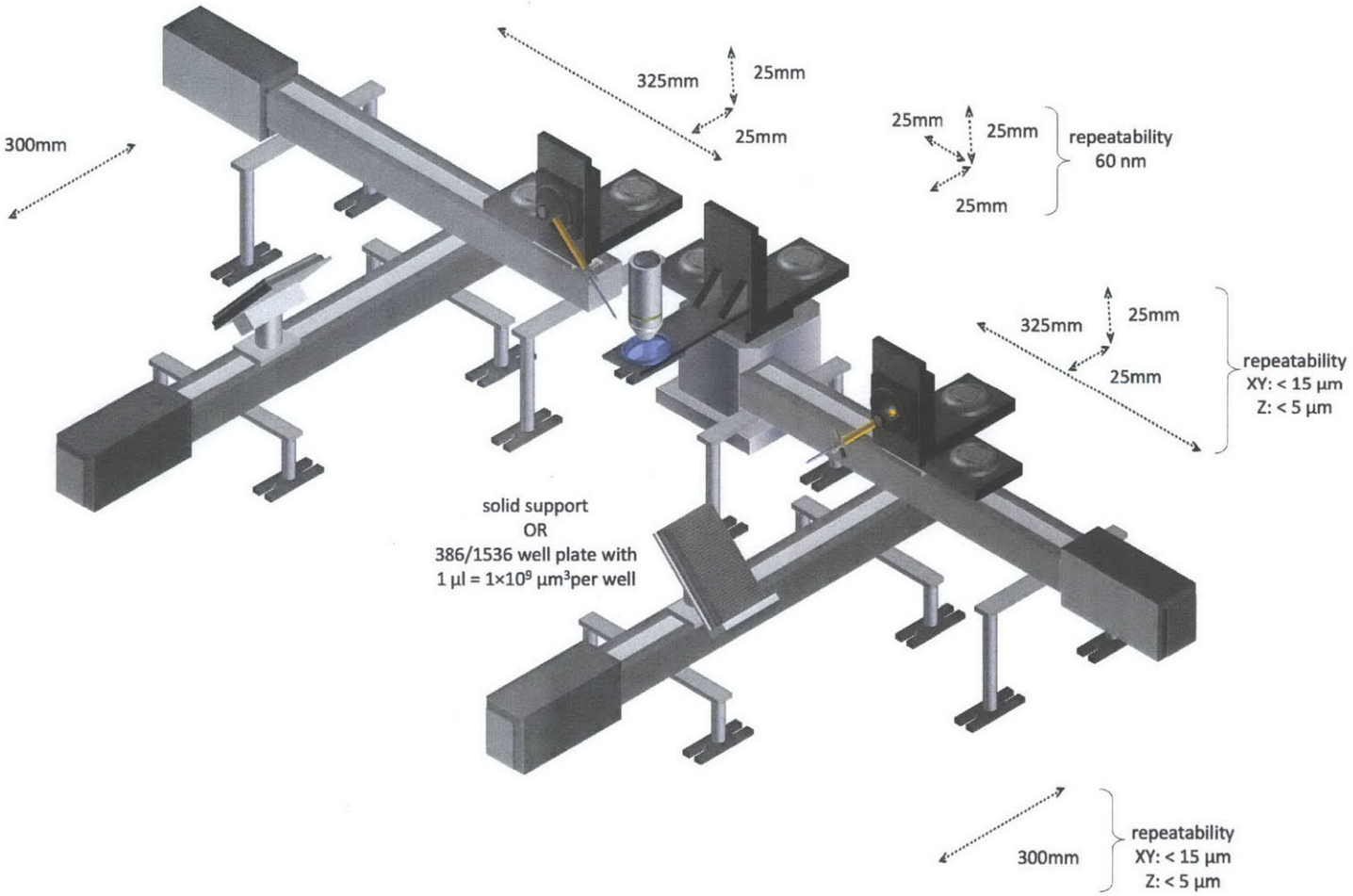

Figure A.7: Version 2 of the dual-micropipette system: (A larger version dual micropipette system discussed in Figure 2.5)

Appendix B

General Analytics for Experiments

B.1 Imaging

A 16×0.8 NA water-dipping objective was used on an FN-1 upright electrophysiology microscope (Nikon), utilizing bright field and epi-fluorescence. For SCE development a Hitachi KP-M2RU near-infrared monochrome CCD camera was used in conjunction with either a Nikon TRITC HQ cube or a FITC HQ (both Nikon). For single-cell sampling development a Hamamatsu Orca was used for a camera in conjunction with A dual-bandpass (Cy3, FITC) emission/dichroic/excitation set (Chroma). A multi-focal Visitech vtHawk confocal imaging unit, CoolSnap HQ camera, and PIFOC-400 400 μm travel piezo were used for high-speed imaging of cells after transfection and for analyzing dendritic spine density. For spine imaging, a 60×1.0 NA objective (Nikon) was used, while for lower resolution/magnification images, the 16×0.8 NA objective was used. When collecting data for dendritic spine analysis, z-stack slices were taken at 0.5 μm increments, and for low-magnification images, z-stack slices were taken at 2 μm increments. For immunohistochemistry imaging, a TE-2000 microscope equipped with either a 20×0.7 NA or 60×1.4 NA oil immersion objective and Nikon Elements Advanced Research software was used.

B.1.1 Image Handling

Plots of quantitative data were generated using either MATLAB and its associated packages, or python and matplotlib using the prettyplot library written by Olga Botvinnik[1]. Figure creation was carried out using Microsoft PowerPoint, GNU Image Manipulation Program (GIMP), ImageJ, FIJI, and the Python packages numpy and matplotlib.

B.1.2 Immunohistochemistry

For immunohistochemistry, slices were rinsed in Tris-Buffered Saline and Tween-20 (TBST) for five minutes, followed by fixation for 10 minutes at room temperature in 4% Paraformaldehyde in Phosphate Buffered Solution (PBS). TBST was introduced to the fixing solution before aspirating and rinsing twice in TBST. Slices were permeabilized in 0.1% Triton X-100 for 20 minutes at room temperature before rinsing twice in TBST, and then incubated in 1% casein in TBST for 60 minutes at room temperature or overnight at 4° C. Slices were subsequently cut out of their membrane inserts and placed into 24 well plates and incubated with antibody (anti-myc pre-conjugated to Alexa Fluor 555 from Millipore) in TBST containing 0.4% casein for three hours at room temperature. Slices were then rinsed in TBST with rocking for thirty minutes changing TBST every ten minutes before being mounted on slides in Vectashield under cover glass, sealed with nail varnish, and being stored at 4 degrees Celsius in the dark. Using the described protocol we rarely saw significant loss of native fluorescence in Cerulean and therefore did not need to use anti-bodies for its imaging. In cases where longer fixation (20 to 30 minutes) was used,fluorescent protein expression could become too low, and in such cases an anti-GFP primary antibody was used in conjunction with an appropriate secondary antibody conjugated to Alexa Fluor 647 or 680.

B.1.3 Dendritic Spine Density Analysis Statistics

Dendritic spines were manually counted by analyzing z-stack projections. Image files were randomized using a MATLAB script to preclude bias from counting and analysis. Only after image sets were analyzed were numbers matched with conditions. A one-way ANOVA test was used for cross-cell comparisons. or in

[1] http://olgabot.github.io/prettyplotlib/

the case of individual comparisons Welch's modification on a student's t-test was used. All results are reported as mean ± s.d.

B.1.4 Gel Analysis for Quantification

For gel runnout analysis, images were taken using GedDoc-It Imaging System (UVP) at varying exposures. Images were captured as TIFFs and analyzed using the ImageJ (NIH). Measurements were extracted from images of serial dilutions of murine whole brain lysate (or other known RNA source such as synthetic YFP mRNA) run out on the same gel as samples and were plotted against concentration of starting material. A best fit curve was fitted to the data using either MATLAB or python numpy packages. In the case of high-expression genes (β-Actin and GAPDH), these curves were then used to generate estimates of total cellular RNA content present in wells as long as they were in the linear range of standard curve, which generally stopped in the 0.1 to 1pg range. In the case of other genes, including cell-type specific markers like β-III tubulin, GFAP, or neural subtype markers like GAD-1 or vGLut1, reliable quantification standard curves could not be generated because the concentration of Replicates were carried out on all primer sets investigated and used to provide rough ranges in which accurate quantitation could be assayed in the case of house-keeping genes with murine brain lysate or YFP in the case of synthetic RNA.

B.2 Tissue Harvest and Maintenance

Organotypic slicing technique varied across the work shown in this thesis, but was primarily based on the publications by DeSimoni et al. described previously[143]. The majority of SCE system development was carried out using cultured septo-temoporal slices of the hippocampus of P5 to P9 Sprague-Dawley rat pups. The specimens were sacrificed quickly before the brain was coarsely dissected and subsequently sliced at 300 to 350 μm thickness using a Vibratome in chilled, EBSS + 10 mM HEPES buffered to pH 7.4. Slices were cultured on 6-well plate membrane inserts (Millipore PICM0RG50) using media described in Table B.10. Slices were kept for up to six weeks, although generally used between 5 and 21 days post-harvest. in the case of acute rat hippocampal slices, slices were harvested as described above, however In the For organotypic work, slice media was changed 24 hours following slicing and every third day afterwards. To avoid contamination, organotypic slices were rinsed in pre-warmed Rat Ringers

Solution (buffered to pH 7.4) containing 100 U/mL penicillin and 100 μg/mL streptomycin and were returned to a well containing fresh media, containing both containing antibiotics at above concentration and 60 ng/mL of Nystatin immediately following either transfections or imaging in the slice bath. Using this methodology as well as standard techniques during slicing, contamination of organotypic cultures was extremely rare. For transfections in acute slices, the bath chamber was perfused with warmed Rat Ringer's solution that was continuously bubbled in carbogen (95% O2/5% CO2). Acute slices were maintained for up to three hours in this environment. All animal work was approved by the MIT Committee of Animal Care and Division of Comparative Medicine and abided by institutional, state, and federal guidelines for animal welfare.

B.3 DNA and RNA Preparation

Plasmids for all phases of work were grown in the conventional bacteria strains XL-1 Blue, DH5, or TOP10. All plasmids were harvested using Qiagen Endo-Free Maxi Kits, and stored in TE Buffer or DI water at 1 to 6 μg/μL concentration, determined by a Qubit dsDNA Broad Range Kit (Invitrogen), or NanoDrop (Thermo Scientific) . All plasmids were acquired from Addgene unless otherwise specified:

- pCAG-EGFP, pCAG-YFP, pCAG-dsRed (Addgene plasmids 11150, 11180, and 11151, respectively)[144]
- pEGFP-N1 (Clontech)
- pCI-tdTomato, (courtesy of Dr. Rachael Neve)
- mCherry Lac-REP (Addgene plasmid 18985)[145]
- Cerulean (Addgene plasmid 15214)[146]
- pEAK10-His-Myc-Kal7 (Addgene plasmid 25454) [147]
- pEAK10-His-Myc-Kal5 and pEAK10-His-Myc-Kal9 (Addgene plasmids 25440 and 25441, respectively)[93]

pCAG-Cerulean was constructed by removing the Cerulean gene from its native Clontech backbone using the AgeI and BsrGI restriction endonucleases (New England Biolabs) and sub-cloning into the pCAG plasmid[146]. In all

cases, concentration of fluorescent-protein-encoding plasmids was 300 ng·μL^{-1}, while for the plasmids encoding Kalirin-5, Kalirin-7, and Kalirin-9, plasmid concentrations were 250, 300 and 373 ng·μL^{-1}, respectively to provide equivalent molarity of delivered plasmids.

B.3.1 Manufacture of synthetic mRNA

For generation of synthetic mRNA, sequences for EGFP, mCherry, and EYFP were inserted via subcloning (using *NheI* and *AgeI* or *BsrGI* restriction enzymes) into a previously described RNA manufacturing vector featuring HBB[2] 3' and 5' untranslated regions (UTRs)[148]. These UTRs enabled high levels of expression in murine and rat neural tissue in multiple cell types including neurons, astrocytes, and neural fibroblasts. Template for RNA synthesis was created either through 20-cycle PCR of vectors using forward primer TAATACGACTCACTATAGGGACATTTGCTTCTGACACAACTGTG and reverse primer GCAATGAAAATAAATGTTTTTTATTAGGCAGAATCCAGATG followed by *in vitro* transcription using a kit from Trilink Biosciences. RNA was tailed so that poly-A length was approximately 150 bp long. In later work from 2013 onward, fluorescent proteins the PCR step was avoided and mRNA was transcribed directly off of a linearize plasmid.

B.3.2 SCE of mRNA

mRNA was diluted to a concentration of 10 ng/μL for transfection. Superase RNAse inhibitor (Life Technologies) was added to solution to prevent degradation.

B.3.3 Bulk Transfection of Tissue Slices with mRNA

For bulk transfection of cells in tissue slices, Lipofectamine 2000 (Life Technologies) was mixed at a 1μL:1 μg ratio with mRNA in 25 μL of Optimem (Life Technologies) prior to a brief (5 minute) incubation and careful deposition onto the surface of slices. A standard coronal slice taken from a P1 murine pup has a cross-sectional area of approximately 0.5 cm^2 and would receive 0.5 to 1 μg of total mRNA for sufficient expression levels.

[2]Human hemoglobin β

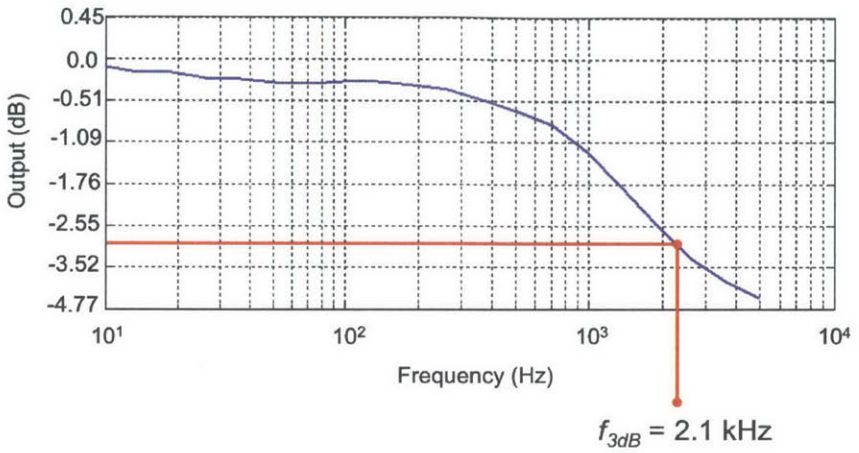

Figure B.1: The electrical model of a glass micropipette consists of a distributed RC network (with the internal ionic solution modeled as a longitudinal resistance and the glass of the micropipette as a shunt capacitance). These properties result in a significant bandwidth limitation on the system as shown, in which $f_{-3dB} \approx 2.1kHz$. As a result, the variety of signals applied to the tip is greatly limited,with even square waves at 1 kHz showing significant bandwidth limitation artifacts.

B.4 Electrical Characterization of Micropipettes

Let's assume that in a glass micropipette the internal diameter r_i and outer diameter r_o maintain a constant ration p such that

$$p = \frac{r_o}{r_i} \tag{B.1}$$

If we assume the micropipette geometry is such to effectively electrically isolate the internal volume from the external volume, the differential shunt capacitance dC_s of a micropipette submerged in a bath can be approximated as

$$dC_s = \frac{2\pi m \epsilon_r \epsilon_o dl}{d} \tag{B.2}$$

where m is the average cross-sectional radius:

$$m = \frac{r_o + r_1}{2} \tag{B.3}$$

With ϵ_o is the permittivity of free space ($8.85 \times 10^{-12} F \cdot m^{-1}$), ϵ_r is the relative permittivity of borosilicate glass ($\epsilon_r \approx 11.8$), dl is the differential longitudinal

distance, and d is the thickness of the glass micropipette wall at that point in l. Substituting and canceling the appropriate values we achieve;

$$\frac{dC_s}{dl} = \frac{\pi(p+1)\epsilon_r\epsilon_o}{p-1} \tag{B.4}$$

The differential longitudinal resistance of the micropipette dR can be calculated as follows:

$$dR = \pi r_i^2 \rho_s dl \tag{B.5}$$

where ρ_s is the resistivity of the ionic solution inside the micropipette.

$$\tau = \frac{dR}{dl} \times \frac{dC}{dl} = \frac{\pi^2 r_i^2 \rho_s (p+1)\epsilon_r\epsilon_o}{p-1} \tag{B.6}$$

Most of these parameters are independent of micropipette geometry and can therefore be lumped into a constant K

$$K = \frac{\pi^2 \rho_s (p+1)\epsilon_r\epsilon_o}{p-1} \tag{B.7}$$

so that

$$\tau = K r_i^2 \tag{B.8}$$

B.5 Detergents for Release of Material

In addition to SDS, we also tested the presence of several other detergents in the RT-PCR workflow since it has been reported that non-ionic detergents can in some instances offset the deleterious effect of anionic detergents on enzymatic reactions. Non-ionic detergents, such as Triton X-100 and NP-40, which lack denaturing capabilities are often reported as being compatible with RT and/or PCR reactions, however we found little quantitative data in the literature regarding the usage of these detergents in high concentration environments in the lower volumes (several μL) and lower starting materials (single to low tens of pg) of single-cell experiments. Addition of 0.1% Triton X-100 to the solution completely inhibited downstream readout.

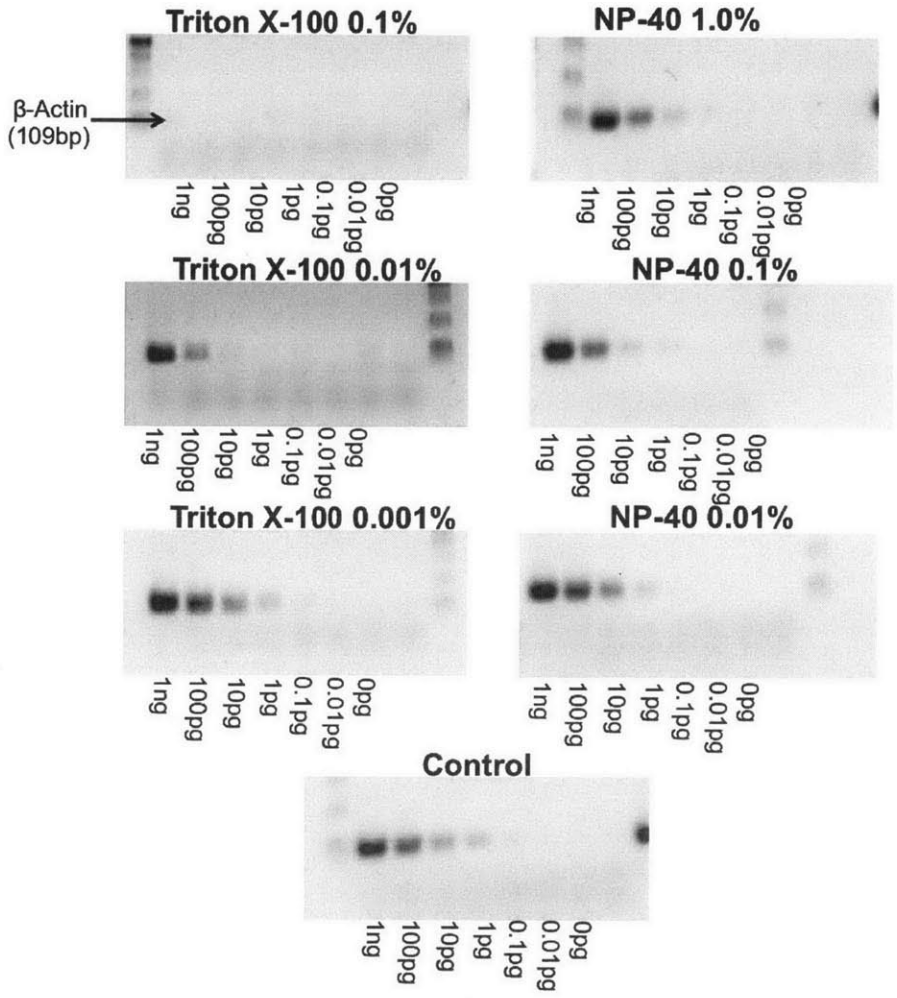

Figure B.2: In an effort to improve deposition into plates, we added non-ionic detergents to the solution. Interestingly, while both Triton X-100 and NP-40 are often listed as RT-PCR compatible detergents because of their non-denaturing capabilites, complete to partial inhibition of the RT-PCR reactions takes place at varying levels of Triton X-100 and to a lesser degree, with NP-40. Care must be taken in using these reagents at such levels since while they seem to not inhibit product at higher concentrations they can completely eliminate it at lower levels on the order of single cells

SCE Pulse Parameters	Observed Efficiency
200 Hz, 20% duty cycle, -10 V, 1second	27.1% (8 in exps**, n = 96)
50 Hz, 2.5% duty cycle, -10 V, 1 second	48.7% (6 in exps, n = 78)
50 Hz, 2.5% duty cycle, -12 V*, 1 second	54.8% (7 in exps, n = 73)
50 Hz, 2.5% duty cycle, -15 V*, 1 second	21.6% (5 in exps, n = 51)
50 Hz, 2.5% duty cycle, -8 V, 1 second	16.7% (5 in exps, n = 60)
50 Hz, 0.5% duty cycle, -10V, 1 second	61.8% (6 in exps, n = 76)
100 Hz, 1% duty cycle, -10 V, 0.5 second	65.6% (6 in exps, n = 64)
100 Hz, 1% duty cycle, -10 V, 0.25 second	44.0% (4 in exps, n = 50)
1 kHz, 10% duty cycle, -10 V, 0.1 second	81.7% (6 in exps, n = 93)
1 kHz, 10% duty cycle, -12 V*, 0.1 second	58.4% (6 in exps, n = 89)
1 kHz, 10% duty cycle, -8 V, 0.1 second	20.3% (5 in exps, n = 59)
1 kHz, 10% duty cycle, -10 V, 0.05 second	60.1% (5 in exps, n = 69)
1 kHz, 10% duty cycle, -10 V, 0.2 second	62.5% (6 in exps, n = 56)

Table B.1: Measured efficiencies for different electroporation pulse parameters for a micropipette tip with approximately 8 M resistance filled with 300 ng·μL-1 pEGFP-N1 and 50μM Alexa Fluor 594 hydrazide in standard Ringers solution. Efficiency was determined from expression of EGFP at 24 hours post-transfection. n = total number of cells that were electroporated in the indicated number of independent experiments. Rise/Fall time of the micropipettes used was measured at 0.23±0.015 ms (n = 8). *Signals were created from an amplifier with ±18V power supply rails driven by a scaled signal from the NIDAQ card. For all -10V signals, the electrode voltage was applied directly by the NIDAQ card. **independent experiments

B.6 Additional SCE Information

We experienced inconsistent and inefficient transformation efficiencies using standard SCE electrical pulse parameters reported in the literature[54, 49] and therefore screened a variety SCE pulse parameters, including different pulse repetition frequencies and pulse duty cycles using our platform. Examples of transfection efficiencies with different pulse parameters are shown in Table B.1. We found that a short 100 millisecond burst of -10V 1 kHz (10% duty cycle) provided the highest efficiency in our system compared to more commonly used lower repetition rate pulses with long total durations such as a 200 Hz (20% duty cycle) or 50 Hz (2.5% duty cycle) repetition rate for a one second duration. Using these pulse parameters with front-loaded micropipettes, we transfected cells in the pyramidal cell layer (PCL) of the CA1 within approximately 40 μm of the surface of organotypic hippocampal slices with 300 ng·μL^{-1} pEGFP-N1 and 50μM Alexa Fluor 594 hydrazide for visualization in standard Ringers solution.

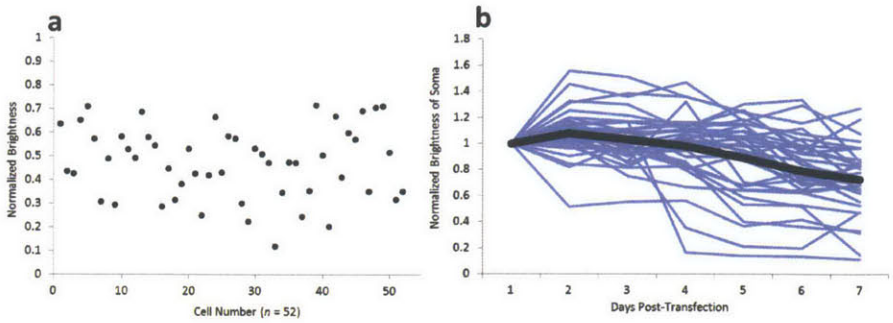

Figure B.3: (a) CA1 pyramidal cells were transfected with pCAG-EGFP using SCE, and the average fluorescence of their soma was measured at 24 hours post-transfection. Brightness was normalized to maximum possible value (214 bits=16384 values). Average normalized brightness was 0.47 ± 0.15 ($n = 52$). (b) Cells were transfected with pCAG-YFP and their fluorescence was monitored over time in a manner similar to in part a. Values were normalized to the first data point taken at 24 hours post-transfection. Black line shows average of all normalized brightness levels (n=35). At 7 days post-transfection, fluorescence intensity was 67.6% of peak value.

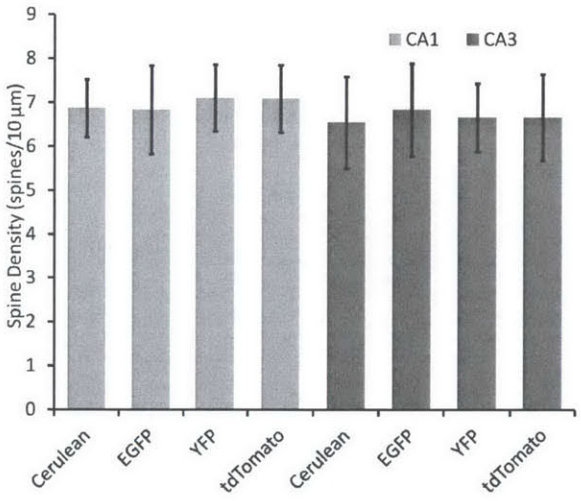

Figure B.4: Cells in both the CA1 (n=50) and CA3 (n=70) of hippocampal organotypic slices were transfected with one of the four fluorescent proteins, Cerulean, EGFP, YFP, or tdTomato, and the linear spine densities of their basal dendritic arbors were sampled (n=600 dendritic spine segments). For each cell type, no significant difference exists in spine density count among the subsets of cells labeled with different fluorescent reporters (ANOVA results: Fcrit = 2.63, F=0.29 and 0.62 for CA1 and CA3, respectively).

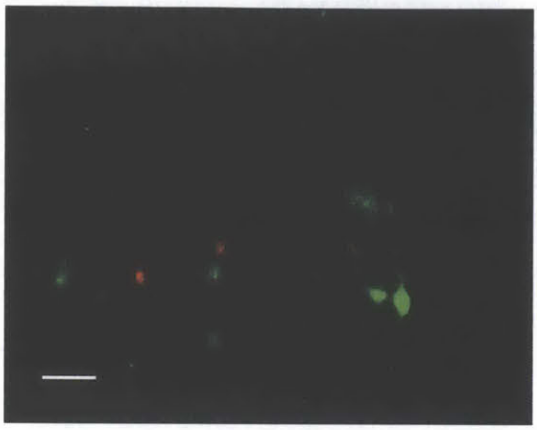

Figure B.5: Cells in the CA1/CA2 region of a hippocampus were transfected in short succession with Alexa Fluor 594 hydrazide (orange) and Alexa Fluor 488 hydrazide (green). Electroporation efficiency, the percentage of cells electroporated by targeting was 95.3±4.2% with mean targeting and electroporation time per cell of 26.5±8.9 seconds per cell in acute slices (n=62 in five separate experiments) Scale bar 30 μm.

Cell Type	Transfection Efficiency
CA3 Pyramidal	79.4% (27/34)
CA1 Pyramidal	65.6% (21/32)
Granule Cell	35.9% (14/39)
Cortical Pyramidal (Layer IV/V)	76.2% (16/21)

Table B.2: Transfection efficiency of plasmids into several cell types in rat tissue using SCE at optimal electrical parameters. Efficiency is assayed as expression of fluorophore at 24 hours post-transfection. Totals are lumped sums over two experiments

B.7 Cell-type Variability in SCE Efficiency

In carrying out experiments, we found distinctive differences in efficiency between certain cell types. In particular pyramidal cells from both were found to be easier to transfect than granule cells from the dentate gyrus region of the (and in general provided higher transfection efficiencies when assayed for fluorescence at 24 hours) as shown in Table B.2. Variability in transfection efficiency between cell types is common knowledge in the field.

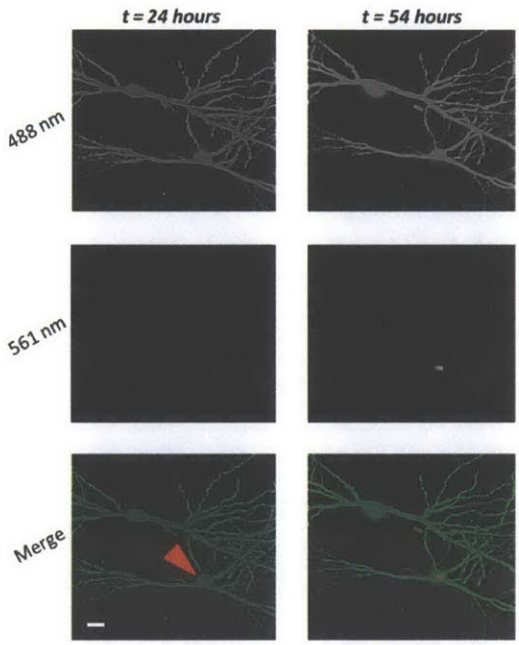

Figure B.6: CA2/CA3 cells were rapidly transfected with pCAG-EGFP using our system. At 24 hours following first-transfection 23 out of 30 cells (efficiency: 76.7%) expressed EGFP. Twelve of the expressing cells were then re-transfected by our system at 30 hours following first-transfection with a nuclear-localization-mCherry plasmid (red-arrow). 24 hours following second-transfection, cells were analyzed for expression. 100% (n=11) of non re-transfected (control) cells continued to expressed EGFP. 16.7% (2/12) of re-transfected cells were no longer visible, 41.7% (4/12) were expressing both mCherry NLS and EGFP, and 50% (6/12) expressed only EGFP. Scale bar 15 μm.

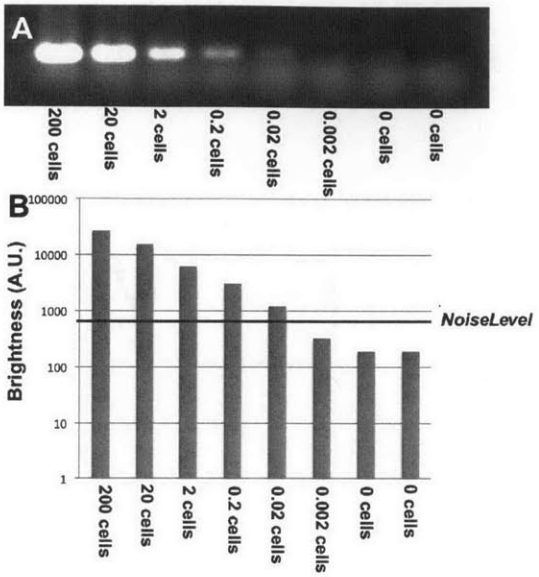

Figure B.7: Serial dilutions of estimated cellular content of total RNA (A) were used to generate standard curves from fluorescent readout (B)

B.8 Additional SCS Analytical Information

B.8.1 Semi-Quantitative Analysis of Recovered Material

For experiments where we develop an estimate of recovered cellular material (including initial deposition experiments using synthetic YFP), serial dilutions of murine whole-brain lysate were used to develop standard curves using a linear least squares method, one of which is shown in Figure B.7. Making the rough assumption of relatively uniform distribution of house-keeping genes across all cell types, we could then match up quantified fluorescence of PCR products at the correct location with the corresponding point in the derived standard curve (Figure B.8).

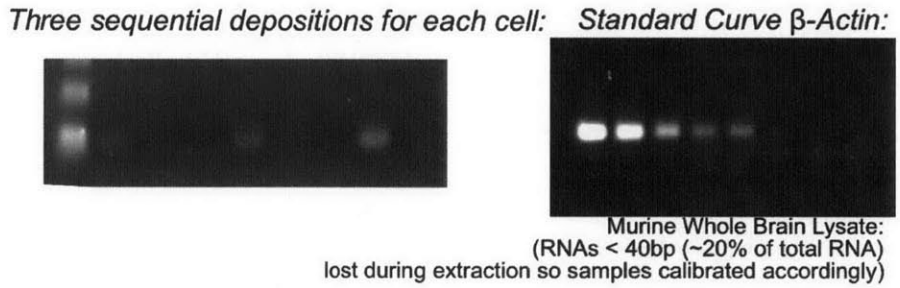

Figure B.8: Readout from an experiment (left) is compared to its standard curve (right).

B.8.2 RT-PCR Analysis

Two types of RT-PCR analysis were carried out depending on the experiment: Direct RT-PCR and Nested RT-PCR. In both cases, the RT step (Reverse Transcription) was carried out identically. In all cases, following cell harvesting and deposition of content into PCR-compatible 384 well plates (Bio-Rad), samples were quickly frozen at -80 °C. Reverse Transcription was carried out in sterile PCR strip tubes using the recipe found in Table B.5. Because sample volume would sometimes vary based off of experiment or even evaporation, final reaction volume could vary by ± 1 μL, however generally it was less. We verified that this variability in volume had non-detectable effect on overall reaction efficiency. Samples were incubated at 42°C for 50 minutes followed by storage at 4°C.

Direct PCR:

In all cases of PCR, components were sourced from Kapa HiFi Hotstart PCR kit components (Kapa Biosystems). In Direct PCR, only one gene was analyzed per reaction. These experiments were used generally for transcript species known to exist in high numbers such as "housekeeping" genes such as β-Actin or GAPDH. 2 μL of sample was taken from RT reaction (approximately 6 μL following incubation) and mixed with PCR components as described in Table B.6. The PCR program used was an initial denaturation step 95°C for 3 min followed by 34 cycles of 98°C for 30 sec, 65°C for 15 sec, and 72°C for 40 sec, and a final extension step of 72°C for 3 min. Following this, samples in their entirety were run out in 1.5% agarose gels and subsequently imaged for analysis. Length of product was used to confirm the amplification of the correct product.

Nested PCR:

Nested PCR is used to analyze multiple transcripts and is based on previously published protocols [124]. It was used primarily in analyzing cell cross-contamination where we looked at multiple, possibly low-expression level markers, many of which are listed in Table , for example. The entire RT sample was used as input for a pre-amplification step in which lowered concentrations of all primer sets of interest were added. Generally primer concentrations were 10% of what they were in single-step PCR, however traditional housekeeping genes were generally less, down to 1% (100 nM). The pre-amp PCR volume was approximately 24 μL as shown in Table B.7. Reaction conditions were as follows: an initial denaturation step 95°C for 3 min followed by 20 cycles of 98°C for 30 sec, 65°C for 15 sec, and 72°C for 40 sec, and a final extension step of 72°C for 3 min. Following this pre-amplification step, 2 μL of sample from first reaction

Primer	Sequence
YFP-1 Forward	ACGTAAACGGCCACAAGTTC
YFP-1 Reverse	CTGCTTGTCGGCCATGATATAG
YFP-2 Forward	GCTGACCCTGAAGTTCATCTG
YFP-2 Reverse	CGATGTTGTGGCGGATCTT
β-Actin Forward	CTCCCTGGAGAAGAGCTATGA
β-Actin Reverse	CACAGGATTCCATACCCAAGAA
GAPDH Forward	GTGCTGAGTATGTCGTGGAG
GAPDH Reverse	GGATGCAGGGATGATGTTCT
β-III-Tubulin Forward	GGAGATCGTGCACATCCAG
β-III-Tubulin Reverse	GCACCACTCTGACCAAAGATA
GFAP Forward	CACCAAACTGGCTGATGTCTA
GFAP Reverse	CCAGGGTGGCTTCATCTG

Table B.3: Primer sequences for initial verification of cellular collection.

were added to the recipe found in Table B.8. The amplification program for this second program was as follows: an initial denaturation step 95°C for 3 min followed by 35 cycles of 98°C for 30 sec, 65°C for 15 sec, and 72°C for 40 sec, and a final extension step of 72°C for 3 min. Following this, samples in their entirety were run out in 1.5% agarose gels and subsequently imaged for analysis. Length of product was used to confirm the amplification of the correct product.

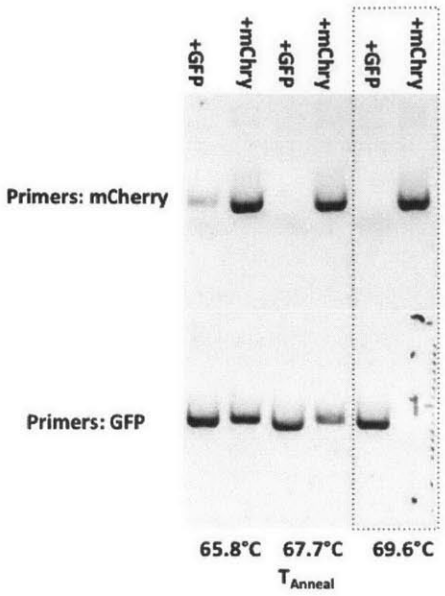

Figure B.9: Eight sets of primers (four for EGFP and four for mCherry) were designed and ordered. Because of the high sequence similarity between EGFP and mCherry, in order to determine exclusive detection of desired signal, the sets had to be analyzed with varying anneal temperatures. While, many sets showed near indistinguishable responses to both EGFP and mCherry, one EGFP set (#4) and one mCherry set (#3) were found to show sufficient exclusivity at an anneal temperature of 69.6 degrees Celsius. (Correct Temperature is enclosed by dashed box).

Future work will analyze for the presence/absence of known artificial markers, including the two fluorescent species EGFP and mCherry. Primer sets have been developed for this experiment and are shown in Figure B.9.

B.8.3 Cell Sampling Real-Time Analysis

B.9 Oil Deposition

In conducting in initial experiments to determine the best means of sample deposition from a micropipette, we briefly pursued deposition into oil[3] before turning to focus on deposition into small $\approx 5\mu L$ water volumes. There were two main reasons for this switch: First, the introduction of oil into the workflow resulted in additional complexities that we chose to avoid (clogging of tip, etc...).

[3]Idea Credit: Yao Zhou

Primer	Sequence
β-III-Tubulin-1Forward	CTAGATGTCGTGCGGAAAGAG
β-III-Tubulin-1 Reverse	AGTAGGTCTCGTCTGTGTTCT
β-III-Tubulin-2Forward	AATGACCTGGTGTCCGAGTA
β-III-Tubulin-2 Reverse	CTTTAACCTGGGAGCCCTAATG
β-III-Tubulin-3Forward	GATTCCCTGGTCAGCTCAAT
β-III-Tubulin-3 Reverse	TCGTCCACCTCCTTCATAGA
GFAP Forward	GAAAGTCCCTGAGGCAAAGT
GFAP Reverse	GTCTTCCAGAGAACGGGTTATT
GAD1-3 Forward	CTTCCGGATGGTCATCTCTAAC
GAD1-3 Reverse	CTTCAGTGAGATGGCCTAGATG
vGlut1 Forward	GGCAGTGACGAAAGTGAAATG
vGlut1 Reverse	GAGGCAGTTGAGAGGGAAAG
TH Forward	CTACTGTCTGCCCGTGATTT
TH Reverse	GGTAGGTTTGATCTTGGTAGGG
SST Forward	CCCAGACTCCGTCAGTTTC
SST Reverse	GGTCTGGCTAGGACAACAATA
PV Forward	CCTCCTGAGTTTCTGTTCAGTT
PV Reverse	TGGGAAAGGTGCAGAGATTG
NPY Forward	GCTCTGCGACACTACATCAA
NPY Reverse	ACAACAACAACAACAAGGGAAA
TBR1 Forward	CTTGTCTTGGCCTCCCTATTT
TBR1 Reverse	GTGAGAAAGCCACCACTATGA
TBR2 (EOMES) Forward	GAATGAGCCCACCTGTCTTC
TBR2 Reverse	TGCCTTTGGAGGTGTCTTTAC
FezF2 Forward	GCCTTCCATCAGGTCTACAATC
FezF2 Reverse	GTCATCGAGGACACGTTTACAT
DLX1 Forward	GTGTCTGCTGTCCTCATTCTAC
DLX1 Reverse	CACTCCATGTCCCAGAGAATTT
DLX2 Forward	CTCACCCAAACTCAGGTCAA
DLX2 Reverse	TCTGCGAAGGATGCAGAAG
DLX5 Forward	CTCTCTAGGACTGACGCAAAC
DLX5 Reverse	GCAAGAGAAAGTAGCCCATCTA
DLX6 Forward	GGAAGCCTCGGACCATTTATT
DLX6 Reverse	GTCACATCATCTGTGGTCTCTG
mCherry Forward	GACTACTTGAAGCTGTCCTTCC
mCherry Reverse	CTTCAGCCTCTGCTTGATCTC
GFP Forward	GGAGCGCACCATCTTCTT
GFP Reverse	GGGTGTTCTGCTGGTAGTG

Table B.4: Primer sequences Cell Selectivity Assay

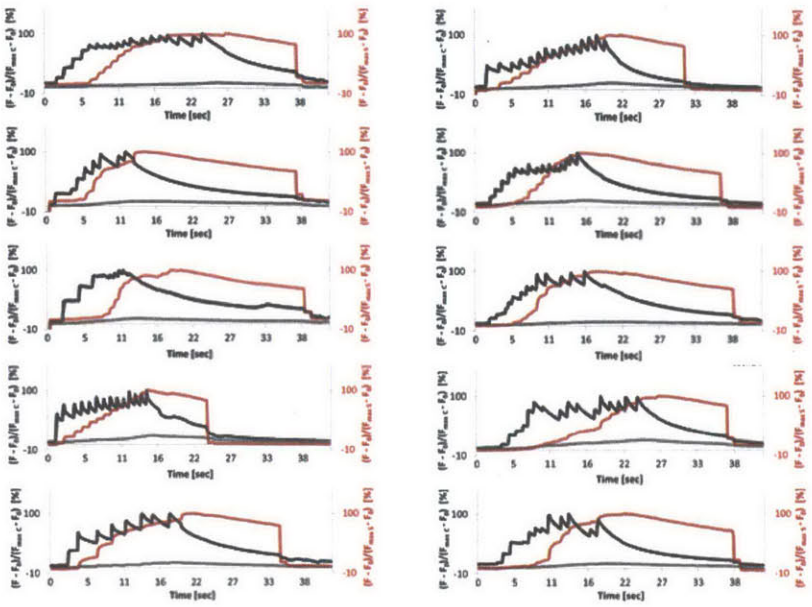

Figure B.10: Ten separate cell samplings shown here were recorded and analyzed as discussed in Section 4.4.1 and Figure 4.9

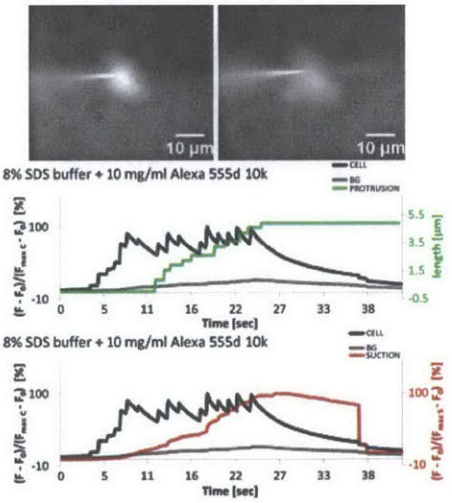

Figure B.11: Injection of SDS resulted in overall growth of the cell, through a combination of volume increase from the bulk of the lysis buffer and integration of SDS into the membrane of the cell. The integration was not always uniform, however, oftentimes resulting in distinct protrusion outgrowths of cells during the course of injection and collection. (See the outgrowth in the lower left corner of the cell between the left and right panel.

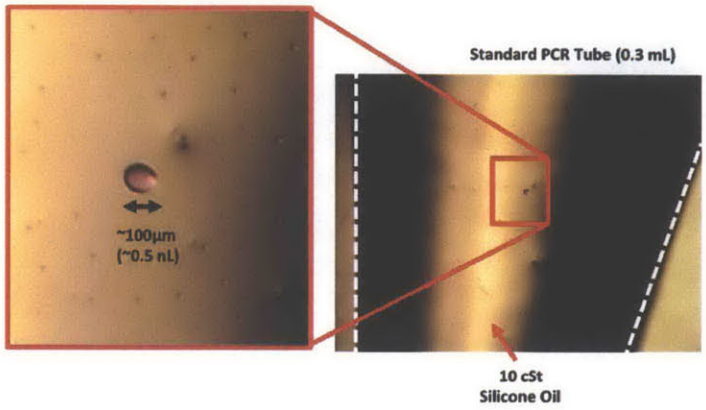

Figure B.12: Solution from a micropipette deposited into an oil environment remains together, allowing a means to transfer the contents out of a micropipette while minimizing dilution. This may prove beneficial in future work adapting this technique to protein analysis.

Second, in order to emphasize the flexibility in applying this technique to standardized techniques, we decided to remove this unproven step and instead focus on the novel sampling method

The oil-deposition provided a potential means of freeing the sample from the confines of the micropipette tip while still allowing it to stay together because of the separation of its aqueous environment from the oil environment. Silicone oil (25 cSt) (Sigma-Aldrich) was used for experiments. As shown in Figure B.12, droplets on the order of nL could be generated and were stable. A basic oil-collection workflow was developed and is shown in Figure B.13.

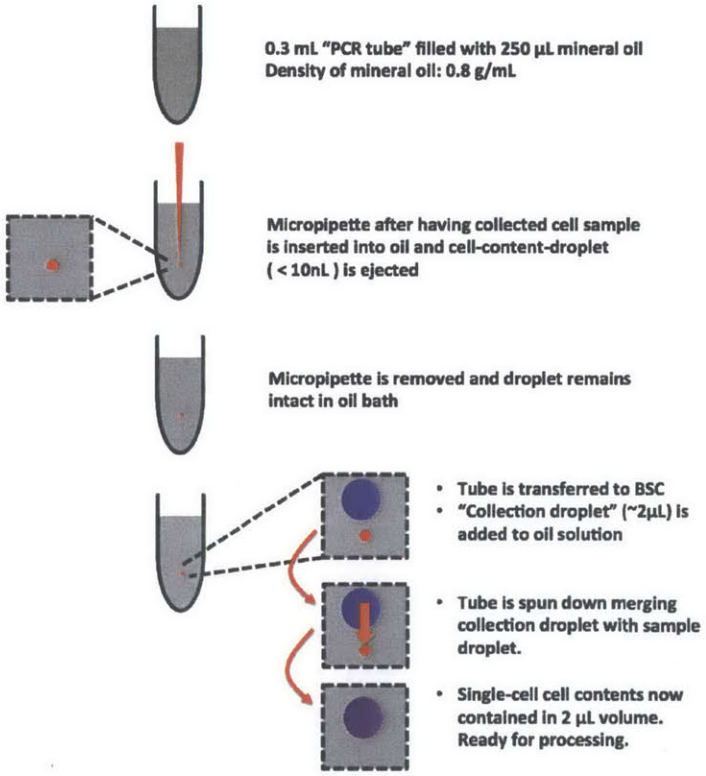

Figure B.13: Basic Oil Collection Workflow.

Component	Quantity per reaction
10 mM dNTP	0.35 µL
5X ProtoScriptII Buffer	1.4 µL
ProtoScript II RT (200 U/µL)	0.35 µL
100 mM DTT	0.35 µL
20U/µL Superase^{TM} Inhibitor	0.35 µL
0.1% SDS Buffer	1.00 µL
Cell Sample	3.00 µL
Total	7.15 µL

Table B.5: First-Strand Synthesis Reaction Components

Component	Quantity per reaction
Water	3.63 µL
HiFi w/ Mg^{+2} Buffer	1.6 µL
10 mM dNTP	0.48 µL
20 µM primers	0.128 µL
Kapa HiFi Hotstart Polymerase	0.16 µL
RT Sample	2.0 µL
Total	8.0 µL

Table B.6: Non-nested Single-Step PCR Reaction Formula

B.10 Solutions and Formulas

Component	Quantity per reaction
Water	10.89 µL
HiFi w/ Mg^{+2} Buffer	4.8 µL
10 mM dNTP	1.44 µL
Primer Mix*	0.384 µL
Kapa HiFi Hotstart Polymerase	0.48 µL
RT Sample	6.0 µL
Total	24.0 µL

Table B.7: Nested-PCR Step 1 Reaction Formula. *Primer Mixes varied depending on reaction condition, however the concentration of most primers was 1 µM, with the exception of β-Actin and GAPDH, which were 0.1 µM

Component	Quantity per reaction
Water	3.63 µL
HiFi w/ Mg^{+2} Buffer	1.6 µL
10 mM dNTP	0.48 µL
20 µM primers	0.128 µL
Kapa HiFi Hotstart Polymerase	0.16 µL
Pre-Amp Sample	2.0 µL
Total	8.0 µL

Table B.8: Nested-PCR Step 2 Reaction Formula

Component	Concentration
Tris-HCl	50 mM
SDS	2.0%
Glycerol	5.0%
EDTA	5.0 mM
NaF	1.0 mM

Table B.9: Base Lysis Buffer

Component	Quantity
MEM+GlutaMax^{TM}	100 mL
Earle's Balanced Salt Solution	38 mL
HI Horse Serum	50 mL
720 mM D-Glucose Stock	12 mL
Nystatin 10,000U/mL	120 µL
Total	200 mL

Table B.10: Organotypic Slice Culture Formula

Primers were designed to have a T_M of approximately 55°C, which in the higher salt conditions of Kapa Bioscience PCR kits, was generally found to be 68°C. An anneal temperature of 65°C was subsequently used to ensure high yield with minimal off-target signal in PCR.

B.11 Tissue Culture Solutions

Component	Concentration
NaCl	135 mM
KCl	5.5 mM
$MgCl_2 \cdot 6H_2O$	1.5mM
$CaCl_2 \cdot 2H_2O$	1.5mM
HEPES	5mM
Total Osmolarity:	295 mOsm

Table B.11: Ringers Solution used in Rat Slice Culture

Bibliography

[1] T. Nawy, "Single-cell sequencing," *Nature Methods*, vol. 11, pp. 18–18, Dec. 2013.

[2] P. C. Blainey and S. R. Quake, "Dissecting genomic diversity, one cell at a time," *Nature Methods*, vol. 11, pp. 19–21, Dec. 2013.

[3] J. Eberwine, J.-Y. Sul, T. Bartfai, and J. Kim, "The promise of single-cell sequencing," *Nature Methods*, vol. 11, pp. 25–27, Dec. 2013.

[4] Nature, "Method of the Year 2013," *Nature Methods*, vol. 11, pp. 1–1, Dec. 2013.

[5] P. Fara, "A microscopic reality tale.," *Nature*, vol. 459, pp. 642–4, June 2009.

[6] J. Carey, *Eyewitness to Science*. Harvard University Press, 1997.

[7] T. Schwann, *Microscopical researches into the accordance in the structure and growth of animals and plants*. 1849 engli ed., 1838.

[8] I. B. Levitan and L. K. Kaczmarek, *The Neuron*. New York, New York: Oxford University Press, 3 ed., 2002.

[9] J. Pawley, *Handbook of Biological Confocal Microscopy*. Springer, 3rd ed., 2006.

[10] Y. Okada, *Patch Clamp Techniques*. Springer Protocols, 2012.

[11] A. P. Minton, "The influence of macromolecular crowding and macromolecular confinement on biochemical reactions in physiological media.," *The Journal of biological chemistry*, vol. 276, pp. 10577–80, Apr. 2001.

[12] M. Zeiler, W. L. Straube, E. Lundberg, M. Uhlen, and M. Mann, "A Protein Epitope Signature Tag (PrEST) library allows SILAC-based absolute quantification and multiplexed determination of protein copy numbers in cell lines.," *Molecular & cellular proteomics : MCP*, vol. 11, p. O111.009613, Mar. 2012.

[13] Y. Sasagawa, I. Nikaido, T. Hayashi, H. Danno, K. D. Uno, T. Imai, and H. R. Ueda, "Quartz-Seq: a highly reproducible and sensitive single-cell RNA sequencing method, reveals non-genetic gene-expression heterogeneity.," *Genome biology*, vol. 14, p. R31, Apr. 2013.

[14] S. Qiu, S. Luo, O. Evgrafov, R. Li, G. P. Schroth, P. Levitt, J. A. Knowles, and K. Wang, "Single-neuron RNA-Seq: technical feasibility and reproducibility.," *Frontiers in genetics*, vol. 3, p. 124, Jan. 2012.

[15] I. J. Fijalkowska, R. M. Schaaper, and P. Jonczyk, "DNA replication fidelity in Escherichia coli: a multi-DNA polymerase affair.," *FEMS microbiology reviews*, vol. 36, pp. 1105–21, Nov. 2012.

[16] L. Cai, N. Friedman, and X. S. Xie, "Stochastic protein expression in individual cells at the single molecule level.," *Nature*, vol. 440, pp. 358–62, Mar. 2006.

[17] E. M. Ozbudak, M. Thattai, I. Kurtser, A. D. Grossman, and A. van Oudenaarden, "Regulation of noise in the expression of a single gene.," *Nature genetics*, vol. 31, pp. 69–73, May 2002.

[18] M. B. Elowitz, A. J. Levine, E. D. Siggia, and P. S. Swain, "Stochastic gene expression in a single cell.," *Science (New York, N.Y.)*, vol. 297, pp. 1183–6, Aug. 2002.

[19] A. Raj, C. S. Peskin, D. Tranchina, D. Y. Vargas, and S. Tyagi, "Stochastic mRNA synthesis in mammalian cells.," *PLoS biology*, vol. 4, p. e309, Oct. 2006.

[20] S. L. Spencer, S. Gaudet, J. G. Albeck, J. M. Burke, and P. K. Sorger, "Non-genetic origins of cell-to-cell variability in TRAIL-induced apoptosis.," *Nature*, vol. 459, pp. 428 32, May 2009.

[21] T. L. Yuan, G. Wulf, L. Burga, and L. C. Cantley, "Cell-to-cell variability in PI3K protein level regulates PI3K-AKT pathway activity in cell populations.," *Current biology : CB*, vol. 21, pp. 173–83, Mar. 2011.

[22] T. F. Weiss, *Cellular Biophysics: Electrical Properties.* MIT Press, 1998.

[23] S. M. Potter and T. B. DeMarse, "A new approach to neural cell culture for long-term studies.," *Journal of neuroscience methods*, vol. 110, pp. 17–24, Sept. 2001.

[24] B. Marte, "Tumour heterogeneity.," *Nature*, vol. 501, p. 327, Sept. 2013.

[25] A. Abbott, "Laboratory animals: the Renaissance rat.," *Nature*, vol. 428, pp. 464–6, Apr. 2004.

[26] J. Livet, T. A. Weissman, H. Kang, R. W. Draft, J. Lu, R. A. Bennis, J. R. Sanes, and J. W. Lichtman, "Transgenic strategies for combinatorial expression of fluorescent proteins in the nervous system.," *Nature*, vol. 450, pp. 56–62, Nov. 2007.

[27] S. Hampel, P. Chung, C. E. McKellar, D. Hall, L. L. Looger, and J. H. Simpson, "Drosophila Brainbow: a recombinase-based fluorescence labeling technique to subdivide neural expression patterns.," *Nature methods*, vol. 8, pp. 253–9, Mar. 2011.

[28] W. D. Lyman, M. Tricoche, W. C. Hatch, Y. Kress, F. C. Chiu, and W. K. Rashbaum, "Human fetal central nervous system organotypic cultures.," *Brain Research. Developmental brain research*, vol. 60, pp. 155–60, July 1991.

[29] V. M. Vostrikov, N. S. Kolomeets, O. P. Aleksandrova, I. V. Viktorov, N. A. Uranova, and G. T. Sukhikh, "Organotypic cultures of free-floating slices of human embryo medulla oblongata.," *Neuroscience and Behavioral Physiology*, vol. 35, pp. 9 15, Jan. 2005.

[30] R. W. H. Verwer, E. J. G. Dubelaar, W. T. J. M. C. Hermens, and D. F. Swaab, "Tissue cultures from adult human postmortem subcortical brain areas.," *Journal of cellular and molecular medicine*, vol. 6, no. 3, pp. 429–32.

[31] N. Al-Jaberi, S. Lindsay, S. Sarma, N. Bayatti, and G. J. Clowry, "The Early Fetal Development of Human Neocortical GABAergic Interneurons.," *Cerebral cortex (New York, N.Y. : 1991)*, pp. bht254 , Sept. 2013.

[32] A. Ernst, K. Alkass, S. Bernard, M. Salehpour, S. Perl, J. Tisdale, G. Possnert, H. Druid, and J. Frisén, "Neurogenesis in the striatum of the adult human brain.," *Cell*, vol. 156, pp. 1072–83, Feb. 2014.

[33] J. A. O'Brien and S. C. R. Lummis, "Biolistic transfection of neuronal cultures using a hand-held gene gun.," *Nature Protocols*, vol. 1, pp. 977–81, Jan. 2006.

[34] G. Woods and K. Zito, "Preparation of gene gun bullets and biolistic transfection of neurons in slice culture.," *Journal of visualized experiments : JoVE*, Jan. 2008.

[35] D. Karra and R. Dahm, "Transfection techniques for neuronal cells.," *The Journal of neuroscience : the official journal of the Society for Neuroscience*, vol. 30, pp. 6171–7, May 2010.

[36] R. C. Murphy and A. Messer, "Gene transfer methods for CNS organotypic cultures: a comparison of three nonviral methods.," *Molecular Therapy*, vol. 3, pp. 113–21, Jan. 2001.

[37] I. R. Wickersham, S. Finke, K.-K. Conzelmann, and E. M. Callaway, "Retrograde neuronal tracing with a deletion-mutant rabies virus.," *Nature methods*, vol. 4, pp. 47–9, Jan. 2007.

[38] K. K. Ghosh, L. D. Burns, E. D. Cocker, A. Nimmerjahn, Y. Ziv, A. E. Gamal, and M. J. Schnitzer, "Miniaturized integration of a fluorescence microscope," *Nature Methods*, vol. 8, pp. 871–878, Sept. 2011.

[39] J. W. Lichtman, J. Livet, and J. R. Sanes, "A technicolour approach to the connectome.," *Nature reviews. Neuroscience*, vol. 9, pp. 417–22, June 2008.

[40] J. M. Spaethling, D. Piel, H. Dueck, P. T. Buckley, J. F. Morris, S. A. Fisher, J. Lee, J.-Y. Sul, J. Kim, T. Bartfai, S. G. Beck, and J. H. Eberwine, "Serotonergic neuron regulation informed by in vivo single-cell transcriptomics.," *FASEB journal : official publication of the Federation of American Societies for Experimental Biology*, vol. 28, pp. 771–80, Feb. 2014.

[41] E. Taverna, C. Haffner, R. Pepperkok, and W. B. Huttner, "A new approach to manipulate the fate of single neural stem cells in tissue.," *Nature neuroscience*, vol. 15, pp. 329–37, Feb. 2012.

[42] Y. Komarova, J. Peloquin, and G. Borisy, "Microinjection of Protein Samples," *Cold Spring Harbor Protocols*, vol. 2007, pp. pdb.prot4657–pdb.prot4657, Jan. 2007.

[43] Y. Zhang, X. Zhou, J. Lu, J. Lichtman, D. Adjeroh, and S. T. C. Wong, "3D Axon structure extraction and analysis in confocal fluorescence microscopy images.," *Neural computation*, vol. 20, pp. 1899–927, Aug. 2008.

[44] J. A. Lundqvist, F. Sahlin, M. A. Aberg, A. Strömberg, P. S. Eriksson, and O. Orwar, "Altering the biochemical state of individual cultured cells and organelles with ultramicroelectrodes.," *Proceedings of the National Academy of Sciences of the United States of America*, vol. 95, pp. 10356–60, Oct. 1998.

[45] D. Wang, R. Lagerstrom, C. Sun, L. Bishof, P. Valotton, and M. Götte, "HCA-vision: automated neurite outgrowth analysis.," *Journal of biomolecular screening : the official journal of the Society for Biomolecular Screening*, vol. 15, pp. 1165–70, Oct. 2010.

[46] K. Nolkrantz, C. Farre, A. Brederlau, R. I. D. Karlsson, C. Brennan, P. S. Eriksson, S. G. Weber, M. Sandberg, and O. Orwar, "Electroporation of Single Cells and Tissues with an Electrolyte-filled Capillary," *Analytical Chemistry*, vol. 73, pp. 4469–4477, Sept. 2001.

[47] F. RYTTSEN, "Characterization of Single-Cell Electroporation by Using Patch-Clamp and Fluorescence Microscopy," *Biophysical Journal*, vol. 79, pp. 1993–2001, Oct. 2000.

[48] K. Haas, K. Jensen, W. C. Sin, L. Foa, and H. T. Cline, "Targeted electroporation in Xenopus tadpoles in vivo–from single cells to the entire brain.," *Differentiation*, vol. 70, pp. 148–54, July 2002.

[49] J. Rathenberg, T. Nevian, and V. Witzemann, "High-efficiency transfection of individual neurons using modified electrophysiology techniques.," *Journal of Neuroscience Methods*, vol. 126, pp. 91–8, June 2003.

[50] P. Lovell, S. H. Jezzini, and L. L. Moroz, "Electroporation of neurons and growth cones in Aplysia californica," *Journal of Neuroscience Methods*, vol. 151, pp. 114–120, Mar. 2006.

[51] B. Judkewitz, M. Rizzi, K. Kitamura, and M. Häusser, "Targeted single-cell electroporation of mammalian neurons in vivo.," *Nature Protocols*, vol. 4, pp. 862–9, Jan. 2009.

[52] M. Boudes, S. Pieraut, J. Valmier, P. Carroll, and F. Scamps, "Single-cell electroporation of adult sensory neurons for gene screening with RNA interference mechanism.," *Journal of Neuroscience Methods*, vol. 170, pp. 204–11, May 2008.

[53] K. Haas, "Single-Cell Electroporationfor Gene Transfer In Vivo," *Neuron*, vol. 29, pp. 583 591, Mar. 2001.

[54] K. Kitamura, B. Judkewitz, M. Kano, W. Denk, and M. Häusser, "Targeted patch-clamp recordings and single-cell electroporation of unlabeled neurons in vivo.," *Nature Methods*, vol. 5, pp. 61–7, Jan. 2008.

[55] M. Tsukakoshi, S. Kurata, Y. Nomiya, Y. Ikawa, and T. Kasuya, "A novel method of DNA transfection by laser microbeam cell surgery," *Applied Physics B Photophysics and Laser Chemistry*, vol. 35, pp. 135–140, Nov. 1984.

[56] J. D. Steinmeyer, C. L. Gilleland, C. Pardo-Martin, M. Angel, C. B. Rohde, M. A. Scott, and M. F. Yanik, "Construction of a femtosecond laser microsurgery system.," *Nature Protocols*, vol. 5, pp. 395–407, Jan. 2010.

[57] D. R. Tripathy, A. K. Dinda, and S. Dasgupta, "A simple assay for the ribonuclease activity of ribonucleases in the presence of ethidium bromide.," *Analytical biochemistry*, vol. 437, pp. 126–9, June 2013.

[58] B. W. Okaty, K. Sugino, and S. B. Nelson, "A quantitative comparison of cell-type-specific microarray gene expression profiling methods in the mouse brain.," *PloS one*, vol. 6, p. e16493, Jan. 2011.

[59] R. V. Grindberg, J. L. Yee-Greenbaum, M. J. McConnell, M. Novotny, A. L. O'Shaughnessy, G. M. Lambert, M. J. Araúzo-Bravo, J. Lee, M. Fishman, G. E. Robbins, X. Lin, P. Venepally, J. H. Badger, D. W. Galbraith, F. H. Gage, and R. S. Lasken, "RNA-sequencing from single nuclei.," *Proceedings of the National Academy of Sciences of the United States of America*, vol. 110, pp. 19802–7, Dec. 2013.

[60] D. A. Jaitin, E. Kenigsberg, H. Keren-Shaul, N. Elefant, F. Paul, I. Zaretsky, A. Mildner, N. Cohen, S. Jung, A. Tanay, and I. Amit, "Massively parallel single-cell RNA-seq for marker-free decomposition of tissues into cell types.," *Science (New York, N.Y.)*, vol. 343, pp. 776–9, Feb. 2014.

[61] D. W. Y. Ho, Z. F. Yang, K. Yi, C. T. Lam, M. N. P. Ng, W. C. Yu, J. Lau, T. Wan, X. Wang, Z. Yan, H. Liu, Y. Zhang, and S. T. Fan, "Gene expression profiling of liver cancer stem cells by RNA-sequencing.," *PloS one*, vol. 7, p. e37159, Jan. 2012.

[62] I. C. Macaulay and T. Voet, "Single cell genomics: advances and future perspectives.," *PLoS genetics*, vol. 10, p. e1004126, Jan. 2014.

[63] C. Berger, H. Harzer, T. R. Burkard, J. Steinmann, S. van der Horst, A.-S. Laurenson, M. Novatchkova, H. Reichert, and J. A. Knoblich, "FACS purification and transcriptome analysis of drosophila neural stem cells reveals a role for Klumpfuss in self-renewal.," *Cell reports*, vol. 2, pp. 407–18, Aug. 2012.

[64] P. R. Langer-Safer, M. Levine, and D. C. Ward, "Immunological method for mapping genes on Drosophila polytene chromosomes.," *Proceedings of the National Academy of Sciences of the United States of America*, vol. 79, pp. 4381–5, July 1982.

[65] A. R. Buxbaum, B. Wu, and R. H. Singer, "Single β-actin mRNA detection in neurons reveals a mechanism for regulating its translatability.," *Science (New York, N.Y.)*, vol. 343, pp. 419–22, Jan. 2014.

[66] J. H. Lee, E. R. Daugharthy, J. Scheiman, R. Kalhor, J. L. Yang, T. C. Ferrante, R. Terry, S. S. F. Jeanty, C. Li, R. Amamoto, D. T. Peters, B. M. Turczyk, A. H. Marblestone, S. A. Inverso, A. Bernard, P. Mali, X. Rios, J. Aach, and G. M. Church, "Highly Multiplexed Subcellular RNA Sequencing in Situ," *Science*, pp. science.1250212–, Feb. 2014.

[67] R. D. Mitra, J. Shendure, J. Olejnik, Edyta-Krzymanska-Olejnik, and G. M. Church, "Fluorescent in situ sequencing on polymerase colonies.," *Analytical biochemistry*, vol. 320, pp. 55–65, Sept. 2003.

[68] M. F. Haroon, C. T. Skennerton, J. A. Steen, N. Lachner, P. Hugenholtz, and G. W. Tyson, "In-solution fluorescence in situ hybridization and

fluorescence-activated cell sorting for single cell and population genome recovery.," *Methods in enzymology*, vol. 531, pp. 3–19, Jan. 2013.

[69] X. Shi, J. Kleeff, Z.-W. Zhu, B. Schmied, W.-H. Tang, A. Zimmermann, M. W. Buchler, and H. Friess, "Gene-expression analysis of single cells-nested polymerase chain reaction after laser microdissection.," *World journal of gastroenterology : WJG*, vol. 9, pp. 1337–41, June 2003.

[70] M. R. Emmert-Buck, R. F. Bonner, P. D. Smith, R. F. Chuaqui, Z. Zhuang, S. R. Goldstein, R. A. Weiss, and L. A. Liotta, "Laser Capture Microdissection," *Science*, vol. 274, pp. 998–1001, Nov. 1996.

[71] A. Mustafa, C. Cenayko, R. R. Mitry, and A. Quaglia, "Laser microdissection microscopy: application to cell culture.," *Methods in molecular biology (Clifton, N.J.)*, vol. 806, pp. 385–92, Jan. 2012.

[72] O. V. Podgorny, "Live cell isolation by laser microdissection with gravity transfer.," *Journal of biomedical optics*, vol. 18, p. 55002, May 2013.

[73] D. Lovatt, B. K. Ruble, J. Lee, H. Dueck, T. K. Kim, S. Fisher, C. Francis, J. M. Spaethling, J. A. Wolf, M. S. Grady, A. V. Ulyanova, S. B. Yeldell, J. C. Griepenburg, P. T. Buckley, J. Kim, J.-Y. Sul, I. J. Dmochowski, and J. Eberwine, "Transcriptome in vivo analysis (TIVA) of spatially defined single cells in live tissue.," *Nature methods*, vol. 11, pp. 190–196, Jan. 2014.

[74] J. Eberwine, H. Yeh, K. Miyashiro, Y. Cao, S. Nair, R. Finnell, M. Zettel, and P. Coleman, "Analysis of gene expression in single live neurons.," *Proceedings of the National Academy of Sciences*, vol. 89, pp. 3010–3014, Apr. 1992.

[75] B. Lambolez, E. Audinat, P. Bochet, F. Crépel, and J. Rossier, "AMPA receptor subunits expressed by single Purkinje cells.," *Neuron*, vol. 9, pp. 247–58, Aug. 1992.

[76] R. Trouillon, M. K. Passarelli, J. Wang, M. E. Kurczy, and A. G. Ewing, "Chemical analysis of single cells.," *Analytical chemistry*, vol. 85, pp. 522–42, Jan. 2013.

[77] J. Morris, J. M. Singh, and J. H. Eberwine, "Transcriptome analysis of single cells.," *Journal of visualized experiments : JoVE*, Jan. 2011.

[78] J. T. Aerts, K. R. Louis, S. R. Crandall, G. Govindaiah, C. L. Cox, and J. V. Sweedler, "Patch clamp electrophysiology and capillary electrophoresis-mass spectrometry metabolomics for single cell characterization.," *Analytical chemistry*, vol. 86, pp. 3203 8, Mar. 2014.

[79] M. Toledo-Rodriguez, B. Blumenfeld, C. Wu, J. Luo, B. Attali, P. Goodman, and H. Markram, "Correlation maps allow neuronal electrical properties to be predicted from single-cell gene expression profiles in rat neocortex.," *Cerebral cortex (New York, N.Y. : 1991)*, vol. 14, pp. 1310–27, Dec. 2004.

[80] J. Morris, J. M. Singh, and J. H. Eberwine, "Transcriptome analysis of single cells.," *Journal of visualized experiments : JoVE*, p. e2634, Jan. 2011.

[81] J. D. Steinmeyer, *Rapid Single-Cell Electroporation for Labeling Organotypic Cultures.* Master of science in electrical engineering and computer science, Massachusetts Institute of Technology, 2010.

[82] K. T. Brown and D. Flaming, *Advanced Micropipette Techniques for Cell Physiology.* Wiley, 1st ed., 1987.

[83] A. L. HODGKIN and A. F. HUXLEY, "A quantitative description of membrane current and its application to conduction and excitation in nerve.," *The Journal of physiology*, vol. 117, pp. 500–44, Aug. 1952.

[84] E. NEHER and B. SAKMANN, "Single-channel currents recorded from membrane of denervated frog muscle fibres," *Nature*, vol. 260, pp. 799–802, Apr. 1976.

[85] O. P. Hamill, A. Marty, E. Neher, B. Sakmann, and F. J. Sigworth, "Improved patch-clamp techniques for high-resolution current recording from cells and cell-free membrane patches.," *Pflügers Archiv : European journal of physiology*, vol. 391, pp. 85–100, Aug. 1981.

[86] N. R. Herr and R. M. Wightman, "Improved techniques for examining rapid dopamine signaling with iontophoresis.," *Frontiers in bioscience (Elite edition)*, vol. 5, pp. 249–57, Jan. 2013.

[87] J. M. Albrich, C. A. McCarthy, and J. K. Hurst, "Biological reactivity of hypochlorous acid: implications for microbicidal mechanisms of leukocyte

myeloperoxidase.," *Proceedings of the National Academy of Sciences of the United States of America*, vol. 78, pp. 210–4, Jan. 1981.

[88] S. B. Kodandaramaiah, G. T. Franzesi, B. Y. Chow, E. S. Boyden, and C. R. Forest, "Automated whole-cell patch-clamp electrophysiology of neurons in vivo.," *Nature methods*, vol. 9, pp. 585–7, June 2012.

[89] J. D. Steinmeyer and M. F. Yanik, "High-throughput single-cell manipulation in brain tissue.," *PloS one*, vol. 7, p. e35603, Jan. 2012.

[90] G. Saulis, "Comparison of electroporation of different cell lines in vitro," *Acta Physica Polonica Series a*, vol. 115, pp. 1056 – 1058, 2009.

[91] A. M. Lebar, G. C. Troiano, L. Tung, and D. Miklavcic, "Inter-pulse interval between rectangular voltage pulses affects electroporation threshold of artificial lipid bilayers.," *IEEE transactions on nanobioscience*, vol. 1, pp. 116–20, Sept. 2002.

[92] C. Bae and P. J. Butler, "Automated single-cell electroporation.," *BioTechniques*, vol. 41, pp. 399–400, 402, Oct. 2006.

[93] D. M. Johnson, K. R. Illig, M. Behan, and L. B. Haberly, "New features of connectivity in piriform cortex visualized by intracellular injection of pyramidal cells suggest that "primary" olfactory cortex functions like "association" cortex in other sensory systems.," *The Journal of neuroscience : the official journal of the Society for Neuroscience*, vol. 20, pp. 6974–82, Sept. 2000.

[94] X.-M. Ma, J. Huang, Y. Wang, B. A. Eipper, and R. E. Mains, "Kalirin, a multifunctional Rho guanine nucleotide exchange factor, is necessary for maintenance of hippocampal pyramidal neuron dendrites and dendritic spines.," *The Journal of Neuroscience*, vol. 23, pp. 10593–603, Nov. 2003.

[95] X.-M. Ma, Y. Wang, F. Ferraro, R. E. Mains, and B. A. Eipper, "Kalirin-7 is an essential component of both shaft and spine excitatory synapses in hippocampal interneurons.," *The Journal of Neuroscience*, vol. 28, pp. 711–24, Jan. 2008.

[96] P. Penzes, A. Beeser, J. Chernoff, M. R. Schiller, B. A. Eipper, R. E. Mains, and R. L. Huganir, "Rapid Induction of Dendritic Spine Morphogenesis by trans-Synaptic EphrinB-EphB Receptor Activation of the Rho-GEF Kalirin," *Neuron*, vol. 37, pp. 263–274, Jan. 2003.

[97] P. Penzes and K. A. Jones, "Dendritic spine dynamics–a key role for kalirin-7.," *Trends in Neurosciences*, vol. 31, pp. 419–27, Aug. 2008.

[98] M. R. Schiller, F. Ferraro, Y. Wang, X.-m. Ma, C. E. McPherson, J. A. Sobota, N. I. Schiller, R. E. Mains, and B. A. Eipper, "Autonomous functions for the Sec14p/spectrin-repeat region of Kalirin.," *Experimental Cell Research*, vol. 314, pp. 2674–91, Aug. 2008.

[99] M. R. Schiller, F. Ferraro, Y. Wang, X.-m. Ma, C. E. McPherson, J. A. Sobota, N. I. Schiller, R. E. Mains, and B. A. Eipper, "Autonomous functions for the Sec14p/spectrin-repeat region of Kalirin.," *Experimental Cell Research*, vol. 314, pp. 2674–91, Aug. 2008.

[100] J. E. Sommer and E. C. Budreck, "Kalirin-7: linking spine plasticity and behavior.," *The Journal of Neuroscience*, vol. 29, pp. 5367–9, Apr. 2009.

[101] Z. Xie, D. P. Srivastava, H. Photowala, L. Kai, M. E. Cahill, K. M. Woolfrey, C. Y. Shum, D. J. Surmeier, and P. Penzes, "Kalirin-7 controls activity-dependent structural and functional plasticity of dendritic spines.," *Neuron*, vol. 56, pp. 640–56, Nov. 2007.

[102] P. Penzes, R. C. Johnson, R. Sattler, X. Zhang, R. L. Huganir, V. Kambampati, R. E. Mains, and B. A. Eipper, "The neuronal Rho-GEF Kalirin-7 interacts with PDZ domain-containing proteins and regulates dendritic morphogenesis.," *Neuron*, vol. 29, pp. 229 42, Jan. 2001.

[103] A. De Simoni, C. B. Griesinger, and F. A. Edwards, "Development of rat CA1 neurones in acute versus organotypic slices: role of experience in synaptic morphology and activity.," *The Journal of Physiology*, vol. 550, pp. 135–47, July 2003.

[104] S. Cho, A. Wood, and M. R. Bowlby, "Brain slices as models for neurodegenerative disease and screening platforms to identify novel therapeutics.," *Current neuropharmacology*, vol. 5, pp. 19–33, Mar. 2007.

[105] K. Duff, W. Noble, K. Gaynor, and Y. Matsuoka, "Organotypic Slice Cultures from Transgenic Mice as Disease Model Systems," *Journal of Molecular Neuroscience*, vol. 19, pp. 317 320, Dec. 2002.

[106] M. Tanaka, Y. Yanagawa, and N. Hirashima, "Transfer of small interfering RNA by single-cell electroporation in cerebellar cell cultures.," *Journal of Neuroscience Methods*, vol. 178, pp. 80–6, Mar. 2009.

[107] O. Yizhar, L. E. Fenno, T. J. Davidson, M. Mogri, and K. Deisseroth, "Optogenetics in neural systems.," *Neuron*, vol. 71, pp. 9–34, July 2011.

[108] F. Zhang, L.-P. Wang, E. S. Boyden, and K. Deisseroth, "Channelrhodopsin-2 and optical control of excitable cells.," *Nature methods*, vol. 3, pp. 785 92, Oct. 2006.

[109] K. R. Hovis, K. Padmanabhan, and N. N. Urban, "A simple method of in vitro electroporation allows visualization, recording, and calcium imaging of local neuronal circuits.," *Journal of neuroscience methods*, vol. 191, pp. 1–10, Aug. 2010.

[110] H. J. Pi, N. Otmakhov, F. El Gaamouch, D. Lemelin, P. De Koninck, and J. Lisman, "CaMKII control of spine size and synaptic strength: Role of phosphorylation states and nonenzymatic action.," *Proceedings of the National Academy of Sciences of the United States of America*, vol. 107, pp. 14437–14442, July 2010.

[111] Q. Qing, S. K. Pal, B. Tian, X. Duan, B. P. Timko, T. Cohen-Karni, V. N. Murthy, and C. M. Lieber, "Nanowire transistor arrays for mapping neural circuits in acute brain slices.," *Proceedings of the National Academy of Sciences of the United States of America*, vol. 107, pp. 1882–7, Feb. 2010.

[112] E. A. Rancz, K. M. Franks, M. K. Schwarz, B. Pichler, A. T. Schaefer, and T. W. Margrie, "Transfection via whole-cell recording in vivo: bridging single-cell physiology, genetics and connectomics," *Nature Neuroscience*, vol. 14, pp. 527 532, Feb. 2011.

[113] A. Ainla, S. Xu, N. Sanchez, G. D. M. Jeffries, and A. Jesorka, "Single-cell electroporation using a multifunctional pipette.," *Lab on a chip*, vol. 12, pp. 4605–9, Nov. 2012.

[114] N. J. Sucher and D. L. Deitcher, "PCR and patch-clamp analysis of single neurons," *Neuron*, vol. 14, pp. 1095–1100, June 1995.

[115] P. Bochet, E. Audinat, B. Lambolez, F. Crépel, J. Rossier, M. Iino, K. Tsuzuki, and S. Ozawa, "Subunit composition at the single-cell level explains functional properties of a glutamate-gated channel," *Neuron*, vol. 12, pp. 383 388, Feb. 1994.

[116] E. Audinat, B. Lambolez, and J. Rossier, "Functional and molecular analysis of glutamate-gated channels by patch-clamp and RT-PCR at the single cell level," *Neurochemistry International*, vol. 28, pp. 119–136, Feb. 1996.

[117] B. Cauli, E. Audinat, B. Lambolez, M. C. Angulo, N. Ropert, K. Tsuzuki, S. Hestrin, and J. Rossier, "Molecular and physiological diversity of cortical nonpyramidal cells.," *The Journal of neuroscience : the official journal of the Society for Neuroscience*, vol. 17, pp. 3894–906, May 1997.

[118] S. A. Bustin, "Absolute quantification of mRNA using real-time reverse transcription polymerase chain reaction assays.," *Journal of molecular endocrinology*, vol. 25, pp. 169–93, Oct. 2000.

[119] L.-H. Loo, H.-J. Lin, D. K. Singh, K. M. Lyons, S. J. Altschuler, and L. F. Wu, "Heterogeneity in the physiological states and pharmacological responses of differentiating 3T3-L1 preadipocytes.," *The Journal of cell biology*, vol. 187, pp. 375–84, Nov. 2009.

[120] M. Bengtsson, M. Hemberg, P. Rorsman, and A. Stà hlberg, "Quantification of mRNA in single cells and modelling of RT-qPCR induced noise.," *BMC molecular biology*, vol. 9, p. 63, Jan. 2008.

[121] H. Lodish, *Molecular Cell Biology*. W. H. Freeman; 6th edition, 2007.

[122] C.-H. Lee, M.-S. Kim, B. M. Chung, D. J. Leahy, and P. A. Coulombe, "Structural basis for heteromeric assembly and perinuclear organization of keratin filaments.," *Nature structural & molecular biology*, vol. 19, pp. 707–15, July 2012.

[123] A. Finski, "Multiplex Analytical Measurements in Single Cells of Solid Tissues," Mar. 2012.

[124] M. Toledo-Rodriguez and H. Markram, "Single-cell RT-PCR, a technique to decipher the electrical, anatomical, and genetic determinants of neuronal diversity.," *Methods in molecular biology (Clifton, N.J.)*, vol. 403, pp. 123–39, Jan. 2007.

[125] K. D. Dyer and H. F. Rosenberg, "The RNase a superfamily: generation of diversity and innate host defense.," *Molecular diversity*, vol. 10, pp. 585–97, Nov. 2006.

[126] G. Konat, "No Title," in *PCR Technology: Current Innovations* (H. Griffin and A. Griffin, eds.), Boca Raton Florida: CRC Press, Inc, 1994.

[127] A. Helenius and K. Simons, "Solubilization of membranes by detergents.," *Biochimica et biophysica acta*, vol. 415, pp. 29–79, Mar. 1975.

[128] L. Warren, *Single-cell gene-expesion analysis by quantitative RT-PCR.* PhD thesis, California Institute of Technology, 2008.

[129] G. S. Belinsky, M. T. Rich, C. L. Sirois, S. M. Short, E. Pedrosa, H. M. Lachman, and S. D. Antic, "Patch-clamp recordings and calcium imaging followed by single-cell PCR reveal the developmental profile of 13 genes in iPSC-derived human neurons.," *Stem cell research*, vol. 12, pp. 101–18, Jan. 2014.

[130] J. Phillips and J. Eberwine, "Antisense RNA Amplification: A Linear Amplification Method for Analyzing the mRNA Population from Single Living Cells," *Methods (San Diego, Calif.)*, vol. 10, pp. 283–8, Dec. 1996.

[131] A. Ghetti, A. Guia, and J. Xu, "Automated voltage-clamp technique.," *Methods in molecular biology (Clifton, N.J.)*, vol. 403, pp. 59 69, Jan. 2007.

[132] M. Fejtl, U. Czubayko, A. Hümmer, T. Krauter, and A. Lepple-Wienhues, "Flip-the-tip: automated patch clamping based on glass electrodes.," *Methods in molecular biology (Clifton, N.J.)*, vol. 403, pp. 71–85, Jan. 2007.

[133] C. Leisgen, M. Kuester, and C. Methfessel, "The roboocyte: automated electrophysiology based on Xenopus oocytes.," *Methods in molecular biology (Clifton, N.J.)*, vol. 403, pp. 87–109, Jan. 2007.

[134] P. Jonas, C. Racca, B. Sakmann, P. H. Seeburg, and H. Monyer, "Differences in Ca2+ permeability of AMPA-type glutamate receptor channels in neocortical neurons caused by differential GluR-B subunit expression.," *Neuron*, vol. 12, pp. 1281–9, June 1994.

[135] R. Kwak, S. J. Kim, and J. Han, "Continuous-flow biomolecule and cell concentrator by ion concentration polarization.," *Analytical chemistry*, vol. 83, pp. 7348–55, Oct. 2011.

[136] S. H. Ko, S. J. Kim, L. F. Cheow, L. D. Li, K. H. Kang, and J. Han, "Massively parallel concentration device for multiplexed immunoassays.," *Lab on a chip*, vol. 11, pp. 1351–8, Apr. 2011.

[137] D. Juncker, H. Schmid, and E. Delamarche, "Multipurpose microfluidic probe.," *Nature materials*, vol. 4, pp. 622–8, Aug. 2005.

[138] A. Sarkar, S. Kolitz, D. A. Lauffenburger, and J. Han, "Microfluidic probe for single-cell analysis in adherent tissue culture.," *Nature communications*, vol. 5, p. 3421, Jan. 2014.

[139] B. A. Flusberg, A. Nimmerjahn, E. D. Cocker, E. A. Mukamel, R. P. J. Barretto, T. H. Ko, L. D. Burns, J. C. Jung, and M. J. Schnitzer, "High-speed, miniaturized fluorescence microscopy in freely moving mice.," *Nature methods*, vol. 5, pp. 935–8, Nov. 2008.

[140] K. Brown and D. Flaming, *Advanced micropipette techniques for cell physiology*. Wiley, 1986.

[141] J. M. Nitsche, H.-C. Chang, P. A. Weber, and B. J. Nicholson, "A Transient Diffusion Model Yields Unitary Gap Junctional Permeabilities from Images of Cell-to-Cell Fluorescent Dye Transfer Between Xenopus Oocytes," *Biophysical Journal*, vol. 86, pp. 2058–2077, Apr. 2004.

[142] D. M. F. Prazeres, "Prediction of diffusion coefficients of plasmids.," *Biotechnology and Bioengineering*, vol. 99, pp. 1040–4, Mar. 2008.

[143] A. De Simoni and L. M. Y. Yu, "Preparation of organotypic hippocampal slice cultures: interface method.," *Nature Protocols*, vol. 1, pp. 1439–45, Jan. 2006.

[144] T. Matsuda and C. L. Cepko, "Electroporation and RNA interference in the rodent retina in vivo and in vitro.," *Proceedings of the National Academy of Sciences of the United States of America*, vol. 101, pp. 16–22, Jan. 2004.

[145] M. Dundr, J. K. Ospina, M.-H. Sung, S. John, M. Upender, T. Ried, G. L. Hager, and A. G. Matera, "Actin-dependent intranuclear repositioning of an active gene locus in vivo.," *The Journal of Cell Biology*, vol. 179, pp. 1095–103, Dec. 2007.

[146] M. A. Rizzo, G. H. Springer, B. Granada, and D. W. Piston, "An improved cyan fluorescent protein variant useful for FRET.," *Nature Biotechnology*, vol. 22, pp. 445–9, Apr. 2004.

[147] P. Penzes, R. C. Johnson, M. R. Alam, V. Kambampati, R. E. Mains, and B. A. Eipper, "An isoform of kalirin, a brain-specific GDP/GTP exchange factor, is enriched in the postsynaptic density fraction.," *The Journal of Biological Chemistry*, vol. 275, pp. 6395–403, Mar. 2000.

[148] M. Angel and M. F. Yanik, "Innate Immune Suppression Enables Frequent Transfection with RNA Encoding Reprogramming Proteins," *PLoS ONE*, vol. 5, p. e11756, July 2010.